PEOPLE'S DEMOCRATIC REPUBLIC OF ALGERIA
Ministry of Higher Education and Scientific Research
MOHAMED KHIDER UNIVERSITY - BISKRA
Faculty of Exacts Sciences, Nature and Life Sciences
Department of Computer Science

THESIS

To obtain the academic degree of

Doctor in Science in Computer Sciences

Option : computer Sciences

Approche robuste pour la segmentation et la classification d'images médicales

---

Presented by

Fouzia CHIGHOUB

Members of the jury :

- Pr. Labib Sadek Terrissa	University of Biskra	President
- Pr. Rachida SAOULI	University of Biskra	Director of thesis
- Pr. Kamal Eddine MELKEMI	University of Batna	Examinator
- Pr. Mohamed BENMOHAMMED	University of Constantine	Examinator

Acknowledgments

I am profoundly grateful to my supervisor, Pr. Rachida SAOULI, for her unwavering guidance, continuous advice, and the genuine care she has shown me throughout my thesis journey. Her support and mentorship have been invaluable, and I credit her for helping me successfully complete this dissertation.

I also want to extend my heartfelt thanks to the members of my jury, Pr. Labib Sadek TERRISSA, Pr. Kamal Eddine MELKEMI, and Pr. BENMOHAMMED Mohamed, for dedicating their precious time and effort in carefully reviewing and evaluating my thesis.

To my beloved family, including my brothers and sisters, I owe a special debt of gratitude. Your unwavering belief in my abilities and constant encouragement have been a driving force behind my thesis. Your love, support, and understanding have been my pillars of strength, and I am forever grateful for your presence in my life.

Finally, I want to express my deepest appreciation to everyone who has been a part of my thesis. Each one has contributed to this achievement in their unique way, and I am truly blessed to have such amazing people in my life. Your unwavering support has made a significant impact on my academic journey, and I am humbled by your kindness.

Abstract

Image segmentation is a vital process in various fields, including robotics, object recognition, and medical imaging. In medical imaging, accurate segmentation of brain tissues from MRI images is crucial for diagnosing and treating brain disorders such as Alzheimer's disease, epilepsy, schizophrenia, multiple sclerosis, and cancer. This thesis proposes an automatic fuzzy method for brain MRI segmentation.

Firstly, the proposed method aims to improve the efficiency of the Fuzzy C-Means (FCM) algorithm by reducing the need for manual intervention in cluster initialization and determining the number of clusters. For this purpose, we introduce an adaptive split-merge technique that effectively divides the image into several homogeneous regions using a multi-threshold method based on entropy information. During the merge process, a new distance metric is introduced to combine the regions that are both highly similar within the merged region and effectively separated from others. The cluster centers and numbers obtained from the adaptive split-merge step serve as the initial parameters for the FCM algorithm. The obtained fuzzy partitions are evaluated using a novel proposed validity index.

Secondly, we present a novel method to address the challenge of noisy pixels in the FCM algorithm by incorporating spatial information. Specifically, we assign a crucial role to the central pixel in the clustering process, provided it is not corrupted with noise. However, if it is corrupted with noise, its influence is reduced. Furthermore, we propose a novel quantitative metric for replacing the central pixel with one of its neighbors if it can improve the segmentation result in terms of compactness and separation. To evaluate the effectiveness of the proposed method, a thorough comparison with existing clustering techniques is conducted, considering cluster validity functions, segmentation accuracy, and tissue segmentation accuracy. The evaluation comprises comprehensive qualitative and quantitative assessments, providing strong evidence of the superior performance of the proposed approach.

Keywords

Image segmentation, adaptive split-merge stage, spatial information, fuzzy similarity measure, level of noise.

Résumé

La segmentation d'image est un processus essentiel dans divers domaines, notamment la robotique, la reconnaissance d'objets et l'imagerie médicale. En imagerie médicale, une segmentation précise des tissus cérébraux à partir d'images IRM est cruciale pour le diagnostic et le traitement des troubles cérébraux tels que la maladie d'Alzheimer, l'épilepsie, la schizophrénie, la sclérose en plaques et le cancer. Cette thèse propose une méthode floue automatique pour la segmentation IRM cérébrale.

Tout d'abord, la méthode proposée vise à améliorer l'efficacité de l'algorithme Fuzzy C-Means (FCM) en réduisant le besoin d'intervention manuelle dans l'initialisation des clusters et la détermination du nombre de clusters. Dans ce but, nous introduisons une technique de décomposition-fusion adaptative qui divise efficacement l'image en plusieurs régions homogènes à l'aide d'une méthode multi-seuils basée sur les informations d'entropie. Pendant le processus de fusion, une nouvelle mesure de distance est introduite pour combiner les régions qui sont à la fois très similaires à l'intérieur de la région fusionnée et efficacement séparées des autres. Les centres et les nombres de groupes obtenus à partir de l'étape de décomposition-fusion adaptative servent de paramètres initiaux pour l'algorithme FCM. Les partitions floues obtenues sont évaluées à l'aide d'un nouvel indice de validité.

Ensuite, nous présentons une nouvelle méthode pour relever le défi des pixels bruités dans l'algorithme FCM en incorporant des informations spatiales. Plus précisément, nous attribuons un rôle crucial au pixel central dans le processus de regroupement, à condition qu'il ne soit pas corrompu par du bruit. Cependant, s'il est corrompu par du bruit, son influence est réduite. De plus, nous proposons une nouvelle mesure quantitative pour remplacer le pixel central par l'un de ses voisins s'il peut améliorer le résultat de segmentation en termes de compacité et de séparation. Nous effectuons des comparaisons qualitatives et quantitatives avec des techniques de clustering existantes, en considérant les fonctions de validité, la précision de segmentation et la précision des tissus segmentés.

Mots-clés

Segmentation d'image, décompositon-fusion adaptative, information spatiale, mesure de similarité floue, niveau de bruit.

ملخص

إن تقسيم الصور هي عملية مهمة ضمن مجالات مختلفة، مثل: الروبوتات، التعرف على الأجسام، والتصوير بالرنين المغناطيسي. حيث نجد أن صور التصوير بالرنين المغناطيسي للدماغ يركز على تقسيم الأنسجة بدقة، وهو أمر جد مهم للتشخيص وعلاج اضطرابات الدماغ، مثل: مرض الزهايمر، الصرع، فصام الشخصية، التصلب المتعدد والسرطان. الهدف الرئيسي من هذه الأطروحة هو اقتراح طريقة ضبابية تلقائية لتقسيم صور التصوير بالرنين المغناطيسي للدماغ.

أولاً، سنهدف إلى تحسين دقة خوارزمية المتوسطات الضبابية (FCM) عن طريق ادخال طريقة تكيفية تجمع بين خوارزمية التقسيم والدمج مع خوارزمية (FCM)، فقد تم تصميم هذه الطريقة للتغلب على حساسية (FCM) للقيم الابتدائية سواء عدد المجموعات او قيم مراكز المجموعات. حيث سنهدف لتقسيم الصورة بشكل ديناميكي إلى مناطق متجانسة باستخدام معلومات الإنتروبيا متعددة العتبات، ثم نقوم بدمج المناطق المتجانسة باستخدام مقياس مسافة جديد لتقليل عدد المجموعات. ليتم بعد ذلك تطبيق خوارزمية (FCM) باستخدام مراكز المجموعات المحصل عليها، ومن ثم تقييم مختلف التقسيمات وعدد المجموعات الموافق لها عن طريق مؤشر تقييم جديد.

ثانيًا، من اجل تعزيز أداء خوارزمية (FCM) ضد الضوضاء في تجزئة الصور، سنقدم إستراتيجية جديدة تأخذ في الاعتبار المعلومات في الجوار، حيث سنقترح منح وزنًا أكبر للبكسل المركزي في التجزئة إذا لم يتأثر بالضوضاء، مع التقليل من تأثيره في عملية التجزئة إذا كان بكسل يحتوي على الضوضاء. يتم تعريف تأثير البكسلات المجاورة بناءً على مقياس التشابه فيما بينها ومستوى الضوضاء. إضافة إلى ذلك، سنقترح مقياسًا كميًا جديدًا لتحديد البكسل الأمثل الذي سيعوض البكسل المركزي ويحسن أداء تجزئة الصورة. أخيرًا ولإثبات تفوق طريقتنا المقترحة، سنقوم بمقارنتها مع (FCM) وبعض الأعمال الأخرى المنشورة حالياً عن طريق مجموعة من التقييمات النوعية والكمية، كمقياس تقييم المجموعات ودقة التجزئة ودقة تجزئة الأنسجة.

الكلمات المفتاحية:

تجزئة الصورة، مرحلة الانقسام التكيفية، معلومات جوارية، مقياس التشابه الضبابي، مستوى الضوضاء

Contents

List of Figures

List of Tables

Chapter 1

General introduction

Contents

1.1 Thesis Context

Medical image segmentation is a crucial task in which an image is separated into meaningful and non-overlapping regions with similar characteristics. This process is challenging due to the inherent imprecision of medical images. Accurate and reliable segmentation is indispensable for extracting valuable information from medical images. It enables precise analysis, diagnosis, treatment planning, and monitoring of various medical conditions by identifying and isolating specific tissues or structures within an image. By delineating boundaries, segmentation facilitates accurate measurements, quantitative analysis, and the extraction of relevant features. Moreover, it serves as a foundation for advanced image-based techniques such as 3D reconstruction, computer-aided diagnosis, and image-guided interventions. Additionally, precise segmentation contributes to assessing treatment response, disease progression, and patient outcome evaluation.

Manual segmentation is a traditional method of image segmentation that involves an expert or a human operator manually drawing boundaries or contours around objects of interest in an image. This method has long been used as a gold standard for image segmentation, as it allows for precise and accurate identification of regions of interest. However, manual segmentation is a time-consuming and labor-intensive process that can be prone to errors. Moreover, manual segmentation is subjective, and different experts may produce different segmentations. This subjectivity can lead to inconsistencies in diagnosis and treatment planning. Furthermore, manual segmentation may not be feasible in

cases where the images contain a large number of regions, and it is not suitable for large datasets or real-time applications. The limitations of manual segmentation have led to the development of automatic image segmentation methods. These methods employ various algorithms to segment images based on different criteria, including intensity, texture, shape, and spatial information. Unlike manual segmentation, these methods are less prone to operator variability, resulting in more objective and accurate segmentation.

Image clustering is a process that involves grouping pixels or voxels within an image based on their similarity to identify and separate different regions or objects of interest. This approach offers several advantages. It eliminates the need for manual annotation, reducing human effort and subjectivity in the segmentation process. Moreover, image clustering algorithms are efficient in handling large datasets, enabling the analysis of high resolution medical images with improved efficiency. Additionally, image clustering provides a versatile solution applicable to various imaging modalities, such as MRI, CT, and ultrasound, making it suitable for a wide range of medical image segmentation tasks.

In this work, we address the significant challenge of the scarcity of high-quality annotated medical imaging datasets. We focus on clustering methods, which search for patterns in a data set without pre-existing labels. Additionally, this method can also be employed for anomaly detection to identify noisy pixels that do not belong to any cluster.

1.2 Thesis Motivation and Objectives

There are several well-known clustering algorithms proposed in the literature, including K-means, hierarchical clustering, Density-Based Spatial Clustering of Applications with Noise (DBSCAN), and Gaussian Mixture Models (GMM) (Mittal et al., 2021). K-means and hierarchical clustering are distance-based algorithms that assign data points to clusters based on minimizing the distance within clusters. However, they make assumptions of equal-sized and spherical clusters, which may limit their effectiveness in capturing complex cluster shapes. They are also sensitive to the initial parameter choices, which can lead to different cluster assignments. DBSCAN identifies clusters based on the density of data points and their connectivity. It is capable of discovering clusters of arbitrary shapes and sizes, making it more flexible than distance-based algorithms. However, DBSCAN has difficulties handling data with varying densities and may struggle with high-dimensional datasets due to the curse of dimensionality. GMM is a probabilistic model that assumes data points are generated from a mixture of probability distributions. It estimates the parameters of the underlying distributions and assigns data points to clusters based on their membership probabilities. GMM can capture complex data distributions and is robust to noise. However, it assumes a specific parametric form of the data distribution, which may not always be accurate, and determining the optimal number of clusters can be challenging (Yazdani et al., 2015).

In addition to these limitations, clustering algorithms in general can suffer from computational complexity, especially when dealing with large datasets. The subjective nature of determining the number of clusters and making assumptions about the underlying data distribution also adds a level of uncertainty in the clustering process.

In this thesis, we focus on the Fuzzy C-Means (FCM) algorithm, which is one of the most widely used fuzzy clustering algorithms for image segmentation where imprecise decisions are often required. FCM extends the K-means algorithm by introducing fuzziness into the cluster assignments, allowing a pixel to belong to multiple clusters to a certain degree of membership. This makes it more suitable for handling partial volume effects in medical images, where multiple tissues can contribute to the same pixel intensity value. One of the main challenges in FCM is to determine the optimal number of clusters for a given image. This is a crucial step in the segmentation process, as an incorrect choice of the number of clusters can lead to inaccurate segmentation results. In addition, FCM requires an initialization of the cluster centers which is a critical step that can significantly affect the final segmentation result. Without an appropriate initialization, FCM may fall into local minimum solutions, which can lead to suboptimal results. In addition, FCM algorithm is relatively sensitive to noise pixels, as it does not consider the spatial distribution of pixels in an image, which can lead to misclassification of pixels and affect the accuracy of the segmentation results. In this case, FCM tries to minimize the distance between each pixel and each cluster center, hence, noise can cause a pixel to be closer to the wrong cluster center, leading to misclassification.

In this thesis, we propose an automatic image segmentation method that aims to address the limitations of FCM by achieving two main objectives. Firstly, we aim to improve the efficiency of the segmentation process by reducing the need for manual intervention in cluster initialization and determining the number of clusters. To achieve this, we introduce a new strategy based on an adaptive split-merge technique that effectively divides the image into several homogeneous regions using a multi-threshold method based on entropy information. Furthermore, we use a new fuzzy validity index to incorporate compactness and separation information, which helps determine the optimal fuzzy partition. Secondly, we aim to reduce the impact of noisy data on the clustering process, which can cause misclassification of pixels and affect the accuracy of the segmentation results. To overcome this limitation, we propose a novel variant of the Fuzzy C-Means (FCM) algorithm that fully integrates the spatial constraint. The proposed algorithm incorporates comprehensive spatial information to enhance its performance.

1.3 Thesis Contributions

In this thesis, we aim to propose an automatic method for image segmentation to improve the limitations of FCM algorithm. Our contributions are twofold:

Firstly, we introduce an adaptive split-merge technique that effectively divides the image into several homogeneous regions using a multi-threshold method based on entropy information. This adaptive split-merge technique aims to reduce the need for manual intervention in the initialization step and improve the efficiency of the segmentation process. During the split process, the image is recursively divided into smaller regions based on the entropy values of the intensity histogram until a predefined stopping criterion is met. During the merge process, a new distance metric is introduced to combine the regions that are both highly similar within the merged region and effectively separated from others. The cluster centers and numbers obtained from the adaptive split-merge step serve as the initial parameters for the Fuzzy C-Means (FCM) algorithm. Furthermore, we introduce a novel fuzzy validity index that incorporates a new definition for the separation measure. This index is used to select the optimal fuzzy partition with high compactness and separation of clusters, thereby improving segmentation accuracy.

Secondly, we propose a robust fuzzy clustering algorithm in which we fully integrated the spatial constraint to improve image segmentation accuracy. By incorporating spatial information, our proposed algorithm aims to capture complex spatial dependencies between neighboring pixels. We assign varying degrees of importance to each pixel based on its spatial relationships and noise levels. Specifically, we incorporate the central pixel in the clustering process only if it is not corrupted by noise. If it is a noisy pixel, we suppress its influence from the fuzzy clustering process. To express the degree of similarity between the pixels, we use the fuzzy representation and introduce a new term to indicate the noise level of pixels. We then combine these two measures to construct the spatial information. Additionally, we propose a new quantitative metric to select the optimal pixel that could influence the segmentation performance better in terms of compactness and separation. Our proposed algorithm does not require any parameter specification, which makes it easy to use and applicable to a wide range of image segmentation tasks. By achieving a good balance between robustness to imaging artifacts and preservation of image detail information, our proposed algorithm can improve the accuracy and reliability of the segmentation results.

1.4 Thesis Overview

In this work, we propose an automatic method for image segmentation that overcomes the sensitivity of the FCM algorithm to noise and initialization steps. The thesis is organized as follows:

Chapter 2 provides details of image segmentation and presents the challenges of brain MRI segmentation due to intensity inhomogeneity and noise caused by radio frequency coils used in image acquisition. Also, we present reviews of MRI segmentation techniques classified according to the segmentation strategy used.

Chapter 3 presents an overview of different approaches that automatically determine the number of clusters and enhance the initialization process in the FCM algorithm. It also presents numerous FCM derivatives that aim to increase the FCM algorithm's robustness to noise.

Chapter 4 proposes an adaptive split and merge approach that automatically evolves the number of clusters and initializes the cluster centers to prevent the FCM algorithm from converging to the minimum optimal solution. Additionally, it introduces a novel fuzzy validity index that combines compactness and separation information to select the optimal fuzzy partition.

Chapter 5 presents the main steps of our robust fuzzy algorithm that aim to improve the sensitivity of FCM against noise. The proposed algorithm is completely free from any specification parameters step and fully integrates spatial information. Additionally, the importance of the central pixel is determined based on its level of noise. The effectiveness of the proposed algorithm is evaluated qualitatively and quantitatively on synthetic and brain MR images corrupted by different levels of noise, in terms of fuzzy validity indices, segmentation accuracy, and tissue segmentation accuracy.

A summary of the contributions and outlines of future research directions are presented in Chapter 6.

Chapter 2

Brain MRI Image segmentation

Contents

2.1 Introduction

Medical imaging is a crucial tool for non-invasively mapping the anatomy of the human body, providing valuable information for clinical analysis and medical research. By visualizing the functions of organs and tissues, medical imaging plays a critical role in diagnosis and treatment planning. Magnetic resonance imaging (MRI) of the brain is one of the most important medical imaging techniques, particularly in the field of computer-aided detection of medical images. MRI has greatly increased our knowledge of normal and diseased anatomy, enabling more accurate diagnosis and treatment of various neurological disorders. With its ability to provide high-resolution images of the brain, MRI has become an essential

tool for medical professionals in a wide range of specialties, including neurology, oncology, and psychiatry. Accurate segmentation of anatomical structures in brain MR images is essential for medical image analysis, as qualitative evaluation of brain morphological characteristics can be subjective and unreliable. Quantified techniques, such as segmentation, are needed to provide objective and accurate measurements of brain structures, enabling more precise diagnosis and treatment planning.

Segmentation is a fundamental problem in biomedical image analysis and has been extensively studied in the field of computer vision. In this chapter, we provide an overview of image segmentation, including its definition, challenges, and applications. We then focus on brain MRI segmentation, which remains a challenging task due to the presence of intensity inhomogeneity and noise caused by the radio frequency coil used in image acquisition. We review various MRI segmentation techniques and classify them based on the segmentation strategy employed.

2.2 Image Segmentation

Image segmentation is the process of partitioning an image into regions, also known as classes or subsets, that are homogeneous with respect to one or more characteristics or features, such as texture, intensity, or color. This enables more meaningful and easier analysis of objects within the image (Rogowska, 2000; Bezdek, 1973). The extent of homogeneity of the segmented region can be measured using various image properties, such as pixel intensity (Mittal et al., 2021). Classically, the segmentation is the partition of an image I into n sets R_i called regions, whose union is the entire image I. Thus, the sets that make up a segmentation must satisfy

$$\bigcup_{i=1}^{n} R_i = I \tag{2.1}$$

Where $R_i \cap R_j = \emptyset, \forall i, j \in \{1, ..., n\}^2$ for, $i \neq j$, and each R_i is connected. Ideally, a segmentation method finds those regions that correspond to distinct anatomical structures or regions of interest in the image.

When the constraint that regions be connected is removed, the process of determining the regions R_i is called pixel classification, and the regions themselves are referred to as classes. In medical image analysis, pixel classification is often a desirable goal, especially when identifying disconnected regions belonging to the same tissue class. Unlike classical segmentation, pixel classification does not require the regions to be connected, allowing for more flexibility in identifying and analyzing different structures within the image. In practice, the total number of classes n is often assumed to be known based on prior knowledge of the anatomy being considered.

Image segmentation is a fundamental step in many computer vision systems, as it

plays a critical role in image analysis and processing (Chouhan et al., 2019). The goal of segmentation is to partition an image into meaningful regions or objects, based on some predefined criteria, such as color, texture, or intensity. The level of subdivision required depends on the specific problem being solved, and segmentation should stop when the objects of interest in an application have been isolated. In practice, segmentation is often used as a pre-processing step to extract relevant information from an image, such as identifying tumors in medical images or detecting objects in surveillance videos.

Figure 2.1 provides an overview of the image processing pipeline, which typically consists of five main steps: input, pre-processing, segmentation, post-processing, and output. In the input step, an image is acquired and loaded into the system for further processing. The pre-processing step involves various techniques to enhance the quality of the input image, such as deblurring and denoising, to improve the accuracy of subsequent processing steps. The segmentation step partitions the image into meaningful regions or objects based on some predefined criteria, such as color, texture, or intensity. This step is critical in many image processing applications, as it enables the extraction of relevant information from the image. The post-processing step involves further refinement of the segmented regions to remove noise and artifacts and improve the accuracy of the final output. Finally, the output step generates the desired result, which could be a binary mask, a set of segmented regions, or some other form of processed image data.

Figure 2.2 shows an example of a segmented image obtained from the BSD database (Martin et al., 2001), demonstrating the effectiveness of segmentation in extracting meaningful information from an image. By partitioning an image into meaningful regions or objects based on some predefined criteria, such as color, texture, or intensity, we can extract more information from the image, enabling more precise analysis and interpretation in various applications. For example, in medical imaging, segmentation can be used to locate tumors, measure tissue volumes, and study anatomical structures. In satellite imaging, segmentation can be used to locate objects such as roads, forests, and crops, enabling more accurate mapping and monitoring of the Earth's surface.

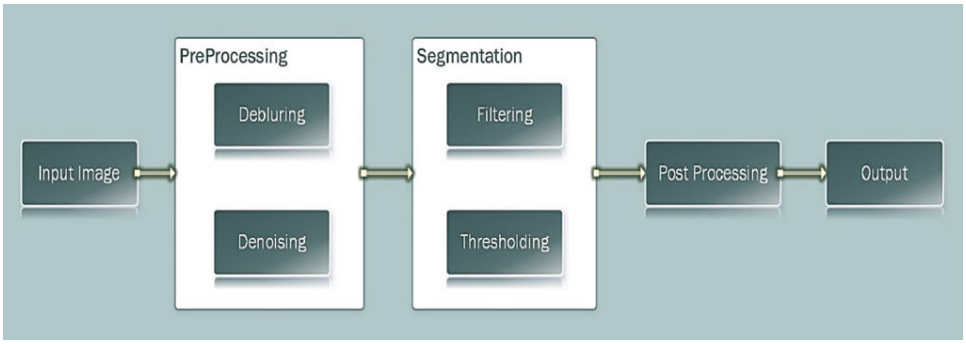

Figure 2.1 – Image segmentation process (Chouhan et al., 2019)

Figure 2.2 – Image segmentation result from BSD (Chouhan et al., 2019)

2.3 Magnetic resonance imaging (MRI)

Magnetic Resonance Imaging (MRI) scanners use a combination of strong magnetic fields and radio waves to create highly detailed images of the tissues and structures inside the brain. When a patient is inside the scanner, the magnetic field causes the hydrogen protons in the brain's tissue to align in a particular way. Short bursts of radio waves are then applied to the area being scanned, causing the protons to move out of alignment. As the protons return to their original state, they emit radio signals that are picked up by a receiver in the scanner. The signals produced by different types of tissue in the brain vary, and this allows the computer to create a highly detailed and accurate picture of the brain's internal structures.

Magnetic Resonance Imaging (MRI) scanners can create clear and detailed pictures of the structure of the brain, which are used by medical professionals to diagnose and treat a wide range of neurological conditions. By using a combination of strong magnetic fields and radio waves, MRI can detect any abnormalities or tumors in the brain, enabling more precise diagnosis and treatment planning. The relaxation times, T1, T2, and T2*, are measured after the scanner's pulse sequence and can be chosen to look at specific tissue within the brain. By selecting different relaxation times and manipulating radio frequencies, specific brain tissue can be highlighted for examination by the physician. This allows for more accurate and targeted diagnosis and treatment of various neurological disorders, such as stroke, tumors, and multiple sclerosis.

The T1 values of most human tissues typically range from 100-1500 ms, as shown in Figure 2.3. These values tend to increase as the magnetic field strength increases. On the other hand, T2 values range from approximately 20-300 ms, as indicated in Table 2.1, and are largely independent of field strength.

Magnetic Resonance Imaging (MRI) provides detailed images of soft tissues, organs, and bones with high-contrast resolution, making it a powerful tool for scientific and diagnostic purposes. The MRI signal intensity can be used to differentiate between different tissues based on their different relaxation times (T1 and T2) and proton densities (Figure 2.4).

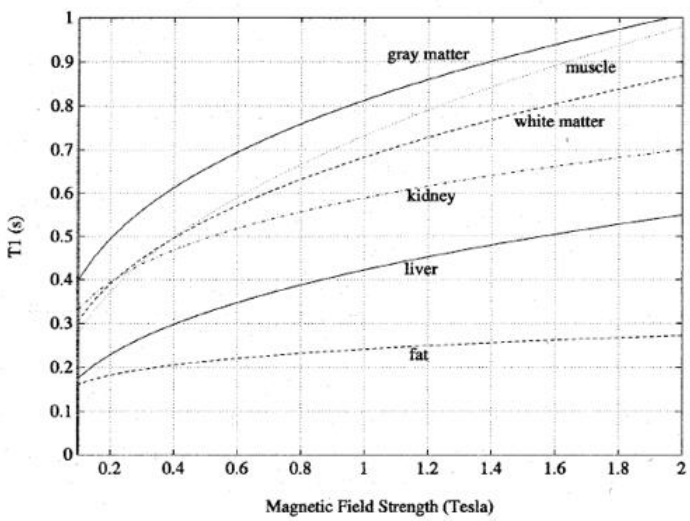

Figure 2.3 – Approximate T1 values as a function of magnetic field (Zhu, 2003)

Table 2.1 – T2 of some normal tissue types

Tissues	**T2 (ms)**
Gray matter	80-100
White matter	40-70
Muscle tissue	40-50
Fat	80-120
Liver	40-50
Kidney	40-60

These images can be further processed to produce new maps of water diffusion, blood flow, and other physiological parameters, which can help study the underlying mechanisms of various diseases and disorders. For example, diffusion tensor imaging (DTI) can be used to study the microstructure of white matter in the brain, while functional MRI (fMRI) can be used to study brain function and connectivity. The wide range of data acquisition and contrast mechanisms of MRI makes it a versatile and powerful tool for various applications in medical diagnosis, research, and treatment planning (Figure 2.5).

Magnetic Resonance Imaging (MRI) scans are generally considered a safe and painless procedure that does not involve exposure to ionizing radiation, unlike X-rays or CT scans. However, in some cases, a patient may experience a reaction to the contrast agent (dye) used during the scan, such as nausea, headache, or allergic reactions. Patients with kidney problems or allergies to contrast agents may be at higher risk of adverse reactions and should inform their doctor before the scan. Pregnant women are usually advised to avoid MRI scans unless it is absolutely necessary, as the effects of a strong magnetic field on the developing fetus are not yet fully understood. In some cases, alternative imaging methods,

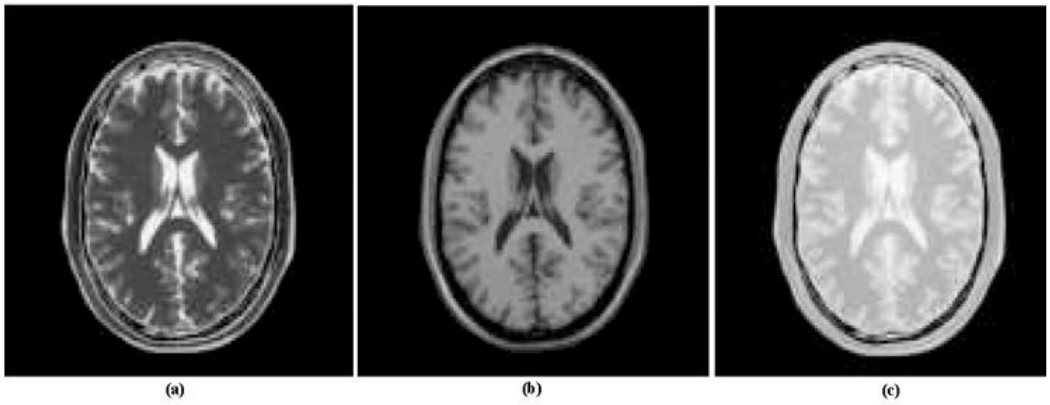

Figure 2.4 – Different MRI modalities (a) T2-weighted (T2), (b) T1-weighted (T1), (c) proton density (PD) (Zhu, 2003)

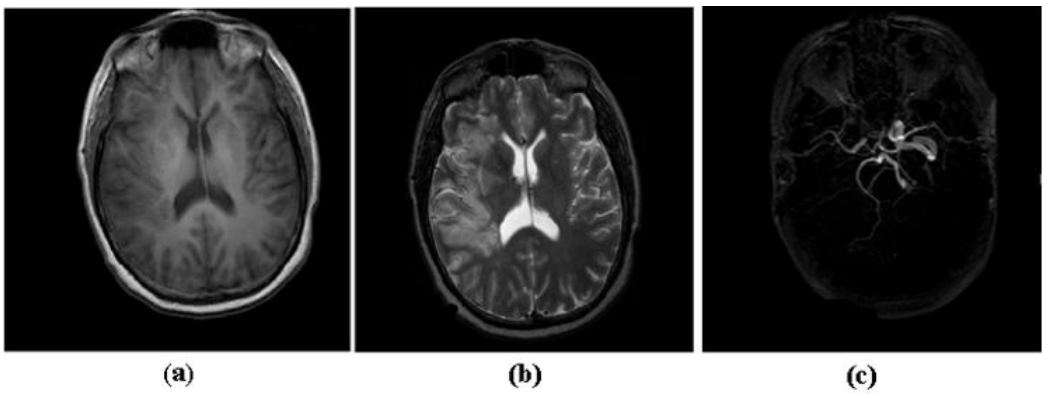

Figure 2.5 – Multiple MR images were acquired to help neurologists diagnose a stroke patient who had middle cerebral artery occlusion in comparison to the right side of the brain. (a) T1-weighted (T1), (b) T2-weighted (T2), (c) 3D MR (Zhu, 2003)

such as ultrasound or MRI without contrast, may be used instead. After the scan, the patient can resume their regular activities immediately, and the radiologist examines the images and provides a report to the doctor, who will discuss the results and any further treatment options with the patient.

2.4 MRI brain images segmentation

Segmentation is a crucial step in medical imaging that involves separating an image into meaningful regions or objects for feature extraction, image measurements, and image display. Depending on the application, segmentation can be used to classify image pixels into anatomical regions, such as bones, muscles, and blood vessels, or into pathological regions, such as cancer, tissue deformities, and multiple sclerosis lesions (Rogowska, 2000).

Brain tissue segmentation is a critical task in medical image analysis that aims to

identify and differentiate the different types of tissues in the brain from MRI images. The brain is composed of various tissues, such as cerebrospinal fluid (CSF), gray matter (GM), and white matter (WM), each with distinct anatomical and functional properties. CSF is not a tissue, but rather a clear, colorless liquid that surrounds the brain and spinal cord. It is produced in the ventricles of the brain and helps to cushion and protect the brain from injury by acting as a shock absorber. It also plays an essential role in the transportation of nutrients, hormones, and waste products within the central nervous system (CNS) (El-Dahshan et al., 2014).

Cerebrospinal fluid (CSF) has distinct imaging characteristics on brain MRI images that depend on the type of MRI sequence used. On T1-weighted MRI images, CSF appears dark or hypo-intense because it contains fewer protons and thus absorbs less radiofrequency energy, while on T2-weighted MRI images, it appears bright or hyper-intense because it contains more protons and thus absorbs more radiofrequency energy. CSF is an essential component of the central nervous system (CNS) and plays a vital role in cushioning and protecting the brain and spinal cord from injury. Gray matter (GM) is another important tissue in the brain that is composed of cell bodies of neurons, as well as glial cells and unmyelinated fibers. It plays a crucial role in brain functions such as memory, perception, and muscle control. GM typically appears darker on T1-weighted MRI images and brighter on T2-weighted MRI images when compared to white matter (WM), which is composed mainly of myelinated axons and plays a critical role in transmitting signals between different regions of the brain. It connects different regions and is essential for cognitive functions such as learning, attention, and memory. It has a distinctive appearance on MRI images, appearing brighter on T1-weighted images and darker on T2-weighted images than gray matter (GM) (Deserno, 2010).

Brain MRI image s a widely used diagnostic tool that provides detailed information about the structure and function of the brain. However, brain MRI images are often affected by intensity inhomogeneity and noise caused by various factors, such as radiofrequency coil used in image acquisition, patient motion, or scanner artifacts. These artifacts can affect the accuracy and reliability of brain image analysis, such as segmentation, registration, or quantification, and can lead to misdiagnosis or inappropriate treatment. Therefore, correction of intensity inhomogeneity and removal of noise are essential preprocessing steps before the segmentation of brain MRI images (Dubey and Mushrif, 2016).

Brain image segmentation plays a crucial role in brain image analysis which extracts brain tissues, white matter (WM), gray matter (GM), and cerebrospinal fluid (CSF) from a brain image by partitioning it into a set of disjoint regions for quantitative brain analysis. Pixels inside each of those regions should be homogeneous in space and intensity (Figure 2.6). Segmentation of normal tissues from brain lesions helps to detect diseases like brain tumor, Alzheimer's disease, Parkinson's disease etc. It also helps in brain disorder identification and whole brain analysis of traumatic injury as well (Dora et al., 2017).

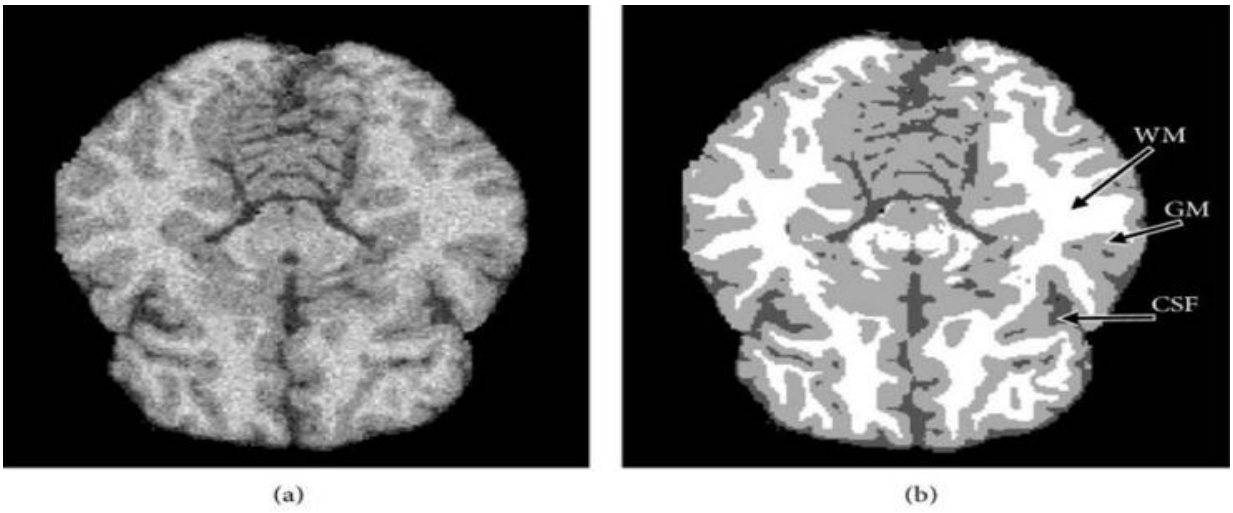

Figure 2.6 – An example of the brain MRI segmentation (Despotović et al., 2015) (a) original image (b) segmented image with three Labels CSF, GM, and WM

2.4.1 MRI image quality limitations

Segmentation of MRI images is a challenging task due to multiple factors that can affect the accuracy and reliability of the segmentation results. These factors include noise, poor contrast, intensity inhomogeneity, and partial volume (Wen et al., 2015).

Noise is one of the primary challenges in MRI image segmentation. MRI images can be affected by various sources of noise, such as scanner hardware, patient and physiological motion, and other factors. The presence of noise in MRI scans is a significant challenge that can make the segmentation difficult to distinguish between different tissues. Moreover, it can lead to inconsistent appearance of tissues in different regions of the image, which can further complicate the task of segmentation.

Intensity inhomogeneity is a major challenge in MRI image segmentation. It refers to the non-uniform distribution of intensities within an MRI image, which can result in the distortion of the image histogram (Yazdani et al., 2015) and the creation of a shading effect. This issue arises due to limitations in the image acquisition process, such as variations in the magnetic field and radiofrequency coil sensitivity, as depicted in Figure 2.7.

There are two primary sources contributing to intensity inhomogeneity. The first source is static field inhomogeneity, bandwidth filtering, and radio frequency transmission and reception inhomogeneity. These factors introduce variations in the magnetic field during image acquisition. These variations can lead to inconsistent intensities across different regions of the image. The second source is related to the characteristics of the imaged object itself, including its magnetic permeability and dielectric properties (Vovk et al., 2007). These properties influence the interaction between the object and the magnetic field, further contributing to intensity variations in the resulting MRI image.

The partial volume is caused by the limited spatial resolution of MRI images. It occurs when a single voxel contains signals from different tissue types. The partial volume effect is especially challenging in MRI brain imaging due to the complex and dynamic nature of the brain, which is characterized by a wide range of tissue properties. The presence of uncertainty in region boundaries can be attributed to the partial volume effect, which leads to a soft segmentation where regions overlap. In contrast, hard segmentation strictly assigns each voxel to a single region, prohibiting simultaneous membership in multiple regions, whether inside or outside (Pham et al., 2000).

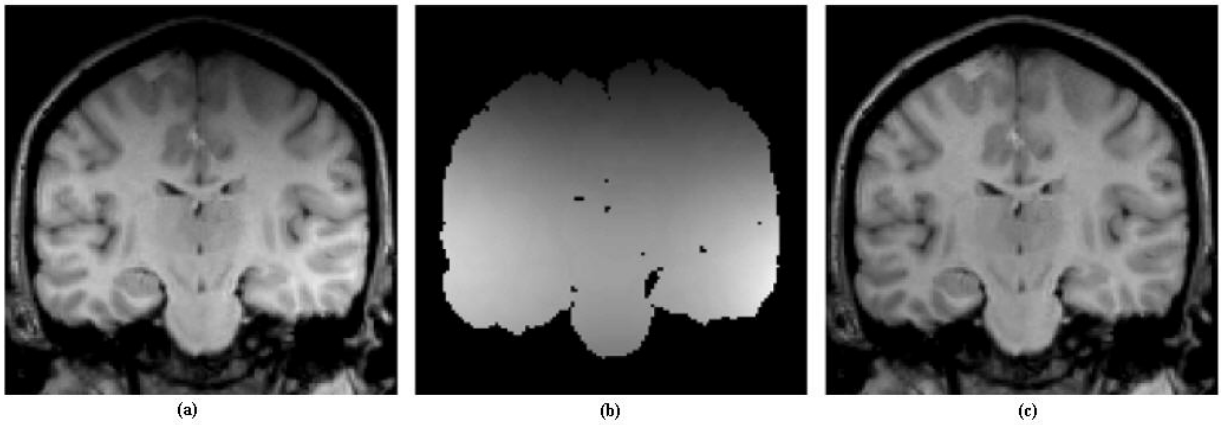

Figure 2.7 – Example of the Intensity inhomogeneity issue in a MRI image (Vovk et al., 2007)
(a) original image (b) Inhomogeneity field (c) The corrected image

2.5 Brain image segmentation approaches

Brain tissue segmentation can be a tedious process due to the highly complicated and overtly sensitive nature of this organ. Moreover, the size and location of the constituent parts may vary from patient to patient. Thus, the use of a simple yet effective segmentation technique can address this issue without further complicating it. Over the years, many popular brain tissue segmentation methods have been proposed in the literature. These methods are applied successfully for disease diagnosis and treatment planning. Nevertheless, in clinical evaluation and neuroscience research, it is considered as a major challenge because medical images suffer from many artifacts such as intensity inhomogeneity (IIH), noise, and abnormal tissues with heterogeneous signal intensities. Further, the performance of brain tissue segmentation methods depends on several factors such as location, size, shape, texture of tissues, and unclear tissue boundary, which are inherent in the modalities used for image acquisition (Fraz et al., 2012).

2.5.1 Thresholding

Thresholding is one of the popular segmentation methods, where the target objects are segmented by comparing their intensity values with one or more thresholds. Thresholding-based methods are of two types, global thresholding, and local (adaptive) thresholding.

Global thresholding is a simple and widely used method that assumes the image has a bimodal histogram, where the intensity values of the object and background pixels are well separated. It assigns intensity values above the threshold to one and below the threshold to zero, respectively. For an image $I(x,\ y)$, a global threshold T segments the image by assigning a value of one to all pixels with intensity values greater than or equal to T, and a value of zero to all pixels with intensity values less than T.

$$S(x,y) = \begin{cases} 1, & \text{if } I(x,y) \geq T \\ 0, & \text{otherwise} \end{cases} \tag{2.2}$$

Where $S(x,y)$ is the thresholded image.

The result of thresholding is a binary image, where pixels with value 1 represent the object and pixels with value 0 represents the background. With the increase in the number of regions, threshold selection becomes a challenging task. It may be noted that brain tissue segmentation requires the segmentation of more than two tissues (i.e., WM, GM, and CSF).

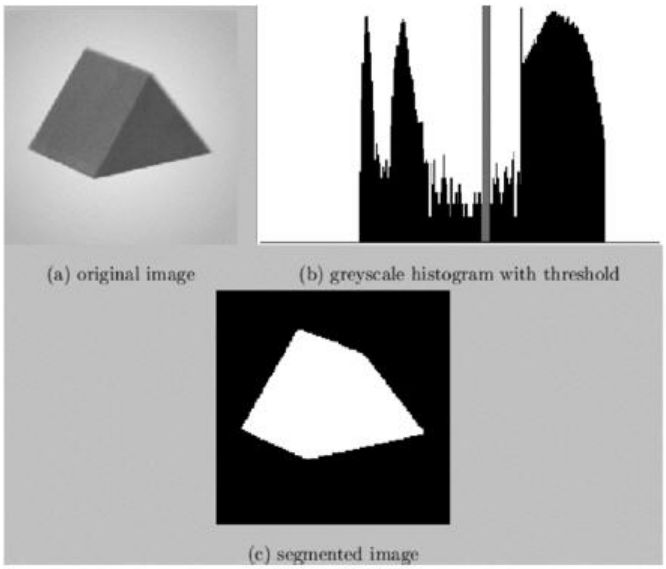

Figure 2.8 – Segmenting a simple image by a single threshold (Rogowska, 2000)

However, in many applications, a global threshold cannot be found from a histogram or a single threshold cannot give good segmentation results over an entire image. This is because the optimal threshold value may vary depending on the characteristics of each

region, such as the intensity distribution and texture. For example, when the background is not constant and the contrast of objects varies across the image, thresholding may work well in one part of the image but may produce unsatisfactory results in other areas.

Local thresholding methods are effective techniques for image segmentation, especially when dealing with images with complex structures and non-uniform intensity. Local thresholds can be determined by examining the image intensities in the neighborhood of each pixel. Prior knowledge or local statistical properties can be used to estimate the threshold values.

For example, Stadlbauer et al. (Stadlbauer et al., 2004) used the Gaussian distribution of pixel intensity levels to determine the threshold value from a T2-weighted MRI. They proposed a method called "adaptive thresholding based on Gaussian mixture modeling" that estimates the threshold value for each pixel based on the local intensity distribution. The method assumes that the intensity values of the image can be modeled as a mixture of Gaussian distributions, where each Gaussian component corresponds to a different tissue type. The threshold value is then estimated as the mean intensity value of the Gaussian component that corresponds to the tissue type of interest. This method was shown to improve the accuracy of brain tissue segmentation compared to other thresholding methods.

Some popular and efficient thresholding-based methods used for brain tissue segmentation of MRI are the entropy method (Kapur et al., 1985), Otsu's method (Otsu, 1979), and evolutionary-based methods (Akay, 2013; Hammouche et al., 2010). Otsu (Otsu, 1979) proposed a popular method that can find thresholds by maximizing the between class variance of intensity levels of the foreground and background. Otsu's method is considered one of the top threshold selection methods for real world images. Nevertheless, the formulation of between class variance is inefficient in the case of multilevel thresholding. As the number of levels grows, the computational time scales exponentially, and its accuracy decreases with each new threshold point (Sezgin and Sankur, 2004). Kapur et al. (Kapur et al., 1985) proposed maximization of entropy, to obtain the optimal threshold values from the histogram. In both methods, computational time increases due to the extensive search strategy with the increase in the number of thresholds (Kittler and Illingworth, 1986). Another thresholding method based on the entropy concept is presented in (Chang et al., 1994). The idea is to find a threshold that minimizes the mismatching between two transition probability distributions resulting from the co-occurrence matrices of an image and thresholded image.

Manikandan et al. (Manikandan et al., 2014) proposed a method for segmenting brain MRI images using a real-coded genetic algorithm with simulated binary crossover to find the optimal threshold values that maximize image entropy. The algorithm starts with a population of candidate solutions, represented as vectors of real numbers, and evaluates their fitness based on the image entropy. The simulated binary crossover operator is used to generate new candidate solutions by combining the information from two parent solutions.

The proposed method was effective in segmenting brain MRI images into multiple tissue types and demonstrates the potential of optimization-based methods for medical image analysis.

Oliva et al. (Oliva et al., 2017) proposed a novel approach for thresholding magnetic resonance (MR) brain images that combines two popular techniques: the Minimum Cross Entropy Thresholding (MCET) criterion and the Crow Search Algorithm (CSA). The MCET criterion has been shown to be effective in identifying the optimal threshold points by minimizing the cross entropy among classes. On the other hand, CSA is an efficient optimization algorithm that mimics the foraging behavior of crows to find the best solution. The proposed approach considers the thresholding process as an optimization problem and uses CSA to search for the optimal threshold points that minimize the cross entropy among classes. CSA generates a set of candidate threshold points that are encoded into a solution at each generation. The objective function evaluates the quality of the proposed solution by measuring the cross entropy. Based on the objective function, CSA generates new candidate solutions using predefined operators to improve the segmentation quality of MR brain images.

Kotte et al. (Kotte et al., 2018) introduced an adaptive wind driven optimization (AWDO) technique using two objective functions including Kapur's maximum entropy thresholding function and Otsu's between-class variance. The adaptive nature of the steps increases the overall performance of the optimization technique. However, due to the lack of spatial information correlation among neighboring pixels, 1D histogram-based methods lag behind in giving accurate segmentation results. Although the authors recognized that 1D histogram-based techniques were not effective in capturing spatial correlation among neighboring pixels. The authors' proposed approach presented better segmentation results compared to other thresholding methods. They suggested that future research could explore more advanced techniques to address these limitations and further improve the segmentation accuracy.

Tarkhaneh and Shen (Tarkhaneh and Shen, 2019) proposed a Differential Evolution (DE) algorithm for optimal multi-level thresholding for MRI brain image segmentation, the proposed algorithm can achieve an optimal balance between exploration and exploitation through a new adaptive approach and new mutation strategies; a new adaptive approach is adopted to generate the optimal solutions by measuring the quality of candidate solutions to evaluate the efficiency of different parts of the proposed algorithm. Moreover, new mutation strategies are adopted to create diversity in the generated solutions to improve global search.

Khairuzzaman and Chaudhury (Khairuzzaman and Chaudhury, 2019) introduced for brain MR image segmentation technique that involves anisotropic diffusion-based filtering, multilevel thresholding through Particle Swarm Optimization (PSO) with Otsu function, and objective image quality evaluation. The first step is to preprocess the MR image using

anisotropic diffusion-based filtering to enhance image quality by mitigating artifacts and noise. Next, multilevel thresholding is executed using PSO to optimize threshold values, facilitated by the Otsu function's histogram-based optimal threshold calculation. The PSO algorithm updates particle positions iteratively, incorporating previous best and global best positions, with termination after a fixed number of iterations. The desired optimum set of thresholds is obtained from the position of the global best particle.

Khorram and Yazdi (Khorram and Yazdi, 2019) presented an optimized thresholding method for MR brain image segmentation, which utilizes the ant colony algorithm. The method consists of five sequential steps. Firstly, the input image is preprocessed to reduce noise and enhance contrast using Gaussian filtering and histogram equalization. Secondly, the image is divided into windows, and each window is assigned a label (WM, GM, CSF) based on the majority pixel class. Thirdly, the optimal threshold values for each window are determined using Ant Colony Optimization (ACO), which involves ant-guided exploration and pheromone deposition. Fourthly, a local search is performed to refine the segmentation by assessing pixel homogeneity and adjusting the labels accordingly. Finally, post-processing is applied to remove any remaining noise and artifacts using morphological operations such as erosion and dilation.

Recently, Panda et al. (Panda et al., 2021) proposed an evolutionary approach to improve optimal multi-level thresholding for brain MR images. The method involved several steps, including preprocessing for noise reduction and contrast enhancement, followed by the construction of a 2D histogram using a normalized local variance method. Initial threshold values were generated uniformly, and fitness evaluation was based on a novel row class entropy measure. The fittest individuals were selected for reproduction through tournament selection, and crossover and mutation operations were applied. Threshold updates were performed using an elitist strategy, and the algorithm terminated based on a maximum iteration criterion. Finally, postprocessing techniques were applied to refine the results, including removing small objects and filling holes in the segmented image.

2.5.2 Region Growing

Region growing, also called region merging, starts with a pixel or a group of pixels (called seeds) that belong to the structure of interest. Seeds can be chosen by an operator, or provided by an automatic seed finding procedure. In the next step neighboring pixels are examined one at a time and added to the growing region, if they are sufficiently similar based on a uniformity test, (also called a homogeneity criterion). The procedure continues until no more pixels can be added. The object is then represented by all pixels that have been accepted during the growing procedure (Rogowska, 2000).

One example of the uniformity test is comparing the difference between the pixel intensity value and the mean intensity value over a region. If the difference is less than a

predefined value, for example, two standard deviations of the intensity across the region, the pixel is included in the region; otherwise, it is defined as an edge pixel. The results of region growing depend strongly on the selection of the homogeneity criterion. If it is not properly chosen, the regions leak out into adjoining areas or merge with regions that do not belong to the object of interest. Another problem of region growing is that different starting points may not grow into identical regions. Moreover, it fails to perform in the segmentation of multiple objects. Region growing has the advantage of considering both visual features and spatial information. It is insensitive to changes in inner parts which result in closed regions. Another advantage is that it generates connected regions (Dora et al., 2017).

Region growing is a commonly practiced technique in brain tissue segmentation. To satisfy homogeneity, it is presumed that the regions of the object of interest have the same or slightly varying intensity values. Therefore, initial seed selection and different homogeneity criteria could alter the segmentation performance. For homogeneous MR images, region growing mostly produce suitable results. Furthermore, it is well suited for medical image segmentation, where images consist of mostly objects and background. A possible measure to ease the problems is combining the region growing method with other methods such as edge detection. Moreover, homogeneity criteria for multiple brain lesions are still to be assessed (Mehnert and Jackway, 1997; Lu et al., 2014).

Pohle and Toennies (Pohle and Toennies, 2001) developed a region growing algorithm that learns its homogeneity criterion automatically from the characteristics of the region to be segmented. The method is based on a model that describes homogeneity and simple shape properties of the region. Parameters of the homogeneity criterion are estimated from sample locations in the region. These locations are selected sequentially in a random walk starting at the seed point, and the homogeneity criterion is updated continuously. This approach was extended to a fully automatic and complete segmentation method by using the pixels with the smallest gradient length in the not yet segmented image region as a seed point.

Pan and Lu (Pan and Lu, 2007) proposed the Dynamic Particle Swarm Optimization and K-means Clustering Algorithm for Image Segmentation, comprising the following steps: Firstly, the input image improves noise reduction and contrast enhancement through preprocessing. Subsequently, K-means clustering is applied to segment the image, grouping similar pixels into clusters. The Particle Swarm Optimization (PSO) algorithm then optimizes threshold values for each cluster; however, PSO's susceptibility to local optima is addressed through the introduction of the Dynamic Particle Swarm Optimization and K-means Clustering Algorithm (DPSOK). DPSOK refines inertia weight and learning factor calculations to achieve equilibrium optimization. Applied to optimize threshold values for each cluster, DPSOK enhances the global search capability and visual quality of K-means clustering in image segmentation.

Ayman et al. (Ayman et al., 2013) presented a new strategy for segmenting brain MRI images with weak boundaries that integrates an evolutionary algorithm, called the Memetic Programming (MP) algorithm, with the Region Growing technique, The MP algorithm generates a new set of automatic threshold functions. These thresholds can be used with the region growing algorithm to perform an efficient segmentation of MRI images.

Zanaty and Asaad (Zanaty and Asaad, 2013) proposed a new region growing algorithm called probabilistic region growing (PRG) in order to improve magnetic resonance image (MRI) segmentation. The proposed approach includes a threshold based on estimating the probability of pixel intensities of a given image. This threshold uses a homogeneity criterion which is obtained automatically from the characteristics of the regions. The homogeneity criterion will be calculated for each pixel as well as the probability of pixel value.

Heydari et al. (Dehdasht-Heydari and Gholami, 2019) proposed an Automatic Seeded Region Growing (ASRG) method for segmenting brain MRI images into different regions based on specific criteria for future processing. The method utilizes a genetic algorithm to automatically select initial points for region growing, aiming to achieve accurate and efficient brain MRI segmentation. The paper explains the steps involved in the proposed method, including the fitness function, chromosome selection, crossover, mutation, and fitness calculation for the next generation. Initially, the method characterizes the initial points for each brain tissue, including white matter, cerebrospinal fluid, and gray matter. Next, a cluster matrix of points from different parts of the image is formed based on the image histogram. The ASRG method employs a genetic algorithm to select initial points for region growing, with steps involving fitness function evaluation, chromosome selection, crossover, mutation, and fitness calculation for the next generation. This approach aims to achieve accurate and efficient brain MRI segmentation by automating the selection of initial points.

2.5.3 Clustering

Clustering is a fundamental technique in unsupervised machine learning that involves the classification of data points or patterns into groups or clusters, such that patterns in the same group are similar to each other while patterns in different groups are dissimilar (Jain et al., 1999). Clustering is widely used in various fields, including image processing, data mining, and pattern recognition. In image processing, clustering is often used for image segmentation, which involves dividing an image into multiple regions or segments based on their visual characteristics. Clustering algorithms can be used to group pixels or image regions with similar color, texture, or intensity values, which can help to identify different objects or regions in the image.

Clustering methods are a type of unsupervised segmentation method used to partition

an image into clusters of pixels or voxels with similar intensities, without using training images (Despotović et al., 2015). Instead, clustering methods use the available image data to train themselves. The segmentation and training are done in parallel by iterating between two steps: data clustering and estimating the properties of each tissue class.

Clustering algorithms are widely used for image segmentation and can be broadly classified into two main categories: hierarchical and partitional (Xu and Tian, 2015). A taxonomy of clustering methods is presented in Figure 2.9. In the following sections, we will discuss each category in more detail and provide examples of commonly used clustering algorithms.

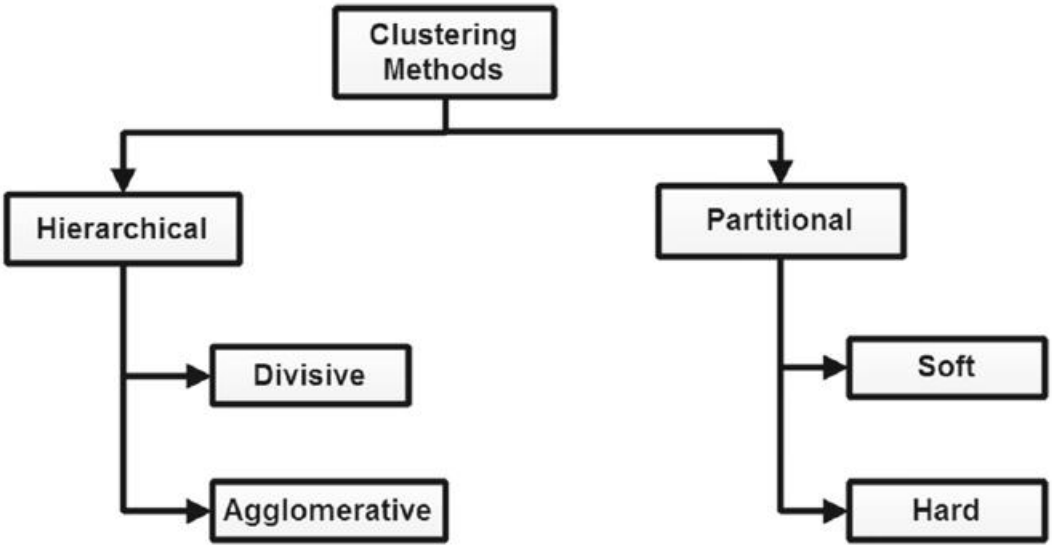

Figure 2.9 – Classification of clustering based image segmentation methods (Xu and Tian, 2015)

.

2.5.3.1 Hierarchical clustering

In the field of clustering algorithms for image segmentation, BIRCH (Balanced Iterative Reducing and Clustering using Hierarchies) (Zhang et al., 1996) is a popular agglomerative approach that is generally used for very large datasets. The BIRCH algorithm constructs a clustering feature tree to discover clusters, but it can only produce spherical and convex shape clusters. Another popular agglomerative approach is CURE (clustering using representatives) (Guha et al., 1998), which utilizes a random sampling approach to cluster all the data items, which are further combined to create the final clusters.

Hierarchical clustering methods are widely used for image segmentation, but they have some limitations. For example, they employ a greedy approach and do not reconsider a data item again after it has been assigned to a cluster, which can result in misclassified data items. They also do not optimize an objective function while forming clusters, and can

perform poorly in the presence of noise and outliers. Additionally, they require knowledge about the number of clusters, and the formation of spherical clusters and the reversal of the hierarchical structure can be distorted. Time complexity is also a major issue when clustering high-dimensional data through a hierarchical approach (Mittal et al., 2021).

2.5.3.2 Partitional clustering

Partitional clustering is a widely used approach for image segmentation that uses the notion of similarity as the measurement parameter. Generally, partitional clustering groups the data points into clusters according to some objective function, with the general notion of the objective function being the minimization of the within-cluster similarity criteria, which is usually computed using Euclidean distance. The objective function represents the goodness of each formed cluster and returns the best representation from the produced clusters. However, partitional clustering methods need to specify the number of clusters to be generated, which can be a challenge in some cases. Partitional clustering methods have some limitations, as they can sometimes assign data items to a cluster even if they are quite far from the respective cluster centroid. This can result in distortion of the cluster shapes or false results, especially in the case of noise or outliers (Mittal et al., 2021). Partitional clustering methods are categorized into soft and hard clustering methods, which are presented in the following subsections.

Soft segmentations are a type of segmentation that allow regions or classes to overlap. In medical imaging, soft segmentations are particularly important due to partial volume effects, where multiple tissues contribute to a single pixel or voxel, resulting in a blurring of intensity across boundaries. Figure 2.10 illustrates how the sampling process can result in partial volume effects, leading to ambiguities in structural definitions. In Figure 2.10 (b), it can be difficult to precisely determine the boundaries of the two objects. A hard segmentation method forces a decision of whether a pixel is inside or outside the object, which can lead to loss of information. Soft segmentation methods, on the other hand, retain more information from the original image by allowing for uncertainty in the location of object boundaries. This is particularly important in medical imaging, where partial volume effects can result in blurred intensity across boundaries.

Pixel classification methods utilize the notion of soft segmentation, which stems from the generalization of a set characteristic function. A characteristic function is simply an indicator function of whether a pixel is inside or outside its corresponding set. For a location $j \in I$, the characteristic function $X_i(j)$ of the region R_i is defined to be 1 if j is inside the region R_i, and 0 otherwise. This allows for a more flexible approach to segmentation, where pixels can have partial membership to multiple regions, rather than

being strictly assigned to a single region.

$$X_i(j) = \begin{cases} 1, & \text{if } j \in R_i \\ 0, & \text{otherwise} \end{cases} \tag{2.3}$$

Characteristic functions can be generalized to *membership functions* (Pham et al., 2000), which need not be binary-valued. The value of a membership function can be interpreted as the contribution of class i to location j. Thus, wherever membership values are greater than zero for two or more classes, those classes are overlapping. Conversely, if the membership function is unity for some value of j and i, then the class is the only contributing class at location j. Soft segmentations based on membership functions can be easily converted to hard segmentations by assigning a pixel to its class with the highest membership value.

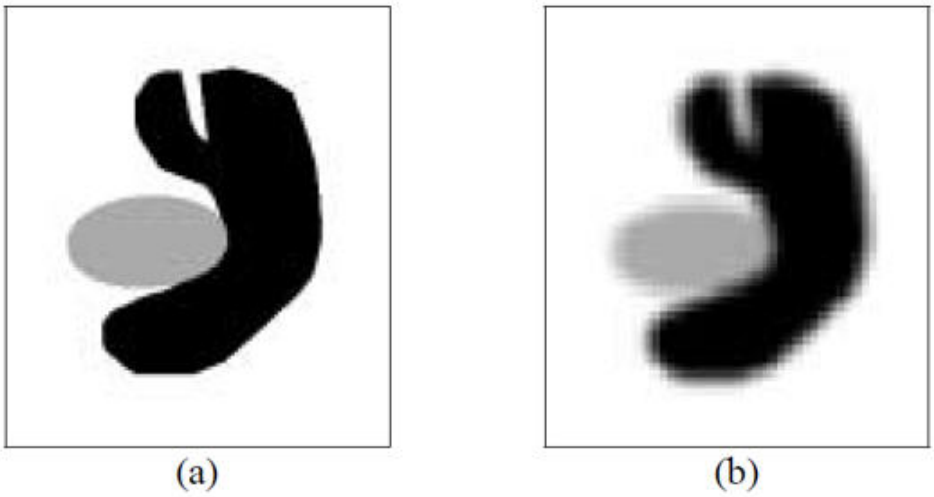

Figure 2.10 – Illustration of partial volume effect (Pham et al., 2000)
(a) Ideal image, (b) acquired image

a)- **Hard clustering methods**

Hard clustering methods iteratively partition the data into disjoint clusters according to an objective function. Typically, the objective function is the sum of the squared Euclidean distance between data and the associated centroid, which is to be minimized. In these methods, the center of the clustered data is considered as the centroid of the clusters. Unlike soft clustering, hard clustering assigns data to a single cluster only, meaning that each data point will have a membership function (degree of belongingness) of either 0 or 1. Hard clustering is a relatively simple and scalable approach with high computational efficiency. It is particularly effective for datasets that have a spherical shape and are well-separated. However, this approach suffers from several drawbacks. For example, the formed

cluster centroids may be relatively poor cluster descriptors, and the method is sensitive to initial parameter settings. Additionally, hard clustering requires prior knowledge about the number of clusters to be formed, which may not always be available or accurate.

- Kmeans clustering algorithm

The K-means clustering algorithm is a popular method for partitioning data into clusters. In this method, the cluster centroid is updated by taking the mean of all the data items assigned to the corresponding cluster. This process is iteratively continued until some defined convergence criterion is met. Although this category of methods has merits such as relatively low time complexity, simplicity, and guaranteed convergence. Generally, this category includes all the methods that are inspired by the K-means method, which is the simplest partitional clustering method.

K-means is a widely used clustering algorithm that aims to group samples into different clusters based on their distance. The core idea of K-means is to iteratively update the center of each cluster, which is represented by the center of the data points assigned to that cluster. This iterative process continues until some criteria for convergence is met.

K-means algorithm partitions a set of data points, $X = \{x_1, x_2, \ldots, x_N\}$, into K clusters based on a similarity criterion, which is usually the sum of squared error defined in Eq.(2.4). Each cluster is represented by its centroid m_i, which is collectively represented as $M = (m_1, m_2, \ldots, m_k)$ for the corresponding clusters $C = \{C_1, C_2, \ldots, C_k\}$. This method iteratively minimizes the criterion function J by updating the formed clusters C and the corresponding centroids M as given by Eq. (2.5) and Eq. (2.6).

$$J = \sum_{i=1}^{K} \sum_{x_j \in C_i} \|x_j - m_i\|^2 \tag{2.4}$$

$$x_j \in C_l \text{ if } \|x_j - m_l\| < \|x_j - m_i\| \tag{2.5}$$

$$m_i = \frac{\sum_{x_j \in C_i} x_j}{|C_i|} \tag{2.6}$$

for j=1,..., n and i=1,..., K

The K-means clustering algorithm clusters data by iteratively computing the mean intensity for each cluster using Eq. (2.6) and then segmenting the image by classifying each pixel into the cluster with the closest mean using Eq. (2.5).

Lai et al. (Lai et al., 2009) proposed a novel and efficient K-means clustering algorithm specifically designed for brain MRI image segmentation. This method introduces a unique approach that leverages center displacements to accelerate the clustering process and improve segmentation accuracy. The algorithm initiates by randomly selecting data points as initial cluster centers and classifies them into static and active groups based on their movement in the previous iteration. An efficient nearest neighbor search technique is employed to assign data points to the nearest cluster centers from both groups. The

algorithm updates the cluster centers by computing the mean of the assigned data points and evaluates the displacement of each center by comparing its current position with the previous iteration. Moreover, the method incorporates a mechanism to reject unlikely candidates during the partition step, further enhancing efficiency. By iteratively repeating these steps until the cluster centers converge,

Isa et al. (Isa et al., 2009) proposed an adaptive fuzzy moving K-means clustering algorithm to overcome the center redundancy, dead centers, and trapped center at local minima problems. Siddiqui and Isa (Siddiqui and Mat Isa, 2012) introduced an optimized K-means (OKM) algorithm that can homogenously segment an image into regions of interest with the capability of avoiding the dead center and trapped center at local minima phenomena.

Krishna and Narasimha (Krishna and Murty, 1999) proposed the Genetic K-Means Algorithm (GKA) as an efficient iterative clustering approach for partitioning data into clusters. Initially, the algorithm randomly generates a population of candidate solutions, each representing a potential cluster partition with user-defined K centroids. Fitness evaluation employs the K-Means Operator (KMO), which measures the negative sum of squared distances between data points and their assigned centroids. The algorithm selects the best solutions based on fitness using stochastic methods like roulette wheel or tournament selection. Subsequently, crossover replaces traditional genetic crossover with the K-means operator, and mutation introduces diversity through distance-based perturbations of cluster centroids. The iterative process continues until a termination condition, such as convergence or reaching the maximum iterations, is met, providing a globally optimal data partition into clusters.

A new image segmentation algorithm called Dynamic Particle Swarm Optimization and K-means Clustering Algorithm (DPSOK) is presented (Li et al., 2015) to improve effectively the global search capability of K-means clustering.

Pei et al. (Jialun et al., 2017) proposed a Brain Image Segmentation Method Based on an Adaptive Clustering Algorithm, which addresses the challenge of accurately segmenting brain images. The method involves three main steps to achieve this goal. Firstly, it corrects the bias field in the input images using the non-parametric N3 algorithm, effectively reducing noise and intensity inhomogeneity. By doing so, the quality of the input images is improved, laying the foundation for more accurate segmentation. Next, the method improves the initial clustering center selection in the k-means algorithm through an adaptive clustering approach that utilizes hierarchical clustering and dendrogram analysis. This enhancement aims to enhance the overall accuracy and stability of the segmentation results, making the algorithm more robust and reliable. Lastly, the proposed method employs evaluation criteria, Peak Signal to Noise Ratio, and Jaccard Similarity index, to determine the appropriate number of clusters (K) in the k-means algorithm. This step ensures that the segmentation achieves the optimal granularity, striking a balance between precision

and computational efficiency.

Mehidi et al. (Mehidi et al., 2020) presented an enhanced K-means clustering algorithm to achieve accurate brain MRI segmentation. They start by applying a median filter for preprocessing, effectively eliminating noise and enhancing image quality. After that, they utilize Histogram-based clustering, which separates pixels based on intensity values, identifying distinct regions within the MRI. Subsequently, the authors employ K-means clustering to further refine the segmentation of the brain into different tissues. Finally, they conclude with Postprocessing, wherein small isolated regions are removed, and any holes in the segmented image are filled, resulting in a more precise and reliable segmentation result.

Atek et al. (Atek et al., 2022) proposed a modified version of the traditional K-means algorithm (HKM), designed to improve segmentation performance while addressing computational complexity. Unlike the conventional K-means that calculates distances between each pixel and cluster centers directly, HKM utilizes image histogram information to derive these distances, resulting in significant computational efficiency. The algorithm's workflow begins with preprocessing the MRI image through a median filter to enhance contrast and remove noise. Next, the histogram of the preprocessed image is computed to understand its intensity distribution. K cluster centers are initialized based on the K highest peaks in the histogram. Each pixel in the image is then assigned to the nearest cluster center, employing histogram-based distance calculations. Subsequently, the cluster centers are iteratively recalculated as the mean of pixel intensities assigned to each cluster until convergence is achieved. Postprocessing is applied to refine the segmented image by removing small isolated regions and filling gaps between regions.

b)- **Soft clustering methods**

- **FCM algorithm**

Soft clustering methods provide an alternative to traditional crisp clustering methods and are classified into two main categories: fuzzy c-means (FCM) and mixture models. In soft clustering, the division of pixels is gradual, meaning that a membership function (based on FCM) or an underlying probability (based on mixture models) is used to define whether a pixel belongs to a cluster or not. FCM-based methods use a membership function to define the degree to which a pixel belongs to a cluster by assigning it a membership grade value. Mixture models assume some distributional form for the underlying probability of the data to cluster into different groups.

FCM is a widely used and popular method in soft clustering approaches (Höppner et al., 1999). It can be regarded as a generalization of ISODATA (Davé and Krishnapuram, 1997) and was first introduced by Bezdek (Bezdek, 1973). FCM attempts to find a fuzzy partition (fuzzy clusters) for a set of data points x_j, $j = 1, \ldots, N$, by minimizing the

following objective function.

$$J(U,V) = \sum_{i=1}^{C}\sum_{j=1}^{N} u_{ij}^{m}\|x_j - v_i\|^2 \tag{2.7}$$

In FCM, the fuzzy partition matrix U and the cluster centers V are used to represent the membership grades of each pixel to each cluster and the centroid values of each cluster, respectively. The objective function is minimized by iteratively updating U and V until convergence is reached. The term $\|x_j - v_i\|^2$ represents the square of the Euclidean distance between the intensity value of the pixel x_j and the centroid value $v_i \in (v_1, v_2, \ldots, v_C)$ of the i-th cluster, where C is the number of clusters. The fuzzy membership u_{ij} of the j-th pixel with respect to the i-th cluster is defined such that the constraint $\sum_{i=1}^{C} u_{ij}$ holds, and the weighting exponent $m \in [1, \infty]$ is a parameter that controls the degree of fuzziness of the obtained classification, which is typically set to 2.

The minimization of the objective function is achieved by an iterative process, in which updating the degree of membership u_{ij} and the cluster centers v_i are done according to the following equations:

$$u_{ij} = \frac{1}{\sum_{k=1}^{C}\left(\frac{\|x_j - v_i\|}{\|x_j - v_k\|}\right)^{\frac{2}{m-1}}} \tag{2.8}$$

$$v_i = \frac{\sum_{j=1}^{N} u_{ij}^{m} \cdot x_j}{\sum_{j=1}^{N} u_{ij}^{m}} \tag{2.9}$$

The FCM clustering process continues until either a specified maximum number of iterations has been reached or convergence has been achieved. Convergence is detected when the change in membership functions for all cluster centers over all pixels is less than the specified tolerance value between two successive iterations. The pseudo-code for FCM is presented in Algorithm 1.

Algorithm 1 FCM Algorithm

Input : The cluster number C and the cluster centers v_i $(i = 1, 2, \ldots, C)$
Output: Cluster centers v_i $(i = 1, 2, \ldots, C)$, and fuzzy partition matrix

Step *1*- *Calculate the membership values and update cluster centers*

Step *2*- *Calculate the membership values using Eq. (2.8)*

Step *3*- *Update cluster centers according to Eq. (2.9)*

Step *4*- *Repeat steps 2 and 3 until there is no change for each cluster*

The FCM algorithm has several limitations, including its sensitivity to local optimal solutions, the need for cluster center initialization, and the requirement to specify the cluster number in advance. Although it can achieve relatively high clustering accuracy and generate approximate solutions quickly by using the probability of belonging, it does not consider spatial information in the image space. As a result, it is highly sensitive to imaging

artifacts and noise, and unable to effectively compensate for intensity inhomogeneities. These problems significantly reduce the efficacy of the FCM method for noisy images and artifacts. While FCM is less sensitive to initialization compared to other techniques, in terms of both speed and stability.(Yazdani et al., 2015).

To overcome the challenges of FCM, researchers have proposed several methods. One such method is the adaptive FCM technique developed by Pham et al. (Pham and Prince, 1999). This method uses a multiplier field to account for the inhomogeneity and includes first and second-order regularization terms in the objective function to ensure the multiplier field varies smoothly and slowly. By addressing these issues, this method provides more accurate and reliable segmentation of MRI images, enabling medical professionals to diagnose and treat brain-related conditions more effectively.

Sikka et al. (Sikka et al., 2009) proposed a Modified Fuzzy C-Mean (MFCM) algorithm for brain MR image segmentation, aiming to achieve enhanced accuracy and automation in the process. The algorithm comprises several key steps to accomplish this goal. It starts with a preprocessing phase, where automatic bias removal and contrast enhancement techniques are applied, followed by the automated retrieval of mean intensity positions for various detected brain tissues. Subsequently, the corrected image is subjected to the MFCM Clustering, utilizing the proposed method's centers as initial input. This approach reduces the number of iterations and significantly improves the quality of the segmentation results. Finally, the algorithm employs a novel postprocessing technique called Neighborhood-Based Membership Ambiguity Correction (NMAC), which incorporates spatial information to smooth tissue class boundaries and eliminate pixel-level noise from the segmented results.

Ji et al. (Ji et al., 2010) proposed a new energy minimization method based on coherent local intensity clustering (CLIC), the proposed approach combines both the local and global intensity information to ensure the smoothness of the derived optimal bias field and improve the accuracy of the segmentations, however, the proposed method has a poor anti-noise ability, for it doesn't consider non-local spatial constraint, for that, (Shi et al., 2013) use the coherent local and non-local spatial constraints. The coherent local information ensures the smoothness of the bias field estimation and the non-local spatial information reduces the noise effect during the segmentation.

Agarwal et al. (Agarwal et al., 2015) proposed a novel method for precise brain tissue segmentation into gray matter, white matter, and cerebrospinal fluid. The process starts with acquiring detailed brain MRI images using magnetic resonance imaging (MRI). To rectify any distortions in the images, a bias-field correction step is performed. Next, the fuzzy c-means (FCM) algorithm is used to categorize tissue types based on pixel intensity. Finally, a level set approach is employed to refine the boundaries between different tissue types using partial differential equations. This approach enhances the accuracy of the segmentation process and provides more precise results.

Many researchers have used evolutionary algorithms like particle swarm optimization to initialize automatically cluster centers in the FCM. For instance, Benaichouche et al. (Benaichouche et al., 2013) used particle swarm optimization to initialize cluster centers in FCM and obtained a global optimum solution. In addition, it uses spatial information and Mahalanobis distance for making the method efficient against noise and misclustering. In order to automatically elicit the proper number and location of cluster centers and the number of pixels in each, a genetic algorithm is integrated along with FCM for Segmentation of MRI Brain Images algorithm (Jansi and Subashini, 2014; Nie et al., 2007).

Mekhmoukh and Mokrani (Mekhmoukh and Mokrani, 2015) proposed a novel approach to MR brain image segmentation, employing Improved Fuzzy C-Means based Particle Swarm Optimization (PSO) initialization and outlier rejection with level set methods. The method involves three main steps: Firstly, MR brain images were preprocessed to remove non-brain tissues, and then Fuzzy C-Means (FCM) algorithm, Kernelized Fuzzy C-Means (KPCM), and Improved KPCM (IKPCM) were utilized to extract brain MR tissues (WM, GM, and CSF). Secondly, in the PSO Initialization step, the authors employed Particle Swarm Optimization (PSO) to optimize the parameters of the FCM algorithm. It was used to find optimal values for the membership function and cluster centers, improving the performance of the FCM algorithm. Lastly, the authors detected and removed outliers using a level set method, a numerical technique for tracking interface evolution in images. A modified level set method combining the Chan-Vese model and the local binary fitting model was used to detect and eliminate outliers in the segmentation process.

Tripathi and Bag (Tripathi and Bag, 2020) introduced a novel approach for segmenting brain MRI images, which utilizes local spatial information to effectively handle noise and inhomogeneity artifacts during the segmentation process. The proposed method incorporates a unique local influence factor that regulates the impact of neighboring pixels, allowing for the adaptive determination of neighboring pixel weights to maximize the use of local information. To effectively separate complex brain MRI data, the authors have also integrated kernel-induced distance into their clustering process.

Papachary et al. (Papachary et al., 2021) proposed a hybrid clustering algorithm aimed at effectively segmenting tissues in MR brain images. The algorithm comprises two main steps. In the first step, a median filter is applied on the input MR brain image to remove noise. The denoised image is then transformed into a data vector, where each element represents the intensity value of a pixel. Subsequently, k-means clustering is applied to partition the data vector into multiple clusters, thereby segmenting the image into different tissue regions. To enhance the segmentation accuracy further, the algorithm proceeds to the second step, where a FCM algorithm is employed which assigns each pixel in the image to a cluster with a degree of membership, adding flexibility and robustness to the segmentation process. Finally, the algorithm estimates the tissue image area using typography and digital imaging units by analyzing the number of white pixels in the segmented output.

- **Mixture models**

In brain image segmentation, the three primary tissue classes that are typically considered are gray matter, white matter, and cerebrospinal fluid. To classify each pixel in an image, a set of features is evaluated, such as the pixel's intensity, and used to create a pattern. These patterns are then used to calculate the belonging probability of each pixel to each class through the use of a probability density function (PDF). The parameters of the PDF can be estimated through both parametric and nonparametric approaches. Nonparametric approaches do not assume a specific distribution form or a predetermined number of clusters, whereas parametric approaches assume a known probability density function (PDF) function such as Gaussian distributions. The Gaussian mixture model (GMM) is a popular statistical model in parametric approaches for brain image segmentation. GMM estimates the intensities of pixels (or voxels) in a region by a Gaussian distribution. To estimate the parameters of GMM, the expectation maximization (EM) algorithm is commonly used. The EM algorithm is a statistical approach that performs the estimation (E) step followed by a maximization (M) step in an iterative manner. The information obtained from the M step is then utilized for the next E step, and the process continues until convergence. However, the use of the EM algorithm to estimate the GMM parameters suffers from the lack of spatial constraint and uncertainty in segmentation (Dora et al., 2017).

In order to improve the robustness of the Gaussian mixture model (GMM) against the complex spatial layout of the tissues, Greenspan et al. (Greenspan et al., 2006) proposed a Constrained Gaussian Mixture Model (CGMM). In the CGMM, each tissue is represented by a large number of Gaussians to capture the complex spatial layout of the tissues. The EM algorithm is used to learn the parameters of the proposed model.

Dong and Peng (Dong and Peng, 2014) proposed a novel approach for accurate brain MR image segmentation with simultaneous bias correction. The method addresses the challenges posed by intensity inhomogeneity often present in MR images, which can negatively impact the accuracy of segmentation algorithms. The approach defines an energy functional with two main components: a local data fitting term based on local Gaussian mixture model (LGMM) to model tissue distributions and a nonlocal spatial regularization term to preserve fine structures and reduce noise influence. Notably, the method simultaneously corrects intensity bias by embedding the bias field function additively into the energy functional.

Bian (Bian, 2022) proposed a novel method for automating the classification of T1-weighted Magnetic Resonance brain scans into the cerebrospinal fluid, gray matter, and white matter consisting of several key steps. Firstly, the pipeline is initialized with a "simple" input generated by Kmeans and tissue prior probability hypothesis. Then, in the expectation step (E-step), the algorithm calculates the posterior probability of each voxel belonging to each tissue class based on the current Gaussian Mixture Model (GMM)

parameters. The method incorporates an entropy-weighted spatial term that combines a posterior term for global constraint characterization and a prior term for local characterization, effectively integrating neighborhood classification results and image spatial resolution. Subsequently, the maximization step (M-step) updates the GMM parameters based on the current posterior probabilities. The E-step and M-step are iteratively repeated until convergence is achieved. Finally, the output of the algorithm is a tissue segmentation map that assigns each voxel to one of the three tissue classes (cerebrospinal fluid, gray matter, or white matter).

— **The Markov random field (MRF)**

Mixture models have a limitation in brain MRI segmentation as they do not incorporate contextual information. To overcome this limitation, researchers have explored the use of Markov Random Fields (MRF), which belong to the category of random field methods. MRF provides a statistical model that considers the relationships between neighboring voxels during segmentation. In MRF, the probability of a label at a given voxel is calculated based on both the voxel intensities and the labels present in its local neighborhood. MRFs have been shown to improve the accuracy of brain MRI segmentation by incorporating contextual information and capturing spatial dependencies. The resulting segmentation becomes smoother as the model accounts for the conditional probability of each voxel based on its neighborhood. Figure 2.11 in (Van Leemput et al., 1999) demonstrates the differences between the segmentation with and without MRF. By using MRF for brain MRI segmentation, the resulting segmentation becomes smoother as the model accounts for the conditional probability of each voxel based on its neighborhood.

MRFs have been shown to offer several benefits for MRI segmentation. They capture important features specific to MRIs, including neighborhood correlations, nonparametric distributions of tissue intensities, and signal inhomogeneities. However, it is important to strike a balance in the MRF model by limiting the number of neighbors considered, especially in brain structures with complex edges. This helps ensure that the segmentation technique remains effective and avoids excessive influence from distant voxels (Held et al., 1997).

Zhang et al. (Zhang et al., 2001) introduced a novel hidden Markov random field (HMRF) model for brain image segmentation. The proposed method comprises several steps. Firstly, the image initializes by assigning each voxel to a specific tissue class, such as gray matter, white matter, or cerebrospinal fluid, based on its intensity value. Next, the HMRF model is employed to capture spatial information and enforce smoothness constraints during segmentation. This model establishes a joint probability distribution among neighboring voxel class labels. The EM algorithm within the HMRF model iteratively estimates parameters and updates voxel class labels. It involves the E-step for label updates, the M-step for parameter estimation, and bias field correction through maximum a posteriori estimation. Finally, the resulting segmentation assigns each voxel to the tissue class

with the highest probability. The postprocessing step refines the segmentation by removing small isolated regions and filling gaps between regions, resulting in an improved final segmentation.

MRFs offer the advantage of being less sensitive to noise compared to other classifiers and clustering techniques. This is primarily due to their ability to incorporate contextual information during the segmentation process. By considering the relationships among neighboring voxels, MRFs can effectively smooth out noisy or inconsistent intensity values, leading to more reliable segmentation results. Another advantageous characteristic of MRFs is their isotropic behavior, which enables the model to capture dependencies and correlations between voxels consistently. This isotropy contributes to the overall accuracy of the segmentation by ensuring an unbiased and comprehensive consideration of spatial relationships.

MRFs can suffer from computational intensity, which can hinder their practical use. Additionally, random field methods require a careful selection of parameters that control the strength of spatial interaction and define the energy function. However, determining these parameters can be challenging in practice. If the parameter controlling spatial interaction is set too high, the resulting segmentation output may overly smooth the image, causing the loss of important structural details. Therefore, it is important to strike a balance in the MRF model by limiting the number of neighbors considered, especially in brain structures with complex edges. This helps ensure that the segmentation technique remains effective and avoids excessive influence from distant voxels (Held et al., 1997).

Rajapakse et al. (Rajapakse et al., 1997) proposed a statistical approach for segmenting cerebral MR images using a finite Gaussian mixture for brain MRI segmentation. The method incorporates a smoothness segmentation based on a Markov random field to make the Gaussian mixture model more robust against noise. The iterative conditional modes (ICM) algorithm is employed to find a suboptimal segmentation while estimating model parameters, and simulated annealing (SA) is utilized to find the optimal segmentation. The approach proves to be effective in achieving accurate segmentation results for medical imaging and brain analysis.

Tohka et al. (Tohka et al., 2010) proposed a new method for tissue classification in brain MRI based on local Markov random fields (MRF). The method involves dividing the image into local brain regions with different intensity statistics using sub-volume probabilistic atlases. The parameters for the local intensity models are obtained without supervision by maximizing the weighted likelihood of a certain finite mixture model using a novel genetic algorithm. These local models for tissue intensities and MRF priors are then combined into a global probabilistic image model, resulting in an inhomogeneous MRF. The proposed method demonstrates improved tissue classification accuracy when the basic tissue characteristics vary across the brain, and the noise level of the images is reasonable. The inhomogeneous MRF is solved using standard algorithms like iterative conditional

modes, allowing the model to effectively capture spatial dependencies and interactions between different brain regions.

Ahmadvand and Daliri (Ahmadvand and Daliri, 2015) proposed a novel approach to accelerate MRI brain segmentation by combining clustering methods and Markov Random Fields (MRF). Their method introduces two preprocessing steps to reduce the computational time of MRF while maintaining segmentation accuracy. The first step involves clustering using Fuzzy C-Means (FCM) or Genetic Algorithm-Gaussian Mixture Model (GA-GMM) for initial segmentation and parameter estimation. The second step selects a subset of pixels based on intensity values. Finally, MRF is applied for post-processing and smoothness of segments, using a smaller subset of pixels to speed up convergence.

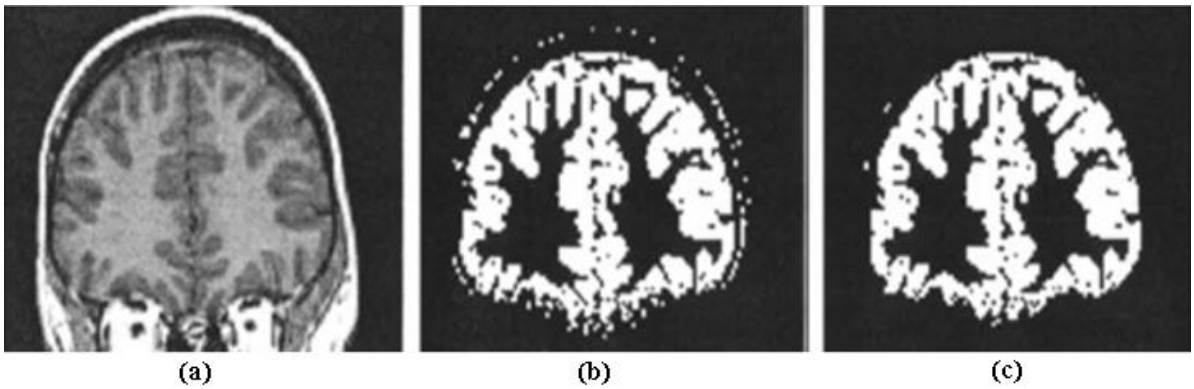

Figure 2.11 – The segmentation of GM with and without MRF (Van Leemput et al., 1999). (a) original image, (b) segmentation without MRF (c) segmentation with MRF

Abhirup and Pradipta (Banerjee and Maji, 2016) introduced a novel approach for brain MRI segmentation, which combines rough-probabilistic clustering with the hidden Markov random field (HMRF) model. The main objective of this approach is to improve the intensity distribution model of the image. To achieve this, they introduced a new probability distribution called stomped normal (SN) distribution, which demonstrated superior performance in representing image classes compared to the Gaussian distribution. Additionally, rough sets were employed to handle uncertainty, vagueness, and incompleteness in the class definition, allowing for efficient treatment of overlapping classes. Furthermore, the HMRF model was incorporated into the approach to capture spatial dependencies between neighboring pixels.

2.5.4 Atlas-based Segmentation Methods

Atlas-based Segmentation Methods are a powerful tool for medical image segmentation when a standard atlas or template is available. The atlas is generated by compiling information on the anatomy that requires segmenting. This atlas is then used as a reference

frame for segmenting new images. Conceptually, atlas-based segmentation approaches are similar to classifiers except they are implemented in the spatial domain of the image rather than in a feature space. The main advantages of this approach are to lend a hand to radiologists in the discovery and identification of diseases, provide a lot of detail, can easily be applied in computer-aided diagnosis to analyze the shape and morphological differences between image regions, and they have the ability to segment the image with no well-defined relation between image pixels and regions (Yazdani et al., 2015).

The standard atlas-based Segmentation Methods consider segmentation as a registration problem. The first step is to identify a one-to-one transformation that maps a pre-segmented atlas image to the target image that requires segmentation. This process is commonly known as atlas warping. While linear transformations can be used for warping, a combination of linear and non-linear transformations is often used due to anatomical variability. Brain warping or registration methods aim to find a transformation that aligns two MRI images voxel-to-voxel, allowing for the definition of variation among the population with fewer parameters. Furthermore, digitized brain atlases can be utilized to modify the description and localization of structures in brain images derived from various subjects and modalities. This allows for correlations between modalities and individuals, and enables precise anatomical measurements within a specific framework by mapping the template to the target brain image. In medical image registration, transformations can be categorized into rigid and non-rigid transformations. However, it is clear that the human body does not conform to an affine or rigid transformation. As a result, most current registration methods involve non-rigid transformation. After a successful non-rigid registration, the segmentation process becomes easier and more efficient between a patient and an atlas (Pham et al., 2000).

Although, atlas-based segmentation provides accurate segmentation results and is generally robust to certain anomalies, however, their dependability on population-specific atlases might limit their applicability to the dataset that is not well represented by the atlas. Due to this, it becomes difficult to segment brain tissue/region types accurately. Moreover, atlas-based segmentation is suboptimal if the patient population in the dataset is considerably different from the atlas model. In this case, these approaches will fail or give inaccurate results due to variability in brain morphology among patients. To overcome these limitations, pattern recognition approaches were proposed that use spatial, intensity, or other information in atlas space as features for the segmentation of different regions (Ramzan et al., 2020). An aligned atlas can be also used as a good initial estimate of the segmentation, which is especially important for an EM algorithm that is guaranteed to converge to local, not global, maxima. In addition, the EM algorithm uses the atlas to constrain the segmentation process where again the correct alignment of the atlas is crucial for successful and accurate segmentation (Despotović et al., 2015).

Aljabar et al. (Aljabar et al., 2009) proposed a multi-atlas based segmentation method

for brain MRI images. The approach involves using a database of pre-segmented images (atlases) to segment a new image, aiming to improve segmentation accuracy by combining information from multiple atlases. To achieve better results, they suggest selecting a custom subset of atlases that are most similar to a given query image. The selected atlases are then combined using a weighted voting scheme to enhance segmentation accuracy by reducing errors associated with individual atlas propagation. To ensure precise alignment of selected atlases with the query image, the authors employed a hierarchical coarse-to-fine registration approach.

Lötjönen et al. (Lötjönen et al., 2010) proposed a pipeline for fast and robust multi-atlas segmentation of brain magnetic resonance images. The process began with preprocessing, where MRI images were preprocessed to remove noise, artifacts, and correct intensity inhomogeneities. Next, a subset of relevant atlases was selected from a larger atlas database based on similarity measures between the target image and the atlases. The selected atlases were then non-rigidly registered to the target image using advanced registration techniques, with different similarity measures used to assess registration quality. After registration, the registered atlases were fused together to generate a segmentation of the target image. Various label fusion methods were evaluated to determine the most effective approach. Lastly, postprocessing was applied to the segmentation, involving the removal of small isolated regions and ensuring topological correctness.

2.5.5 Level set method

Level set method was initially introduced to handle topological changes during curve evolution and has been widely used in the field of image processing, particularly in image segmentation (Osher and Sethian, 1988). The main idea of the level set method is to represent curves or surfaces implicitly as the zero level set of a higher dimensional level set function. This technique not only provides more accurate numerical implementations but also handles topological changes very easily.

The level set method is relatively simple and displays a great advantage in solving problems such as corner point producing, curve breaking, and combining, due to its stability and irrelevancy with topology. However, it updates all the level sets, not just the zero level set, which can result in unbearable computing time and low computational efficiency.

Malladi et al. (Malladi et al., 1993) incorporated gradient information as a stop criterion in their model. The speed definition in their model is intuitive: when the contour approaches the structure boundary, the increase of gradient magnitude decreases the speed value, which slows down the contour. However, this model suffered from leakage due to its dependence solely on the gradient magnitude. As a result, the model can only segment objects with edges defined by gradient, and it is sensitive to noise. The Mumford-Shah model (Mumford and Shah, 1989) was one of the first region-based methods that approximated

the image using a smooth function inside the regions and not just at their boundaries. Several variants of this model have been proposed later (Li et al., 2011; Chan and Vese, 2001). Chan and Vese's model (Chan and Vese, 2001) proposed a new energy functional derived from the Mumford-Shah energy model. The advantages of Chan-Vese's model are that it can detect objects with boundaries that are not necessarily defined by gradient or with very smooth boundaries. Additionally, it can provide a boundary of discrete points, which is crucial for medical image applications when the segmentation result needs to be interpreted by a physician.

Baillard and Barillot (Baillard and Barillot, 2000) proposed a robust evolution model for segmenting structures in 3D images using the level set formalism. The method involves adaptive parameters depending on the data, and it relies on region-based information rather than gradient, via estimation of intensity probability density functions over the image. The method has two main stages: intensity distribution analysis and surface evolution. The evolving surface is processed as a propagating front embedded as the zero level of a 4D scalar function. The evolution rule for the scalar function is defined by a scalar velocity function that depends on the local geometric properties of the front and external parameters related to the input data. The method is versatile and can be applied to various kinds of medical imaging data. It is demonstrated on both brain structures in MR images and carotid arteries in 3D echography. The tuning of the parameters determines the success of the method, but the proposed method requires almost no parameter setting.

Li et al. (Li et al., 2011) proposed a novel region-based image segmentation method that effectively addresses intensity inhomogeneities. The proposed method incorporates a local intensity clustering property derived from a well-established image model and formulates an energy functional within a level set framework. This energy functional aptly accounts for intensity variations within small neighborhoods, leading to precise segmentation results. By considering the local intensity clustering property, the proposed method can effectively handle intensity inhomogeneities, which is a common problem in medical image segmentation. Furthermore, the energy functional is converted into a level set formulation, utilizing vector-valued level set functions to represent the partitioning of the image domain into distinct regions. The authors then optimize the energy functional through an interleaved process involving level set evolution and bias field estimation. The evolution of level set functions is achieved by solving gradient flow equations, while the estimation of the bias field involves solving a Poisson equation.

Zhan et al. (Zhan et al., 2013) proposed an improved variational level set approach to correct the bias and to segment MRI images with inhomogeneous intensity. The authors used a Gaussian distribution with a bias field as a local region descriptor in a two-phase level set formulation for segmentation and bias field correction of the images with inhomogeneous intensities. The proposed method effectively addresses the intensity inhomogeneity problem by modeling the local intensity distribution using a Gaussian distribution with a bias field.

The two-phase level set formulation allows for simultaneous segmentation and bias field correction, resulting in more accurate segmentation results.

Chen and Wu (Chen and Wu, 2019) presented a level set approach for segmenting brain MRI images with asymmetric intensity distributions. The proposed method comprises three main steps: initialization, evolution, and post-processing. In the initialization step, a rough segmentation is obtained through a thresholding technique. In the evolution step, the level set function is modified using a data term, a regularization term, and a spatially varying weighting factor that considers the asymmetric intensity distribution of the images. The proposed method effectively addresses the intensity asymmetry problem by incorporating a spatially varying weighting factor that adapts to the local intensity distribution. Finally, the post-processing step involves obtaining the final segmentation by applying a threshold to the level set function.

2.5.6 Classification based methods

Classification methods play a crucial role in image segmentation. The primary task in classification is to extract a set of features from the image. While the intensity value is the most important feature used for classification, other image properties such as texture can also be considered. The discrete wavelet transform, Gabor filters, gray level co-occurrence matrix, and gray level run length matrix are some of the most commonly used feature extraction methods. However, the presence of a large amount of data for classification is a common challenge with most feature extraction methods. While Principal Component Analysis (PCA) can help solve the dimensionality problem to a certain extent by providing a small set of significant features for accurate classification, there are many classification methods available. Some of the most commonly used methods include k-Nearest Neighbors (kNN) and Artificial Neural Network (ANN). These methods can be used to classify images based on their extracted features, and their effectiveness depends on the specific application and the quality of the extracted features.

2.5.6.1 The k-Nearest Neighbors (kNN)

The nearest neighbor (NN) classifier is one of the simplest classifiers available. The kNN classifier, on the other hand, is a nonparametric classifier that is considered a generalization of the NN classifier. It is an iterative procedure that assigns each unlabeled data point to a cluster based on the majority vote of the k nearest labeled data points. The process continues until all data points are labeled or no additional labelings occur (Duda et al., 1973). This classifier is particularly suitable when a large number of training data are available, and it makes no implicit assumptions about the statistical structure of the data. As shown in Figure 2.12, the circles and triangles represent the training set and the target class values, respectively, providing an example of how data can be represented for

classification purposes.

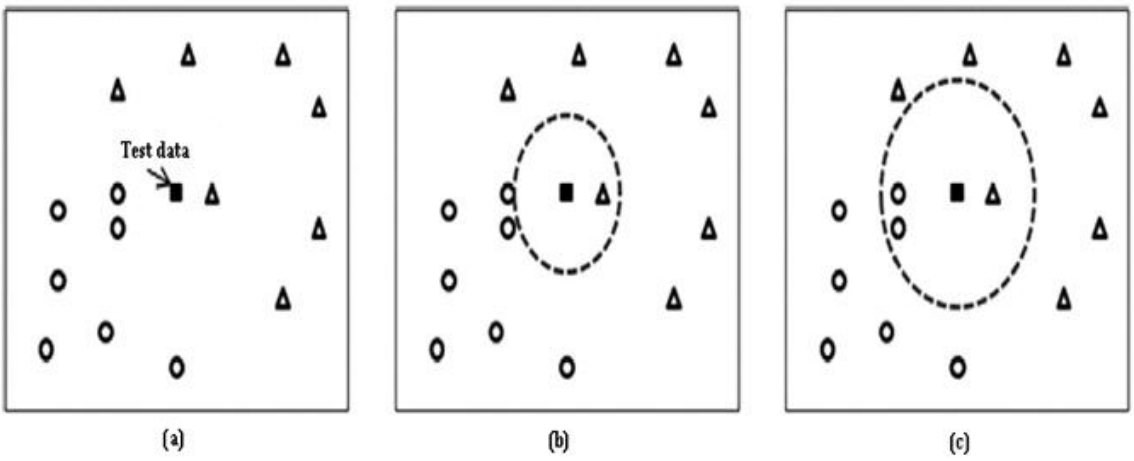

Figure 2.12 – : kNN classifier principle (a) Data set with data of unknown class. (b) Decision boundary with k=1 around unknown class data. (c) Decision boundary with k=3 around unknown test data.

Warfield et al. (Warfield et al., 2000) proposed a novel approach for brain MRI segmentation using the k-nearest neighbor (kNN) classifier. The authors integrated spatial localization of brain structures in the form of a non-rigid registered template, in addition to the intensity information, to enhance the classification. The proposed algorithm alternates between a classification step to identify tissues and an elastic matching step to align an anatomical atlas with the classified tissues and generate a segmentation. The proposed method has been successfully utilized to quantify the normal anatomy and pathology of different types, such as brain tumors, damaged knee cartilage, and multiple sclerosis. However, it should be noted that the method is semi-automatic due to the manual selection of a large number of training data sets for each tissue class during the training phase of the kNN classifier. Additionally, the results are influenced by a suitable selection of the training set. Despite these limitations, the proposed method offers a high potential for accurate and efficient brain MRI segmentation, making it a valuable tool for medical image analysis.

Cocosco et al. (Cocosco et al., 2003) proposed a fully automatic method for selecting training samples for the kNN classifier, which makes it more robust. This method is effective even for anatomies that deviate from the probabilistic atlas. However, it may not perform as well when there is intensity variation within each tissue class. It is worth noting that the two previously mentioned methods, including Warfield et al. (Warfield et al., 2000), require a preprocessing step for bias field correction.

2.5.6.2 Artificial neural network (ANN)

Artificial neural networks (ANNs) have become a popular tool in medical image analysis, with applications ranging from image reconstruction and lesion detection to brain tissue segmentation and noise suppression (Torbati et al., 2014). ANNs are a type of machine learning algorithm that can be used in various ways for image segmentation. One of the most common uses in medical imaging is as a classifier, where the weights are determined using training data, and the network is then used to segment new data. This approach has shown promising results and has the potential to improve the accuracy and efficiency of medical image analysis. ANNs can also be used as an unsupervised clustering method in addition to their supervised classification capabilities. ANNs are known for their ability to perform well even in noisy images due to their many interconnections, which allows for easy incorporation of spatial information into the classification process. Additionally, ANNs are relatively insensitive to the choice of training datasets. Another advantage of ANNs is their inherent parallelism, which enables them to produce outputs in real-time (Pham et al., 2000). Several neural network architectures have been utilized for medical imaging applications, including feed-forward networks, self-organizing maps (SOMs), and radial basis function networks, among others, for the purpose of medical image segmentation.

a- **Feed-forward network**

Feed-forward networks are among the most commonly used neural networks for medical image segmentation. In this type of network, the neurons in each layer are only connected to the neurons in the next layer. These connections are unidirectional, meaning that signals or information being processed can only pass through the network in a single direction, from the input layer, through the hidden layer(s), to the output layer. Feed-forward networks typically use the backpropagation (BP) supervised learning algorithm to dynamically adjust the weight and bias values for each neuron in the network. In a feed-forward network, the modification of weights is carried out using an optimization algorithm called gradient descent, where the weights are updated after each training example is presented to the network. This iterative process allows the network to gradually improve its performance by minimizing the difference between its predicted output and the actual output. A multilayer perceptron (MLP) is a type of feed-forward network that employs three or more layers, with nonlinear transfer functions in the hidden layer neurons. MLPs are particularly suitable for applications in medical imaging where the inputs and outputs are numerical, and pairs of input/output vectors provide a clear basis for supervised training.

Shen et al. (Shen et al., 2005)proposed a method to improve the accuracy of MR image analysis by extending the traditional fuzzy c-means clustering algorithm with neighborhood attraction and neural-network optimization. The method involves preprocessing, initialization, fuzzy clustering, neighborhood attraction, neural-network optimization, iterative

refinement, and stopping criterion. During preprocessing, the MR images are preprocessed to remove noise and enhance contrast. The initialization step randomly selects initial cluster centers from the image, and the fuzzy c-means algorithm is applied to obtain the initial segmentation. The proposed method introduces neighborhood attraction into the objective function of the fuzzy c-means algorithm to improve segmentation accuracy. A simple artificial neural network is employed to optimize the degree of feature attraction and distance attraction in the objective function. The iterative refinement step updates the cluster centers and membership values until convergence is achieved, and the stopping criterion is used to stop the segmentation process.

Assam et al. (Assam et al., 2021) proposed an efficient method for classifying brain MRI images into normal and abnormal categories. The method consists of four steps. First, a median filter is applied to remove noise and unwanted components from the image. In the second step, the authors use the Discrete Wavelet Transform (DWT) technique to extract different features from the images. After that, the set of features is reduced to decrease the computation time. In the last step, the selected features are passed to a feed-forward network for image classification.

b- **Radial basis function networks**

A radial basis function (RBF) network is a type of three-layer supervised feed-forward network that uses a nonlinear transfer function, typically a Gaussian function, for the hidden neurons and a linear transfer function for the output neurons. The Gaussian function is applied to the net input of each neuron to produce a radial function of the distance between each pattern vector and each hidden unit weight vector. This type of network is commonly used for function approximation, classification, and clustering tasks.

RBF networks are known for their inherent flexibility in terms of size and topology, which makes them suitable for a variety of problems. They offer easy design, effective tolerance to input noise, online learning ability, and good generalization (Nilakant et al., 2017).

Valdés-Cristerna et al. (Valdés-Cristerna et al., 2004) proposed a hybrid model for segmenting multispectral brain MRI images. The model combined the Radial Basis Function (RBF) network with a spline Active Contour Model. The RBF network was utilized to analyze and classify the multispectral MRI data, enabling the model to handle the complex intensity variations and anatomical structures present in brain scans. The spline Active Contour Model, on the other hand, employed an energy minimization principle to iteratively adjust the contour shape and accurately delineate the boundaries of brain structures.By integrating these two approaches, the hybrid model proposed by Valdés-Cristerna et al. (Valdés-Cristerna et al., 2004) achieved a high level of performance in terms of evaluation indexes, providing accurate segmentation results. The model effectively captured non-linear relationships in the data while employing a contour-based approach for precise boundary localization.

Rostami et al. (Rostami et al., 2013) proposed a method to improve the accuracy of brain MRI segmentation by combining the FCM algorithm with a Radial Basis Function (RBF) neural network. The FCM algorithm was used to cluster the pixels based on intensity information, but to address misclassifications caused by noise and lack of neighborhood consideration, the researchers employed the RBF neural network. The RBF network was trained using low-level noise images, and pixels that were not confidently classified by FCM were then classified using the trained RBF network. The proposed approach effectively utilized both intensity and neighborhood information, leading to improved segmentation results in the presence of noise and complex image characteristics. By incorporating the RBF neural network, the method was able to address misclassifications caused by noise and lack of neighborhood consideration, resulting in more accurate segmentation of brain MRI images.

c- **Self-organizing maps (SOM)**

The Self-Organizing Map (SOM) is an unsupervised clustering network commonly used in the field of neural networks. It organizes input data into several patterns based on a similarity factor, such as Euclidean distance. Each pattern is assigned to a neuron, which has a weight that depends on the pattern assigned to it. The SOM learns to classify input data according to their grouping in input space, with neighboring neurons learning neighboring patterns in input space.

The SOM is composed of two layers: the input layer and the competitive layer. The input layer has a number of neurons equal to the dimension of the input, while the competitive layer has a neuron corresponding to each class or pattern, with the number of neurons depending on the number of clusters. The neurons in the competitive layer are arranged in regular geometric structures, such as a mesh. In the SOM, each connection from the input layer to a neuron in the competitive layer is assigned a weight vector. The SOM algorithm consists of two main steps (Pateria et al., 2021): finding the winning neuron, which is the most similar neuron to the input based on a similarity factor like Euclidean distance, and updating the weight of the winning neuron and its neighboring neurons based on the input. In other words, the weight of the winning neuron and its neighbors are adjusted towards the input.

Dokur and Ölmez (Dokur and Ölmez, 2003) proposed a novel neural network called the quantiser neural network (QNN) for the segmentation of MR and CT images. The QNN distinguished itself by employing genetic algorithms for training, setting it apart from traditional neural networks. The performance of the QNN was compared to that of a multilayer perceptron and a Kohonen network in the context of MR and CT head image segmentation. The results revealed that the QNN achieved superior classification accuracy with fewer neurons and a shorter training time, indicating that the QNN offers a more efficient and effective approach to image segmentation.

Ortiz et al. (Ortiz et al., 2014) presented a novel MRI segmentation method that utilizes

a Self-Organising Map (SOM) with dual objectives. The first objective involves learning the most discriminative features through SOM optimization using Genetic Algorithms (GA). The second objective is to group voxels into different SOM clusters based on their class. The method involves five stages: preprocessing, feature extraction, feature selection, vector classification using SOMs, and entropy-gradient clustering. Preprocessing involves noise removal and window splitting to reduce data dimensionality. Feature extraction includes extracting first and second-order features using overlapped windows and reducing them through evolutionary computation. The reduced feature vectors are then classified using SOMs, followed by refinement using entropy-gradient clustering to improve segmentation accuracy.

Torbati et al. (Torbati et al., 2014) developed a neural network-based method to improve upon the limitations of self-organizing map (SOM)-based approaches in medical image segmentation. They introduced a modified SOM network called moving average SOM (MA-SOM) and evaluated its performance using a dataset consisting of breast images, brain MRI images, and CT head images. To enhance the input feature space for the network, the authors employed a two-dimensional Discrete Wavelet Transform, resulting in improved segmentation performance compared to both supervised neural network and traditional SOM-based methods. The MA-SOM network, along with the utilization of wavelet transform, represents a promising approach for medical image segmentation.

De and Guo (De and Guo, 2015) utilized the self-organizing map (SOM) technique to segment real brain MRI images obtained from the Internet Brain Segmentation Repository (IBSR). Their approach focused on using Vector Quantization (VQ) for the segmentation task, with the SOM network facilitating adaptive codebook learning for the VQ method. The proposed method aimed to enhance the accuracy and effectiveness of the segmentation process. By utilizing the capabilities of the SOM network for adaptive codebook learning, the algorithm achieved improved representation and clustering of the image data, resulting in enhanced segmentation results for the brain MRI images.

d- **Convolutional Neural Network (CNN)**

A Convolutional Neural Network (CNN) is a type of feed-forward network that uses a specialized multilayer architecture designed for image classification (Jena et al., 2018). It can also be described as a deep multi-layer perception network. CNNs use a local receptive field, shared weights, bias, and pooling to process images. Unlike fully connected neural networks, where the input is represented as a vertical line of neurons, CNNs take the input as a square matrix corresponding to the pixel values of the input image. This allows the original image to be directly processed by the network. In convolutional neural networks (CNNs), each neuron in the hidden layer is connected to a small, localized region of the input image, known as the local receptive field. These neurons are connected to every neuron of the hidden layer. The local receptive field is then slid across the entire input image, starting from the top-left corner, by one pixel at a time, creating the total matrix

of the hidden layer. Each connection from the hidden layer neuron to input neurons bears a weight, and each node in the hidden layer has a bias. The same weight and bias are used by the total hidden neuron matrix, known as shared weight and bias.

In convolutional neural networks (CNNs), the convolutional layers generate feature maps by local connectivity and weight sharing, meaning that the same local features are detected in all locations of the input image. This weight-sharing rule significantly reduces the number of parameters, increasing efficiency and preventing overfitting. A CNN may have many feature maps. Finally, pooling is applied to each feature map separately to reduce the number of features and the dimensionality of the network. The convolution and pooling layers are considered 2D layers, while the output layer is a 1D layer.In CNNs, each 2D layer consists of several planes, and each plane consists of neurons arranged in a 2D array. The reduced pooling layers produce one label per node, resulting in 1D data that is fed to a simple neural network to obtain the required output (Jena et al., 2018).

CNNs have gained popularity in the field of medical image analysis because they do not require a set of handcrafted features for classification. Instead, they learn sets of convolution kernels that are specifically trained for the classification problem at hand. Unlike classical machine learning methods, which use Gaussian kernels to acquire appearance information for image segmentation, CNNs optimize sets of kernels based on the provided training data. This allows the system to automatically extract relevant information from the image, including spatial and intensity information, to distinguish between different classes, this can be learned from the provided information, much like a human observer would recognize objects within a (medical) image.

Moeskops et al. (Moeskops et al., 2016) proposed a CNN-based approach for automatic brain image segmentation that aimed to achieve precise segmentation details and spatial consistency. Their method incorporated multiple patch and convolution kernel sizes to capture multi-scale information for each voxel, and relied on learning relevant information for classification from the training data rather than explicit features. Notably, their approach only required a single anatomical MR image as input.

Kleesiek et al. (Kleesiek et al., 2016) proposed a novel 3D CNN for automatic skull stripping in MRI brain images. Their CNN architecture involves convolving the input data with local filters, followed by nonlinear transformations to extract meaningful features. The network is designed to handle an arbitrary number of modalities and can be trained to process multi-channel data, including non-MRI channels. During training, the filters are optimized using the Kullback-Leibler divergence as the loss function. To enhance generalization and prevent overfitting, data augmentation techniques such as rotation, scaling, and flipping are employed. Before feeding the data into the CNN, a pre-processing step is performed, which involves removing non-brain tissue and normalizing intensity values. The authors used the bias field correction algorithm to address intensity inhomogeneities and the brain extraction tool (BET) to eliminate non-brain tissue. The output of the CNN

is a probability map that indicates the likelihood of each voxel being part of the brain. Post-processing techniques, including thresholding and morphological operations, are then applied to convert the probability map into a binary mask and refine the segmentation results.

Khalili et al. (Khalili et al., 2019) proposed an innovative method for automatic brain MRI image segmentation, employing two fully convolutional networks (CNNs) sharing the same architecture. Their approach consisted of utilizing the first CNN to extract the intracranial volume, while the second CNN was specifically designed to segment the extracted volume into three main brain tissues: white matter (WM), gray matter (GM), and cerebrospinal fluid (CSF). To achieve optimal performance, each CNN was independently trained using stochastic gradient descent and the Adam optimizer with a learning rate set to 0.0001. During the training process, the first CNN effectively utilized 12 slices per subject to extract the intracranial volume, while the second CNN utilized the entire volume for tissue segmentation.

Khaled et al. (Khaled et al., 2023) introduced a novel fully convolutional neural network (CNN) aimed at significantly improving brain segmentation performance. Their method integrated a multi-instance loss technique, effectively distinguishing between brain pixels and background regions. To further enhance segmentation results, the authors leveraged Gabor filter banks and the K-means algorithm, which provided complementary informative details to the machine-learned features. Notably, the CNN utilized complete images as input and employed both max pooling and mean pooling operations for effective data processing.

2.5.7 Discussion

As previously mentioned, there are various approaches for brain MRI image segmentation, each with its own set of advantages and disadvantages. The choice of approach or method is highly dependent on the specific application and the characteristics of the images being analyzed. Despite their differences, these methods offer several advantages. For instance, they are relatively easy to implement and utilize important properties such as the similarity between neighboring pixels. They employ criteria and metrics to separate image groups or classes, often incorporating information and knowledge about shape, orientation, continuity, elasticity, or smoothness through techniques like Atlas-based methods. These methods can be effective in capturing specific features and characteristics relevant to the segmentation task.

However, brain MRI segmentation methods also have certain drawbacks. They often produce suboptimal results and require user interaction, such as selecting appropriate seed points or determining threshold values. These choices play a critical role in the result of the segmentation process. Moreover, these methods can be sensitive to noise, poor

contrast, and acquisition artifacts, which can negatively impact the accuracy of the segmentation results. Additionally, they rely on prior knowledge from domain experts and typically involve manual feature engineering, which can be time-consuming and limit their adaptability to different datasets. Despite these limitations, segmentation methods can be effective in capturing specific features and characteristics relevant to the segmentation task. Table 2.2 provides a comprehensive overview of the advantages and disadvantages of different segmentation methods.

The choice of a specific segmentation approach depends on various factors, including the characteristics of the MRI data, the desired level of accuracy, computational efficiency, the available computational resources, and the expertise of the users. Additionally, the complexity and scalability of the method should be considered, especially when dealing with large datasets or real-time applications. It is important to explore and compare different segmentation techniques, considering their suitability for the specific task at hand. Furthermore, the availability of labeled training data plays a significant role in the selection process, as some methods require a sufficient amount of annotated data for effective training. Researchers need to assess the adequacy of the available training data and determine if additional data acquisition or augmentation is necessary. Moreover, the computational resources available, such as processing power and memory capacity, should be taken into account to ensure the feasibility and efficiency of the chosen method. The parameters that govern the performance of the segmentation method also need to be carefully adjusted. These parameters, such as the degree of spatial interaction or the network architecture, impact the segmentation accuracy and computational complexity. Researchers should conduct parameter tuning experiments to find the optimal configuration that balances accuracy and computational efficiency. Finding a balance between accuracy and computational complexity is indeed crucial when selecting a segmentation method for brain MRI analysis. By considering these factors, researchers can improve both the accuracy and efficiency of brain MRI segmentation.

Table 2.2: Advantages and disadvantages of the most commonly used brain tissue segmentation methods

Method	Advantages	Disadvantages
Thresholding	This approach is effective in segmenting images that have uniform intensity, high contrast, and clear differentiation between the object and background. It is commonly used for brain tissue segmentation due to its simple implementation and computational efficiency (Pham et al., 2000).	One major limitation of this approach is that it does not consider the correlation between pixels, which can result in misclassification of pixels, particularly when there is noise, partial volume effects, and overlapping tissues. These artifacts can significantly affect the image histogram, making segmentation using thresholding a difficult task (Pham et al., 2000).
Level set	It is an effective solution to overcome the limitations of edge-based techniques as it can detect interior contours, making it suitable for medical images with weak boundaries. Additionally, it can effectively handle medical images with inhomogeneity intensity. It is known for its versatility, robustness, and accuracy. It is capable of handling topological changes and accounting for three-dimensional effects (Balafar et al., 2010).	It is limited when applied to images with complex backgrounds and irregular intensities. It is only suitable for images with homogeneous regions. The non-convex and non-unique energy function often leads to convergence to local minima during contour evolution, which can result in undesired segmentation results (Dong and Peng, 2014).

Region growing	It offers the advantage of being insensitive to changes in the inner parts of an object. It has the advantage of considering both visual features and spatial information. It can handle images with non-uniform intensity and complex structures, such as tumors or lesions. (Dora et al., 2017).	it heavily depends on the choice of seed points and the criteria used for merging neighboring regions. This can make it challenging to apply to natural images with complex structures and non-uniform intensity. Additionally, region growing methods may not perform well on images with heterogeneous regions, as they tend to merge regions with similar intensity values, regardless of their spatial location. Furthermore, region growing methods are sensitive to noise, which can result in segmented regions with holes or discontinuities. (Zanaty and Ghoniemy, 2016).
Atlas-based method	It can handle images with large anatomical variations, such as those caused by disease or injury. Additionally, it can be easily applied in computer-assisted analysis, making them a valuable tool for medical image analysis (Dora et al., 2017).	It is typically used for high-resolution, 3D medical images and may not be suitable for other types of images or data modalities. The accuracy of the segmentation is highly dependent on the accuracy of the registration algorithm used to align the atlas with the target image. It can be computationally expensive. It may not always capture the full range of anatomical variation, which can lead to errors in segmentation (Yazdani et al., 2015).

kNN	It is easy to implement. It is capable of preserving information in the training images. It is a non-parametric method, which means it does not assume any specific form of data distribution. It provides interpretability as it assigns labels based on the nearest neighbors, which can help in understanding the decision-making process (Nilakant et al., 2017).	It can be computationally expensive, especially with large datasets or high-dimensional feature spaces. It can be sensitive to noise and outliers in the data. The choice of the optimal value for k (the number of neighbors) in the kNN classifier is crucial. An inappropriate selection of k can lead to underfitting or overfitting, affecting the segmentation accuracy (Nilakant et al., 2017).
K-means	It is simple and easy to implement. It is particularly suitable for real-time image segmentation tasks due to its computational efficiency. It typically converges quickly to a stable solution, especially for well-separated clusters in the (Ezugwu et al., 2021).	It is sensitive to the initial values of the cluster centers and needs to determine the appropriate number of clusters. It is sensitive to outliers and noise. It may not provide accurate segmentation results for regions with irregular shapes or varying sizes (Mittal et al., 2021).
FCM	It does not use a sharp boundary to separate pixels into groups. Instead, it utilizes a membership function to cluster the pixels (Ezugwu et al., 2021).	It is sensitive to noise because it does not consider spatial information. It is difficult to identify the initial partitions. There is no guarantee that ensures FCM converges to an optimum solution (Mittal et al., 2021).
Mixture models	These models have the ability to effectively handle bias field correction and spatial regularization in the local region by employing Gaussian distributions to model the intensity variation of each tissue type. Provide flexibility in adjusting the number of Gaussian components in the mixture, enabling the capture of finer details in the intensity distribution (Balafar et al., 2010).	The performance of Mixture Gaussian models can be sensitive to the choice of initialization parameters, including the initial number of components and their initial locations. The absence of spatial relationships among neighboring pixels within the class leads to the emergence of local optima (Balafar et al., 2010).

MRF	MRF exhibits a lower sensitivity to noise in comparison to other classifiers and clustering techniques, primarily due to its incorporation of contextual information. Another distinguishing feature of MRF is its isotropic behavior and reliance on local dependencies (Yazdani et al., 2015).	One of the major problems of MRF is the need to select appropriate parameters that govern the strength of spatial interaction and the energy function. Determining these parameters can be a difficult task, as setting them too high may result in excessively smooth segmentation outputs, leading to the loss of important structural details. Additionally, the computational complexity of MRF can still pose practical limitations, potentially hindering its practical applicability (Yazdani et al., 2015).
ANN	ANN is able to generate precise results. is a powerful computational model for solving real word problems in all applicable fields. Able to perform well on complicated and multivariate nonlinear domains. Resistance to noise. (Pham et al., 2000).	It needs significant computational complexity and response time. Another significant drawback of using ANN lies in determining the optimal combination of training, learning, and transfer functions for classifying datasets with an increasing number of features and classes (Benos et al., 2021).
CNNs	CNNs are capable of capturing non-linear relationships between input images and segmentation labels. CNNs can automatically learn discriminative features directly from the input data, eliminating the need for manual feature engineering (Puttagunta and Ravi, 2021).	CNNs are often considered as black-box models due to their complex architectures and numerous parameters. Training CNNs can be computationally demanding, necessitating the use of powerful hardware resources, such as GPUs, and resulting in longer training times (Benos et al., 2021).

SOM	It can capture non-linear relationships between input features, enabling it to handle complex variations in brain MRI data. Preserves the topological structure of the input data during the mapping process. It can effectively reduce the dimensionality of high-dimensional data (Torbati et al., 2014).	The lack of explicit spatial constraints. Sensitivity to initialization. It may require substantial computational resources and longer processing times (Torbati et al., 2014).
RBF	It can effectively capture nonlinear relationships in brain MRI data, allowing for accurate modeling of complex intensity distributions and boundaries between different brain tissues. It has the capability to handle nonuniform intensity distributions commonly observed in brain MRI images. It typically has faster training times compared to other neural network architectures (Torbati et al., 2014).	It requires careful tuning of hyperparameters, such as the number and positions of the radial basis functions. It primarily utilizes local pixel intensities and may not fully exploit spatial relationships between neighboring pixels (Pateria et al., 2021).

2.6 Conclusion

Image segmentation is a crucial process that involves dividing an image into multiple segments. The primary goal of image segmentation is to simplify or alter the image's representation, making it easier for further analysis and extracting meaningful information. Effective segmentation results facilitate the subsequent image processing analysis. This chapter has explored various algorithms and approaches for Brain MRI image segmentation, such as thresholding, region growing, clustering-based methods, and classification-based methods. Each method has its own strengths and weaknesses, and the choice of algorithm depends on the specific requirements and perspectives.

In the next chapter, we will present one of the most significant clustering algorithms, the Fuzzy C-Means (FCM) algorithm, and thoroughly discuss its limitations and improvement variants.

Chapter 3

Fuzzy C-Means Based Image Clustering Algorithms

Contents

3.1 Introduction

The objective of Image clustering is to group an image into homogeneous regions based on characteristics such as color, texture, and intensity. However, traditional hard clustering methods that assign each pixel to a single cluster have limitations in dealing with uncertain attributes, such as limited spatial resolution, overlapping intensities, and noise, which makes it challenging to partition the image into distinct clusters.

Fuzzy c-means (FCM) is a popular approach for image clustering as it allows pixels to have membership degrees to each cluster center, indicating the degree of association with each cluster. Compared to hard clustering, FCM provides more information on the structure of the data, particularly for ambiguous points located in "bounding regions."

However, FCM is sensitive to the initialization of cluster centers and can be affected by noise and outliers, which can reduce its clustering performance. In this chapter, we review the traditional FCM algorithm and summarize various techniques aimed at addressing its limitations. Specifically, we discuss approaches for automatically determining the number of clusters and improving the initialization process for cluster centers in the FCM algorithm. Additionally, we present a range of FCM derivatives that aim to enhance the clustering process by speeding it up or making it more robust against noise and other imaging artifacts.

3.2 Traditional FCM algorithm

The FCM algorithm is based on minimizing an objective function that is defined as the weighted sum of the distance of data from cluster centers; the minimizing of the objective function is achieved by iteratively updating the membership matrix and cluster centers. The membership value of each pixel with respect to a particular cluster is considered as the weight of that pixel. The cluster center is a weighted mean of the pixels. The FCM algorithm assigns a higher membership value to a considered pixel that is nearby to a particular cluster, while it assigns lower membership values to the same pixel that is far from the other cluster centers. The updating process is continued until the distance between the cluster centers from two successive iterations does not exceed a certain threshold.

The FCM algorithm is an effective method for image clustering, which is based on minimizing an objective function (Eq. (2.7)) that is defined as the weighted sum of the distance of data from cluster centers. This objective function is achieved by iteratively updating the membership matrix (Eq. (2.8)) and cluster centers (Eq. (2.9)). The membership value of each pixel with respect to a particular cluster is considered as the weight of that pixel. The cluster center is a weighted mean of the pixels, where the weight of each pixel is determined by its membership value.

During the iterative process of updating the membership matrix and cluster centers, the FCM algorithm assigns a higher membership value to a pixel that is closer to a particular cluster center, while it assigns a lower membership value to the same pixel that is far from the other cluster centers. This allows the algorithm to effectively group pixels into non-overlapping regions with homogeneous characteristics. The updating process of the FCM algorithm is continued until the distance between the cluster centers from two successive iterations does not exceed a certain threshold. This means that the algorithm will continue to refine the cluster centers and membership values until a certain level of convergence is reached. This ensures that the final clustering result is as accurate as possible.

3.3 Limitations of Fuzzy c-means (FCM) algorithm

The fuzzy c-means (FCM) algorithm is a popular clustering technique used in image segmentation, where its goal is to divide an image into different regions or segments based on the similarity of their pixel intensities. However, despite its popularity, FCM has several limitations that can significantly impact its performance in certain scenarios.

- One of the primary limitations of the FCM algorithm is that it can become computationally expensive when dealing with large datasets. As the size of the dataset increases, the number of iterations required to achieve convergence also increases, leading to longer processing times. This can make the FCM algorithm impractical for use in real-time applications or when dealing with large datasets.
- Moreover, FCM heavily depends on the initial cluster centers and the number of clusters chosen, which can be challenging to determine. This can significantly affect the accuracy of the segmentation and may lead to suboptimal segmentation quality. When FCM falls into local minimum solutions due to poor initial cluster centers and the number of clusters chosen, the segmentation quality can be further degraded. While the difficulty of determining the cluster number could influence the segmented area and region tolerance for feature variance, the difficulty of obtaining the initial cluster centers could affect the cluster compactness and segmentation accuracy.
- Another limitation of the FCM algorithm is that it only considers the intensity values of the pixels and does not take into account the spatial information of the image. This can result in poor segmentation quality in the presence of imaging artifacts and noises. For example, in medical images, intensity inhomogeneities can occur due to variations in imaging equipment, tissue composition, or patient positioning. The FCM algorithm may not be able to accurately segment regions with intensity inhomogeneities, which can lead to erroneous results.

In the following sections, we provide a detailed overview of some of the most frequently employed FCM variants proposed in the literature. These variants have been designed to address the limitations discussed earlier and enhance the efficiency and accuracy of the FCM algorithm in the context of image segmentation.

3.4 Fast Fuzzy c-Means Clustering Algorithm

To reduce the computational complexity of the FCM algorithm, a multistage random sampling strategy (RSFCM) is introduced in (Chang et al., 1994). The essential idea of the proposed method is to randomly sample and achieve a small subset of the dataset in order to approximate the cluster centers of the whole dataset, this approximation is then applied to decrease the number of iterations. The RSFCM consists of a multistage

iterative process and the conventional FCM algorithm. Since the FCM algorithm is an iterative process the convergence speed of it is lower which makes the algorithm impractical used in image segmentation, to overcome this problem a fast fuzzy c-means clustering algorithm is proposed in (Yong et al., 2004). In this method, the histogram of the image is used as input data for clustering instead of the pixel intensities. Therefore, the size of the input data decreases clearly and clustering is done more quickly. Let consider $G = L_{\min}, L_{\min+1}, \ldots L_{\max}$ as gray level, where $L_{\min}$ is the minimum gray level, $L_{\max}$ is the maximum gray level. For image size $S \times T$, $f(s,t)$ is the gray value of point $p(s,t)$. Let $His(g)$ indicate the number of pixels having gray value g, the histogram function is defined as

$$H(g) = \sum_{s=0}^{S-1} \sum_{t=0}^{T-1} \delta(f(s,t) - g) \tag{3.1}$$

Where

$$\delta(x) = \begin{cases} 0 & \text{if } x \neq 0 \\ 1 & \text{if } x = 0 \end{cases} \tag{3.2}$$

The cluster centers are updated using the following equation

$$v_i = \frac{\sum_{g=L_{\min}}^{L_{\max}} (u_{ig})^m \text{His}(g) g}{\sum_{g=L_{\min}}^{L_{\max}} (u_{ig})^m \text{His}(g)} \tag{3.3}$$

3.5 FCM variants for Improved Initialization

FCM algorithm is widely used for image segmentation due to its ability to handle partial volume effects and imprecise decisions. However, FCM has some limitations that can affect its performance in fully automatic segmentation tasks. One of the main challenges is to determine the optimal number of clusters in a given dataset, which can be a time-consuming and challenging task that often requires expert knowledge or manual intervention. Moreover, FCM is known to converge to a local minimum, which can lead to suboptimal results if the initial cluster centers are not well-chosen. These limitations make the FCM approach semi-automatic and can limit its applicability in some cases.

To address these challenges, researchers have proposed alternative methods, such as Validity Index-Based Methods and Metaheuristic-Based Methods. These techniques can automatically determine the optimal number of clusters and initial cluster centers without the need for any prior knowledge or manual intervention, making the FCM algorithm more suitable for achieving automatic segmentation in various applications.

3.5.1 Validity Index Based Methods

Validity Index Based Methods aim to improve the Fuzzy C-Means (FCM) algorithm by automatically determining the optimal number of clusters for a given dataset. This process

involves defining a range of possible values for the number of clusters, denoted as $C_{\min}$ and $C_{\max}$, which represent the minimum and maximum number of clusters, respectively. For each value of C within this range, the FCM algorithm assigns a fuzzy membership value to each data point, indicating its degree of belonging to each cluster. The algorithm then iteratively updates the cluster centroids and fuzzy membership values until convergence or the stopping criterion is met.

Subsequently, a Cluster Validity Index (CVI) is calculated for each value of C, measuring the quality of the resulting clustering based on separation and compactness measures of clusters. By evaluating the CVI for each C, the algorithm identifies the value that provides the highest or lowest CVI as the optimal number of clusters. Once the optimal number of clusters is determined, the FCM algorithm can be run again with that specific value of C to obtain the final clustering of the data.

The FCM-based splitting algorithm (FBSA) (Sun et al., 2004) is an effective method for automatically determining the number of clusters in a dataset. The algorithm employs a combination of splitting strategies and the basic FCM algorithm to identify and split the worst cluster into two new clusters. The worst cluster is identified based on a specific score, considering both the size and sparsity of the cluster. The candidate cluster selected for splitting has the minimal score value, indicating it is large in volume and sparse in distribution. The FBSA adopts a greedy strategy to split the worst cluster into two new clusters with centers maximally separated from each other, ensuring well-separated clusters. This process iterates until the desired number of clusters, determined by the value of $C_{\max}$, is reached.

To evaluate the quality of the obtained fuzzy partition, the authors introduced a new validity index that combines measures of compactness and separation. The compactness measure evaluates how closely data points are grouped within each cluster, while the separation measure assesses the distinctness of clusters from one another. The proposed validity index provides a quantitative measure of the quality of the obtained fuzzy partition and facilitates comparisons between different fuzzy partitions. By utilizing this validity index, the FCM-based splitting algorithm can evaluate the clustering quality and select the best clustering result. Overall, the FBSA offers a robust and automated approach for generating high-quality clusterings in datasets, eliminating the need for manual cluster number specification.

An adaptive optimization scheme for fuzzy C-means clustering is proposed in (Beringer and Hullermeier, 2007), where the number of clusters is dynamically adjusted based on the quality of the resulting fuzzy partition. Initially, the method starts with a small number of clusters and applies fuzzy C-means clustering to the data. Subsequently, it computes the validity measure for the fuzzy partition using a modified Xie-Beni index (Xie and Beni, 1991). If the validity measure falls below a certain threshold, the number of clusters is increased by 1, and the clustering process is repeated. Conversely, if the validity measure

exceeds the threshold, the number of clusters is decreased by 1, and the clustering process is repeated. This adaptive process continues until the validity measure no longer improves or a maximum number of iterations is reached.

Yan-ling and Yi (Li and Shen, 2010) proposed an automated modified Fuzzy C-Means (FCM) algorithm, termed AMFCM, for image segmentation with the primary goal of determining the optimal number of clusters automatically without requiring expert user intervention. AMFCM incorporates spatial information to enhance segmentation quality. The algorithm starts with the hard c-means to find two initial centroids closest to the real cluster centers. Then, the FCM algorithm calculates the membership matrix iteratively. The optimal number of clusters is determined based on the pixel proportion of clusters, with at most two clusters having values below a parameter d, representing the smallest percentage for an existing cluster. Clusters with an area less than 10% are discarded. If the optimal cluster number is not reached, the algorithm increments the number of clusters and repeats the process until the optimal clustering is achieved.

The new adaptive fuzzy clustering algorithm (AFCM) proposed in (Liang et al., 2010) uses a hierarchical clustering approach to adjust the number of clusters for the FCM algorithm. The algorithm starts by initializing the number of clusters to be explored and the fuzzy weighting exponent. Then, it applies the FCM algorithm to the data set to obtain the initial clustering result. Next, the algorithm uses Ward's method to split each cluster into two based on the biggest decrement of the error sum squares of clusters. The algorithm then computes the index of each resulting cluster using a new index based on cluster variance. The index is defined as the ratio of the sum of the distances between each data point and the cluster center to the sum of the distances between each data point and the nearest cluster center. The algorithm replaces the original cluster with the one that has the highest index and repeats the splitting process until the optimum number of clusters is reached. The optimum number of clusters is determined by the maximum value of the index.

FCM with automatic cluster centers initialization is presented in (Yang and Nataliani, 2017). The sample space is divided into grids and a list of grids with high density is formed. From the list, the highest density grid is taken iteratively. Afterward, the chosen grid and grids with similar properties to select one are removed from the list. This process is repeated until the list is empty. At last, cluster centers are initialized at the centers of selected grids. The proposed method requires more time-consuming.

Zanaty (Zanaty, 2012) proposed a kernelized fuzzy C-means algorithm (KFCM) for automatic medical image segmentation. The algorithm's robustness is enhanced by replacing the original Euclidean distance with a Gaussian radial base function. To determine the optimal number of clusters, KFCM algorithm is applied to the dataset with varying numbers of clusters. Many cluster validity indices are computed for each number of clusters and plotted against them to identify the most effective clustering solution. The optimal number

is typically identified where the validity indices values are stable or reach a maximum or minimum. Finally, KFCM algorithm is run again using the optimal number of clusters to obtain the final segmentation result.

The self-adaptive Fuzzy C-Means (SAFCM) algorithm (Ren et al., 2016) is a clustering method designed to improve the stability and convergence of the traditional FCM algorithm. Unlike traditional methods, this algorithm generates high-quality initial cluster centroids instead of choosing them randomly. It does so by calculating the distance between each data point and all existing centroids and selecting a data point with the maximum potential to be a new centroid. This process is repeated until the desired number of centroids is obtained. Moreover, the SAFCM algorithm automates the determination of the maximum number of clusters in a dataset, thereby reducing the number of iterations required to find the optimal number of clusters. It uses a two-step process to estimate the maximum number of clusters. First, it calculates the average distance between data points and their closest centroid. Then, it estimates the maximum number of clusters based on the features of the dataset.

3.5.2 Metaheuristic-Based Methods

Metaheuristic-Based Methods have emerged as a powerful tool to tackle the problem of sensitivity to initial parameters in the FCM algorithm. These optimization algorithms can efficiently search for the optimal solution in large search spaces, which helps the FCM algorithm converge to a better solution and avoid getting stuck in local optima.

The Fuzzy Variable String Length Genetic Algorithm (FVGA) (Maulik and Bandyopadhyay, 2003) is a clustering technique that automates the determination of the optimal number of clusters in a dataset using FCM algorithm. This approach uses a population of candidate partitions, which are represented as chromosomes that are encoded with real-valued genotypes. Each chromosome contains a diverse number of candidate cluster centers, this enables chromosomes to encode a diverse number of cluster centers and automatically determine the optimal number of clusters in a dataset. The fitness function is evaluated using the Xie-Beni validity index (V_{XB}) (Xie and Beni, 1991), and selection, crossover, and mutation are used to create new offspring chromosomes. To ensure that offspring chromosomes have at least two cluster centers, the crossover operator is modified. Additionally, the mutation operator is applied to every gene within the chromosome when its location is inside the probability of mutation. The authors also included a one-step clustering center recomputation process in FVGA. This step fine-tunes each candidate partition by using FCM cluster centers that are optimized and well-defined. This step leads to more accurate and efficient clustering results.

Maulik and Saha (Maulik and Saha, 2009) proposed an algorithm called Fuzzy-VGAPS, which is a dynamic clustering algorithm based on the FVGA algorithm. Fuzzy-VGAPS

modifies the objective function and genetic operators used in FVGA to improve its performance in handling noisy or incomplete data. The fitness function used in Fuzzy-VGAPS is the fuzzy Sym-index, which is a modified version of the PS-index. The PS-index measures the quality of a clustering solution based on point symmetry, but the fuzzy Sym-index uses fuzzy logic to handle uncertainty in the data. This makes it more robust in the presence of noise or incomplete data, which can improve the accuracy of the clustering results. The genetic operators used in Fuzzy-VGAPS have also been modified to work with variable string length chromosomes. This allows the algorithm to handle a diverse number of clusters and adapt to the complexity of the data distribution. By using variable string length chromosomes, the algorithm can explore a wider range of possible solutions and improve the fitness of the population over time.

Alsmadi (Alsmadi, 2014) proposed a hybrid approach that combines the Firefly Algorithm (FA) and the Fuzzy C-means algorithm to address the challenges of MRI brain segmentation. The proposed clustering method consists of two phases: In the first phase, the FA initializes a population of fireflies, controls their movements towards brighter fireflies in the search space, updates their brightness based on the objective function value, and terminates the algorithm when the maximum number of generations is reached to determine the optimal cluster centers. The objective function is defined as the distance between the centroid of each cluster and the data points assigned to that cluster. In the second phase, the Fuzzy C-means algorithm is initialized based on the evaluated results in the first phase to refine the cluster centers and overcome the drawbacks of the Fuzzy C-means algorithm, such as getting stuck in the local optimum and being susceptible to initialization sensitivity.

The proposed approach in (Chen and Ludwig, 2014) is a novel clustering algorithm based on Particle Swarm Optimization (PSO) that addresses the challenge of automatically determining the optimal number of clusters. The algorithm starts by initializing the PSO parameters, including the number of particles, the maximum number of iterations, the inertia weight, the acceleration coefficients, and the threshold vector. The data set is randomly partitioned into a preset number of clusters, which serves as the starting point for the PSO optimization process. Each particle's fitness value is computed using a reconstruction criterion based on the distance between data points and cluster centers. The PSO equations are then used to update the velocity and position of each particle, incorporating personal best and global best positions. The process iteratively repeats until termination conditions are met. The optimal number of clusters is determined based on the threshold vector and the fitness values, allowing the algorithm to adaptively adjust the number of clusters. Finally, the cluster centers are decoded, and each data point is assigned to the nearest cluster center.

The multi-objective spatial fuzzy clustering algorithm (MSFCA) proposed by (Zhao et al., 2015) is a novel approach to image segmentation that utilizes non-local spatial in-

formation, global fuzzy compactness, and fuzzy separation to improve the segmentation quality. The algorithm incorporates a genetic algorithm step that optimizes the cluster centers and membership values using a real-coded genetic representation. This step allows the algorithm to automatically determine the number of clusters in the image. The non-dominated sorting genetic algorithm II (NSGA-II) is used to generate a set of non-dominated solutions that represent the trade-off between the various objective functions of the algorithm. The algorithm then uses a cluster validity index that incorporates non-local spatial information to select the best clustering solution from this set. The cluster validity index ensures that the clustering solution has high intra-cluster similarity and low inter-cluster similarity while taking into account the spatial relationships between pixels.

Ding and Fu (Ding and Fu, 2016) described a novel clustering algorithm that utilizes fuzzy C-means clustering, a genetic algorithm, and a kernel function to enhance the performance of traditional clustering techniques. The algorithm involves several steps, including mapping the original feature space to a high-dimensional space using a kernel function and applying the FCM algorithm to generate initial cluster centers. A genetic algorithm is then used to optimize the initial cluster centers and membership values. The genetic algorithm begins by generating a random set of solutions that represent the initial population, each including cluster centers and membership values. Fitness evaluation is based on the accuracy of cluster assignments and the proximity of data points to their assigned cluster centers. A subset of the population is selected based on fitness scores for reproduction, generating a new solution by combining the genetic information of two parent solutions through the crossover. A small percentage of the population is randomly selected for mutation, introducing new genetic diversity that can change both the cluster centers and membership values. The genetic algorithm then replaces the least fit individuals in the population with the newly generated solutions to improve overall fitness.

Zhao et al. (Zhao et al., 2018) proposed a multi-objective evolutionary clustering algorithm (MOECA) for image segmentation that can handle noisy and complex data distributions. It uses a real variable string length coded strategy, a noise-robust mechanism, and a multi-objective fitness function allows for a more flexible and adaptive clustering solution that can automatically determine the number of clusters based on the data characteristics. The use of a crowded binary tournament selection method, crossover, and mutation operators also helps to improve the diversity of the population and increase the chances of finding a high-quality clustering solution. Singh et al. (Singh et al., 2020) proposed a method for segmenting MRI data using a combination of an antlion optimization algorithm and fuzzy c-means clustering. The goal of their method is to produce effective segmentation of MRI data that is completely user independent. The authors proposed to use a multi-objective antlion optimization algorithm (Mirjalili et al., 2017) which is a nature-inspired optimization algorithm to determine the optimal initialization of cluster centers for the FCM algorithm, by minimizing both the cluster compactness and fuzzy hyper-

volume fitness functions. The result of multi-objective optimization is a set of solutions, each representing a different segmentation result. The optimal solution is chosen based on the minimum value of the partition entropy index. The authors also introduced a new cluster validity index. This index evaluates the quality of the clustering results based on the within-cluster and between-cluster distances. By combining the multi-objective FCM segmentation and the new cluster validity index, the proposed algorithm can automatically determine the optimal number of clusters and provide accurate segmentation results without the need for user intervention.

Alomoush et al. (Alomoush et al., 2022) proposed a novel grayscale image segmentation algorithm that combines the Firefly mate algorithm (FMA) with Fuzzy C-means (FCM) to improve the segmentation accuracy. The algorithm utilizes FMA to optimize the number of clusters and initial cluster centers' values, which serve as the search space for FCM. A population of fireflies is generated, with each firefly representing a candidate solution in the search space. The brightness of each firefly represents its fitness value, which is evaluated using the FCM objective function. This function measures the degree of membership of each pixel to each cluster and is used to determine how well the corresponding solution performs in the segmentation task. The movement of the fireflies is assured by the attractiveness and randomness factors, where the attractiveness factor is proportional to the brightness of the firefly being attracted, and the randomness factor is a random number between 0 and 1. As the fireflies move towards each other, their brightness decreases with increasing distance between them. After a maximum number of iterations, the best solution is selected as the one with the highest brightness and is considered as the number of clusters and initial cluster centers' values for the FCM algorithm.

3.6 FCM Clustering Methods with Spatial Constraints

The Fuzzy C-Means (FCM) algorithm is a popular clustering algorithm that is widely used for clustering data. However, it is known to be sensitive to noise and other imaging artifacts, which can significantly affect the clustering results. This is because FCM treats each data point independently, without considering its neighboring pixels. As a result, noisy or outlier pixels can be assigned to the wrong cluster, or neighboring pixels that belong to the same cluster can be assigned to different clusters. This limitation can be more severe when the data is highly noisy, making it difficult for FCM to identify meaningful clusters in the data. To overcome this limitation, various spatial FCM algorithms have been proposed that incorporate spatial information. These algorithms utilize the spatial relationships between pixels to identify spatially coherent regions and assign them to the same cluster. This can reduce the impact of noise and other imaging artifacts on the clustering results and lead to more accurate and reliable segmentation. The FCM variants with spatial constraints can be broadly categorized into two types: Input image generation-

based methods that preprocess the input data to generate a new image for FCM algorithm and objective function modification-based methods that modify the objective function by considering both the spatial and intensity information.

3.6.1 Input image generation-based methods

Input image generation-based methods preprocess the input data by generating a new image that retains the local data structure while minimizing the noise impact. This new image is then used as input for the FCM algorithm. The generated image serves as a representation of the input data with reduced noise, resulting in an improved suitability for clustering.

Szilàgyi et al. (Szilagyi et al., 2003) introduced their enhanced fuzzy C-mean (EnFCM) algorithm in which a linearly-weighted sum of the input image and the average image is generated using the following equation

$$g_l = \frac{1}{1+\alpha}\left(x_l + \frac{\alpha}{N_R}\sum_{r\in N_r} x_r\right) \tag{3.4}$$

In the clustering process, the grey level histogram is used instead of pixel intensity values; the objective function of EnFCM used for clustering image g is defined as

$$J = \sum_{i=1}^{C}\sum_{l=1}^{L}\gamma_l u_{il}^m \|g_l - v_i\|^2 \tag{3.5}$$

Where L denotes the number of gray levels in the image, and $_l$ is the number of pixels having an intensity equal to g_l. The membership values and the cluster centers are updated using the following equations

$$u_{il} = \left(\frac{\|g_l - v_i\|^2}{\sum_{k=1}^{C}\|g_l - v_k\|^2}\right)^{\frac{1}{m-1}} \tag{3.6}$$

$$v_i = \frac{\sum_{l=1}^{L}\gamma_l u_{il}^m g_l}{\sum_{l=1}^{L}\gamma_l u_{il}^m} \tag{3.7}$$

The segmentation result of EnFCM is comparable to FCM algorithm, and it is converged faster. However, it still shares a common challenge to specify which controls the trade-off between the original and the neighboring information, the selection of α is not an easy task. The EnFCM assigns the same weight to the neighboring pixels, thus may accelerate the clustering process, nevertheless, the image blurring is unavoidable, which may lead to inaccurate clustering.

Cai et al. (Cai et al., 2007) proposed a Fast Generalized FCM algorithm (FGFCM) for robust clustering, the authors introduced a new similarity measure S_{ij} that integrates

both local spatial S_{ij}^{s} and grey level S_{ij}^{g} information to form a non-linearly weighted sum image, the similarity measure S_{ij} is represented according to the following equation

$$S_{ij} = \begin{cases} S_{ij}^{s} \times S_{ij}^{g}, & \text{if } i \neq j \\ 0, & \text{if } i = j \end{cases} \tag{3.8}$$

S_{ij} is the distance from x_i to one of its neighboring pixels x_j, and it is defined as follows

$$S_{ij}^{s} = \exp\left(-\frac{\max(|p_{c_j} - p_{c_i}|, |q_{c_j} - q_{c_i}|)}{\lambda_s}\right) \tag{3.9}$$

S_{ij}^{g} denotes the difference between the grey level of pixel x_i and the grey level of its neighbors x_j

$$S_{ij}^{g} = \exp\left(-\frac{\|x_i - x_j\|^2}{\lambda_g \times \sigma_i}\right) \tag{3.10}$$

Where σ_i is defined as

$$\sigma_i = \sqrt{\frac{\sum_{j \in N_i} \|x_i - x_j\|^2}{|N_i|}} \tag{3.11}$$

Where $(p_{c_i},\ q_{c_j})$ describe the co-ordinates of the pixel x_i, $_i$ is the average grey-level difference between x_i and its neighbor pixels x_i, and λ_s and λ_g represent scaling factors. The new generated image g is calculated using the following equation

$$g_i = \frac{\sum_{j \in N_i} S_{ij} x_j}{S_{ij}} \tag{3.12}$$

The FGFCM algorithm shows fast clustering convergence and robust segmentation results. However, it does not directly apply to the original image. It requires some specification parameters step that to control the trade-off between robustness to noise and the effectiveness of preserving the details. The selection of these parameters is not an easy task and has to be performed by experience or by utilizing the trial-and-error method.

Wang et al. (Wang et al., 2020) proposed a robust fuzzy c-means (FCM) clustering algorithm for noise image segmentation. The algorithm includes two main steps: In the first step, a fast bilateral filter is applied to the original image for incorporating the local spatial information. In the second step, the filtered image and the original image are used to perform fuzzy clustering. The bilateral filter used in the algorithm takes into account both the spatial location and intensity differences between pixels. It is defined by the following equation:

$$w(x_j) = \exp\left(-\frac{(p_j - p_r)^2 + (q_j - q_r)^2}{2\sigma_d^2} - \frac{\|x_j - x_r\|^2}{2\sigma_r^2}\right) \tag{3.13}$$

The filtered value $\bar{x}_j$ for each pixel x_j in the image is given by

$$\bar{x}_j = \frac{\sum_{r \in N_j} x_r w(x_j, x_r)}{\sum_{r \in N_j} w(x_j, x_r)} \tag{3.14}$$

Where σ_d and σ_r are geometric spread and photometric spread respectively. σ_d controls the spatial extent of the filter while σ_r controls the range of intensities that are included in the filtering process. Specifically, σ_d determines the size of the neighborhood around each pixel that is considered in the filter, while σ_r determines how much weight is given to the intensity difference between the center pixel and its neighbors.

The objective function of the proposed method is defined as

$$J_{\text{FCM\_SICM}} = \sum_{i=1}^{C} \left(\sum_{j=1}^{n} \left(\alpha u_{ij}^m \left\| x_j - v_i \right\|^2 + \beta u_{ij}^m \left\| (\bar{x}_j) - v_i \right\|^2 \right) \right) / \left(\ln^2 \left(\sum_{e=1}^{n} u_{ie+1} \right) \right) \tag{3.15}$$

The objective function includes two terms: the first term measures the distance between the data point and the cluster center, while the second term measures the distance between the data point and the local mean of the filtered image.

The parameters α and β are used as constraints to control the influence of the two terms in the objective function. When the intensity difference between the original pixel and the bilateral filtered pixel is larger, the segmentation result is largely influenced by the bilateral filtered image (β is larger) and less influenced by the original image (α is small). α and β are defined using the following equations

$$\beta = \left\| x_j - \bar{x}_j \right\| \tag{3.16}$$

$$\alpha = \frac{1}{\left\| x_j - \bar{x}_j \right\|} \tag{3.17}$$

The membership function and cluster centers are modified using both the fast bilateral filtered image and the original image. This is achieved by updating the membership function and cluster centers using the following modified equations, respectively:

$$u_{ij} = \frac{\left((1 - k(x_j, v_i)) + \alpha (1 - k(\bar{x}_j, v_i)) \right)^{-\frac{1}{(m-1)}}}{\sum_{k=1}^{C} \left((1 - k(x_j, v_k)) + \alpha (1 - k(\bar{x}_j, v_k)) \right)^{-\frac{1}{(m-1)}}} \tag{3.18}$$

$$v_i = \frac{\sum_{j=1}^{N} u_{ij}^m (\alpha x_j + \beta \bar{x}_j)}{\sum_{j=1}^{N} u_{ij}^m \left(\frac{1+\beta^2}{\beta} \right)} \tag{3.19}$$

3.6.2 Objective function modification-based methods

In this section, we will discuss a class of methods for spatial FCM algorithm that aim to modify the objective function of the standard FCM by incorporating additional spatial

information into the clustering process. These methods have been developed to address the limitations of traditional FCM, which is based solely on the pixel intensity values and does not consider the spatial relationships between pixels. The objective function is modified to consider both the spatial and intensity information. Typically, the objective function contains two terms: the traditional FCM objective function that minimizes the distance between each pixel and its assigned cluster center, and a regularization term that incorporates the spatial information. The regularization term can be formulated in different ways. Moreover, these algorithms can effectively balance the impact of spatial information and image intensity values on the clustering results. These methods help to reduce the impact of noise and improve the accuracy and robustness of image segmentation results.

Ahmed et al. (Ahmed et al., 2002) proposed a modified version of the Fuzzy C-Means (FCM) algorithm called FCM_S. The objective function of FCM_S includes an additional term that incorporates spatial information into the clustering process by allowing the pixel labeling to be influenced by its neighboring pixels. The objective function is defined as:

$$J_m = \sum_{i=1}^{C}\sum_{j=1}^{n} u_{ij}^m \|x_j - v_i\|^2 + \frac{\alpha}{N_R}\sum_{i=1}^{C}\sum_{j=1}^{n} u_{ij}^m \sum_{r\in N_j} \|x_r - v_i\|^2 \tag{3.20}$$

Where d (x_j,v_i) is the distance between the pixel x_j and the cluster center v_i, N_j is the set of neighbors of x_j, N_R is the cardinality of neighbors in a window around x_j, α controls the effect of the penalty. The membership values and the cluster centers are updated using the following equations

$$u_{ij} = \left(\frac{\left(\|x_j - v_i\|^2 + \frac{\alpha}{N_R}\sum_{r\in N_j}\|x_r - v_i\|^2\right)^{-\frac{1}{m-1}}}{\sum_{k=1}^{C}\left(\|x_j - v_k\|^2 + \frac{\alpha}{N_R}\sum_{r\in N_j}\|x_r - v_k\|^2\right)^{-\frac{1}{m-1}}} \right) \tag{3.21}$$

$$v_i = \frac{\sum_{j=1}^{n} u_{ij}^m (x_j + \frac{\alpha}{N_R}\sum_{r\in N_j} x_r)}{(1+\alpha)\sum_{j=1}^{n} u_{ik}^m} \tag{3.22}$$

FCM_S is effective in segmenting images corrupted by noise, outliers, and other imaging artifacts, However, its convergence speed is slower than the traditional FCM algorithm, and it may result in the loss of fine detail image information due to the penalty term. Chen and Zhang (Chen and Zhang, 2004) proposed two low complexity variants to the FCM_S algorithm to address its slow convergence. The (FCM_S1) and (FCM_S2) algorithms replace the neighboring term with the mean and median of neighboring pixels falling within a window centered at x_j, respectively. These variants have a similar objective function as FCM_S, but with a different term for neighborhood influence. The optimized objective function can be written as

$$J(U,V) = \sum_{i=1}^{C}\sum_{j=1}^{n} u_{ij}^m ||x_j - v_i||^2 + \alpha\sum_{i=1}^{C}\sum_{j=1}^{n} u_{ij}^m ||(\overline{x}_j - v_i)||^2 \tag{3.23}$$

To minimize this objective function, the following equations are iterated:

$$u_{ij} = \frac{\left(\|x_j - v_i\|^2 + \alpha \|\bar{x}_j - v_i\|^2\right)^{-\frac{1}{(m-1)}}}{\sum_{k=1}^{C}\left(\|x_j - v_k\|^2 + a \|\bar{x}_j - v_k\|^2\right)^{-\frac{1}{(m-1)}}} \tag{3.24}$$

$$v_i = \frac{\sum_{j=1}^{n} u_{ij}^m (x_j + \alpha \overline{x}_j)}{(1+\alpha)\sum_{j=1}^{n} u_{ij}^m} \tag{3.25}$$

These variants are computationally simpler and have a faster convergence speed than FCM_S. However, they may also result in the loss of fine image details due to the use of the mean or median of neighboring pixels.

The authors replaced the traditional Euclidean distance with a Gaussian kernel-induced distance in their objective function. Specifically, they defined a kernel version of the objective function as:

$$(J(U,V))^K = \sum_{i=1}^{C}\sum_{j=1}^{n} u_{ij}^m (1 - k(x_j, v_i)) + \alpha \sum_{i=1}^{C}\sum_{j=1}^{n} u_{ij}^m (1 - k(\overline{x}_j, v_i)) \tag{3.26}$$

The resulting update equations for minimizing this objective function are:

$$u_{ij} = \frac{((1 - k(x_j, v_i)) + \alpha(1 - k(\bar{x}_j, v_i)))^{-\frac{1}{(m-1)}}}{\sum_{k=1}^{C}((1 - k(x_j, v_k)) + a(1 - k(\bar{x}_j, v_k)))^{-\frac{1}{(m-1)}}} \tag{3.27}$$

$$v_i = \frac{\sum_{j=1}^{n} u_{ij}^m \left(k(x_j, v_i)x_j + \alpha k(\overline{x}_j, v_i)\overline{x}_j\right)}{\sum_{j=1}^{n} u_{ij}^m k(x_j, v_i) + \alpha k(\overline{x}_j, v_i)} \tag{3.28}$$

where $K(x_j, v_i) = \exp\left(\frac{-|x_j - v_i|}{\sigma^2}\right)$

Different kernel functions can be used in place of the Euclidean distance to customize the clustering algorithm for different purposes. However, the Gaussian kernel function is often preferred for its versatility and effectiveness in practice. In summary, Chen and Zhang's modification of the FCM algorithm using a Gaussian kernel-induced distance allows for more flexible clustering that can capture non-linear relationships between data points and centroids. The Gaussian kernel function is a widely used and effective option for incorporating local structure and relationships in the clustering process.

The influence of neighboring terms in FCM_S clustering can be controlled by adjusting the parameter for spatial bias correction. However, this parameter has a significant impact on the clustering results, making it crucial to be able to adjust each spatial bias correction term separately for each cluster. To address this, Yang and Tsai(Yang and Tsai, 2008) proposed a modified objective function that replaces the overall parameter α with η_i,

which is correlated to each cluster i. The new objective function is defined as

$$J_m^G = \sum_{i=1}^{C}\sum_{j=1}^{n} u_{ij}^m(1-k(x_j,v_i)) + \sum_{i=1}^{C}\sum_{j=1}^{n} \eta_i u_{ij}^m(1-k(\bar{x_j},v_i)) \tag{3.29}$$

The parameter η_i is calculated using the following equation

$$\eta_i = \frac{\min_{i'\neq i}(1-k(v_{i'},v_i))}{\max_k(1-k(v_k,\bar{x}))} \tag{3.30}$$

The separation of the data set of the i-th cluster is measured by $\min_{i'\neq i}(1-k(v_{i'},v_i))$ where a larger value indicates that it is well separated from other clusters. The total separation of the data set is measured by $\max_k(1-k(v_k,\bar{x}))$ and the ratio of these two terms can be used to effectively measure the cluster separation strength.

The update equations for the membership function and cluster centers are defined according to the equations

$$u_{ij} = \frac{((1-k(x_j,v_i)) + \eta_i(1-k(\bar{x_j},v_i)))^{-\frac{1}{m-1}}}{\sum_{k=1}^{C}((1-k(x_j,v_k)) + \eta_i(1-k(\bar{x_j},v_k)))^{-\frac{1}{m-1}}} \tag{3.31}$$

$$v_i = \frac{\sum_{j=1}^{n} u_{ij}^m\left(K(x_j,v_i)x_j + \eta_i K(\bar{x_j},v_i)\bar{x}\right)}{\sum_{j=1}^{n} u_{ij}^m K(x_j,v_i) + \eta_i K(\bar{x_j},v_i)} \tag{3.32}$$

Yang and Tsai (Yang and Tsai, 2008) proposed a method that allows for adjusting the spatial bias correction term separately for each cluster, leading to improved cluster separation and higher accuracy in certain datasets. This approach also demonstrates better resilience to noise and outliers compared to traditional FCM. However, one drawback of this method is the increased computational resource requirement due to the additional calculations necessary for adjusting the spatial bias correction term for each cluster. Moreover, in datasets with highly overlapping clusters, the separation strength measure may not accurately capture the extent of overlap between clusters, which can impact the method's performance.

Chuang et al. (Chuang et al., 2006) presented a novel method for image segmentation that integrates spatial information into the membership function. The membership function is defined as the sum of memberships in the neighborhood of each pixel considered, represented as:

$$h_{ij} = \sum_{r\in N_j} u_{ir} \tag{3.33}$$

The proposed method assumes that a pixel x_j belongs to cluster i if the majority of its neighboring pixels belong to that cluster. The final membership function is obtained by combining the spatial information and the global membership function, using the following

equation

$$u'_{ij} = \frac{u_{ij}^p h_{ij}^q}{\sum_{k=1}^{C} u_{ik}^p h_{ik}^q} \tag{3.34}$$

The sFCM algorithm requires the specification of two parameters: p and q. These parameters control the importance of the spatial information and global membership function, respectively. However, using spatial information in sFCM may lead to a loss of detail on region boundaries.

Krindis and Chatzis (Krinidis and Chatzis, 2010) proposed a robust fuzzy local information c-means clustering algorithm (FLICM), which incorporates a new factor into the objective function of FCM. This factor is defined by the following equation

$$G_{ij} = \sum_{r \in N_i, j \neq r} \frac{1}{d_{jr}+1}(1-u_{ir})^m \|x_r - v_i\|^2 \tag{3.35}$$

The factor G_{ij} is not affected by any specification parameter and expresses the importance of pixels within the local window. It adapts flexibly according to its distance from the central pixel, using Euclidean distance. The factor reflects the damping extent of the neighbors based on spatial distance from the center pixel. The balance between insensitivity to noise and preservation of image details is automatically achieved by the fuzziness of each pixel. The objective function and membership function of FLICM have been redefined as follows:

$$J = \sum_{i=1}^{C} \sum_{j=1}^{n} u_{ij}^m \|x_j - v_i\|^2 + G_{ij} \tag{3.36}$$

$$u_{ij} = \frac{(\|x_j - v_i\|^2 + G_{ij})^{\frac{1}{m-1}}}{\sum_{k=1}^{C} (\|x_j - v_k\|^2 + G_{kj})^{\frac{1}{m-1}}} \tag{3.37}$$

The proposed fuzzy factor aims to enhance the similarity of membership degrees among pixels within a local window, thereby reducing the impact of noise on the image. However, treating adjacent pixels as a single category may not be appropriate in all scenarios, especially when dealing with high levels of noise, as it can adversely affect the segmentation results. To address this issue, it is preferable to assign similar pixels to the same cluster rather than strictly relying on adjacency-based membership. Additionally, relying solely on Euclidean distance may result in the exclusion of pixels located farther away from the central pixel, further compromising segmentation accuracy. Nonetheless, FLICM offers the advantage of parameter-free selection and demonstrates promising performance in image segmentation tasks.

Gong et al. (Gong et al., 2013) extended the FLICM algorithm to kernel space (KWFLICM) to achieve a balance between kernel-based fuzzy local factors and kernel

space distance metrics. The kernel fuzzy factor, G_{ij}, is defined as follows:

$$G_{ij} = \sum_{r \in N_i, j \neq r} w_{jr}(1 - u_{ir})^m \|\Phi(x_r) - \Phi(v_i)\|^2 \tag{3.38}$$

Where $\phi()$ is a nonlinear mapping method. The weight w_{jr}, is defined as the product of spatial information constraint w_{SC} and intensity information constraint w_{gc}.

$$w_{jr} = w_{sc} \cdot w_{gc} \tag{3.39}$$

The spatial information constraint, w_{SC} is defined as:

$$w_{sc} = \frac{1}{d_{jr} + 1} \tag{3.40}$$

Where d_{jr} is the Euclidean distance between the spatial coordinates of j-th and r-th pixels. The intensity information constraint, w_{gc}, is defined as

$$w_{gc} = \begin{cases} 2 + \varphi_{jr}, & C_r < \bar{C} \\ 2 - \varphi_{jr}, & C_r > \bar{C} \end{cases} \tag{3.41}$$

Where C_r is the coefficient of variation of pixel intensity, calculated as

$$C_r = \frac{\text{var}(x_r)}{(x_r)^2} \tag{3.42}$$

And $\bar{C}$ is the average coefficient of variation of pixel intensity in the neighborhood of the central pixel. The value of C_r is mapped into kernel space using Ξ_{jr}, which is calculated as

$$\Xi_{jr} = \exp(-(C_r - \bar{C})^2) \tag{3.43}$$

Finally, φ_{jr} is obtained by normalizing Ξ_{jr} to get the weight of the neighbor pixel x_r to the central pixel x_j

$$\varphi_{jr} = \frac{\Xi_{jr}}{\sum_{k \in N_j, j \neq k} \Xi_{jk}} \tag{3.44}$$

KWFLICM improves the segmentation accuracy of FLICM by incorporating a kernel-based fuzzy local factor and a kernel space distance metric. It shows promising results in image segmentation, particularly in handling complex and noisy images. However, it has limitations in terms of computational efficiency and requires careful parameter selection.

FLICM is a widely used clustering method for image segmentation, but it faces limitations when dealing with noisy images. To address this limitation, Zhang et al. (Zhang et al., 2017) proposed an enhancement to the FLICM algorithm by incorporating non-local information. They introduced the concept of the damping extent, which determines the

influence of neighboring pixels on the central pixel. In traditional FLICM, the damping extent is calculated based on the Euclidean distance between the neighboring pixels and the central pixel. However, this approach may not be reliable for noisy pixels as the influence of neighboring pixels cannot be accurately assessed.

To overcome this limitation, Zhang et al. (Zhang et al., 2017) utilized non-local information to estimate the damping extent. They defined the damping extent as the patch similarity between the considered pixels, taking into account the similarity between patches of neighboring pixels and the central pixel. This enabled a more accurate estimation of the damping extent, even in the presence of noisy pixels. The authors incorporated this non-local information into the fuzzy factor G_{ij} of the FLICM algorithm, which represents the impact of neighboring pixels on the central pixel. They used Eq. (3.45) to calculate the new fuzzy factor that incorporates non-local information

$$G_{ij} = \sum_{r \in N_i, j \neq r} w_{jr} \left(1 - u_{ir}\right)^m \left\|x_r - v_i\right\|^2 \tag{3.45}$$

where w_{jr} is a weight parameter, u_{ir} is the membership of the central pixel, x_r is the intensity value of the neighboring pixel, and v_i is the cluster center of the central pixel.

The introduced method utilizes Eq. (2.9) and Eq. (3.37) for updating the membership and cluster centers, respectively. However, significant enhancements have been made to the algorithm. Firstly, it considers the influence of faraway pixels that exhibit similar configurations to the central pixel, which can have an impact on the central pixel as well. Secondly, non-local information is incorporated to estimate the damping extent, defined as the patch similarity between the considered pixels. These improvements enhance the robustness of the algorithm and improve its ability to handle image noise.

Wang et al. (Wang et al., 2008) proposed an extension to the Fuzzy C-Means (FCM) clustering algorithm that incorporates both local and non-local neighboring information to improve its sensitivity to noise. The distance measurement between a data point x_j and a cluster center v_i is defined as follows:

$$D(x_j, v_i) = \alpha_j d_{nl}^2(x_j, v_i) + (1 - \alpha_j) d_l^2(x_j, v_i) \tag{3.46}$$

Where $d_n l(x_j, v_i)$ and $d_l(x_j, v_i)$ represent the non-local and local distance measures, respectively, and α controls the trade-off between them. The local distance measure is given by:

$$d_l(x_j, v_i) = \frac{\sum_{r \in N_j} e^{-\frac{|x_r - x_j|}{\delta^2}} d^2(x_r, v_i)}{\sum_{r \in N_j} w_l(x_r, x_j)} \tag{3.47}$$

Here, δ is a spatial scale factor that controls the size of the local window, and $\bar{x_j}$ represents the mean intensity of the pixels within the window N_j. The non-local distance measure is

defined as

$$d_{\mathrm{nl}}(x_j, v_i) = \sum_{x_r \in I} w_{\mathrm{nl}}(x_r, x_j) d^2(x_r, v_i) \tag{3.48}$$

Where w_{nl} represents the weights of neighboring pixels in a larger spatial region centered at x_j. The weight w_{nl} (x_r,x_j) is calculated based on the similarity between the pixel intensities of x_j and x_r. The weight function w_{nl} is defined as

$$w_{\mathrm{nl}}(x_r, x_j) = \frac{1}{Z(x_j)} e^{-\frac{|v(\eta_r) - v(\eta_j)|}{h^2}} \tag{3.49}$$

Where η_j is the vector of neighboring intensities of x_j, and its components are denoted by $v(\eta_j)$. The intensity value x_r has a significant effect on x_j if η_r is more similar to η_j. $Z(x_j)$ is a normalized factor, defined as:

$$Z(x_j) = \sum_{x_r \in I} e^{-\frac{|v(\eta_r) - v(\eta_j)|}{h^2}} \tag{3.50}$$

The decay of the exponential function in w_{nl} is controlled by the parameter h, which is defined as:

$$h = \left(\sum_{r \in N_j} (x_r - x_j)^2 \right)^{1/2} \tag{3.51}$$

The proposed algorithm offers several advantages, such as effective noise handling, robustness against intensity variations, and preservation of image details. However, it also has some drawbacks. Firstly, the algorithm exhibits high computational complexity and memory requirements due to the large number of pixels and the need to calculate distances between each pixel and cluster centers. This can limit its applicability to large-scale datasets or resource-constrained environments. Additionally, the algorithm's performance is highly dependent on the proper tuning of its parameters, such as the spatial and intensity bandwidths. Finding the optimal parameter values can be challenging and may require extensive experimentation and domain knowledge.

The conditional spatial fuzzy C-means algorithm (csFCM) introduced in (Adhikari et al., 2015) defines a probability function f_{ij} for each pixel x_j based on its neighboring pixels. The equation for f_{ij} is:

$$f_{ij} = \frac{N_{ij}}{M_j} \tag{3.52}$$

Where M_j is the total number of neighboring pixels x_k of x_j, N_{ij} is the number of neighboring pixels of x_j that belong to the i-th cluster according to the current segmentation result. The modified objective function of csFCM is defined as:

$$J(U, P,) = \sum_{i=1}^{C} \sum_{j=1}^{n} u_{ij}^m \left\| x_j - p_i \right\|^2 + \alpha f_{ij}^{-1} \xi_{ij}^m \left\| \bar{x}_j - p_i \right\|^2 \tag{3.53}$$

Where Ξ is a new membership matrix, in which xi_{ij} indicates the belonging value of x_j. The iterative optimization of csFCM is achieved according to the following equations:

$$\xi_{ij} = (f_{ij})^{\frac{1}{m-1}} \Big/ \left(\sum_{k=1}^{C} \left(\frac{f_{kj}\bar{d}_{ij}^2}{\bar{d}_{kj}^2} \right)^{\frac{1}{m-1}} \right) \tag{3.54}$$

$$p_i = \frac{\sum_{j=1}^{n} \left(u_{ij}^m x_j + \alpha f_{ij}^{-1} \xi_{ij}^m \bar{x}_j \right)}{\sum_{j=1}^{n} \left(u_{ij}^m + \alpha f_{ij}^{-1} \xi_{ij}^m \right)} \tag{3.55}$$

Where $\bar{d}_{ij}^2 = \|\bar{x}_j - p_i\|^2$ and $d_{ij}^2 = \|x_j - p_i\|^2$ the final membership is defined by combining the membership of the central pixel x_j and the membership of neighboring ξ_{ij}. The membership function and the cluster center are derived as:

$$u'_{ij} = \frac{u_{ij}^p \xi_{ij}^q}{\sum_{k=1}^{C} u_{ik}^p \xi_{ik}^q} \tag{3.56}$$

$$v_i = \frac{\sum_{j=1}^{n} u_{ij}'^m x_j}{\sum_{j=1}^{n} u_{ij}'^m} \tag{3.57}$$

The parameters p and q are used to control the importance of both membership functions. The weight f_{ij} is updated in each iteration of the csFCM algorithm. Therefore, after determining the membership z_{ik}, a segmentation result can be achieved by assigning each pixel to the class that maximizes its membership value.

The csFCM algorithm combines both local and global spatial information, making it robust in handling noisy images to a certain extent. The parameter α controls the influence of the neighborhood of a pixel on itself. In other words, csFCM incorporates neighborhood information into the objective function, leading to an immediate update of the membership function by combining the neighborhood information. The final membership function update can be seen as an additional step that utilizes neighborhood information to improve memberships and reduce noise. However, in cases where the image is heavily corrupted by noise and inhomogeneity, the csFCM algorithm may yield undesired results. Incorporating spatial information and inhomogeneity into the membership function can be a suitable technique to enhance its performance.

In the presence of high levels of noise in an image, the neighboring pixels of a pixel may also contain abnormal features, and fuzzy clustering algorithms based on local spatial information may not achieve satisfying segmentation performance. For each pixel, there are multiple pixels that have a similar neighborhood configuration with a particular pixel, so it is more appropriate to use these pixels to describe the spatial information of that pixel. This kind of information is called non-local spatial information. In (Zhao, 2013) a fuzzy c-means clustering algorithm with self-tuning non-local spatial information FCM_SNLS is introduced. In FCM_SNLS, the non-local spatial information is used instead of spatial

information, and the calculation of the filtering degree parameter is achieved by studying the statistical characteristics in the search window. For pixel x_j, its spatial information is defined according to the following formula:

$$\theta_j = \sum_{r \in N_j} w_{jr} x_r \tag{3.58}$$

Where N_j is the search window centered at x_j. This reveals that the spatial information θ_j is the weighted average gray value of the neighboring pixels x_r of the pixel x_j. The weight w_{jr} depends on the similarity between the neighborhood configurations of the pixel x_j and its neighboring pixels x_r. The weights w_{jr} are calculated using the following equation

$$w_{jr} = \frac{1}{Z(x_j)} \exp\left(-\frac{\|v(\eta_r) - v(\eta_j)\|_\sigma^2}{h_j h_r}\right) \tag{3.59}$$

Where $Z(x_j)$ is a normalization factor, $v(\eta_r)$ and $v(\eta_j)$ are feature vectors for pixels x_r and x_j, respectively, h_j and h_r are the filtering degree parameters for pixels x_j and x_r, respectively.

The filtering degree parameter h plays a crucial role in determining the quality of spatial information. However, setting an appropriate value for h remains an open problem. If h is set too large, the non-local spatial information of a pixel may lose important image details, especially near edges. On the other hand, if h is set too small, the non-local spatial information may be overly influenced by image noise. Ideally, h should be adaptively determined based on the noise level present in the corrupted image. In the proposed approach, the authors address this issue by adopting an adaptive h value for each pixel, rather than using a single h value for all pixels. For a pixel x_j, its filtering degree parameter h_j can be obtained by analyzing the statistical characteristics within its search window. Specifically, h_j is defined as:

$$h_j = \min_{k \in N_j} \|v(\eta_k) - v(\eta_j)\| \tag{3.60}$$

We indicate that h_j is measured by the similarity between the neighborhood configurations of the pixel x_j and its closest pixel $x_j l$. If this similarity is large, it reveals that the pixel xj, the pixel $x_j l$, and their neighbor pixels are not seriously corrupted by noise, so the filtering degree parameter hj should be small, and vice versa. The determination of h_j can reflect the noise level of the image to some degree. The objective function of FCM_SNLS is defined as:

$$J(U, V) = \sum_{i=1}^{C} \sum_{j=1}^{n} u_{ij}^m \|x_j - v_i\|^2 + \beta \sum_{i=1}^{C} \sum_{j=1}^{n} u_{ij}^m \|\theta_j - v_i\|^2 \tag{3.61}$$

The update equations for the membership function and cluster center in FCM_SNLS

are as follows:

$$u_{ij} = \frac{(\|x_j - v_i\|^2 + \beta\|\theta_j - v_i\|^2)^{\frac{1}{m-1}}}{\sum_{k=1}^{C}(\|x_j - v_k\|^2 + \beta\|\theta_j - v_k\|^2)^{\frac{1}{m-1}}} \tag{3.62}$$

$$v_i = \frac{\sum_{j=1}^{n} u_{ij}^m (x_j + \beta\theta_j)}{(1+\beta)\sum_{j=1}^{n} u_{ij}^m} \tag{3.63}$$

Zhang et al. (Zhang et al., 2021) proposed improvements to the FCM_s (BCFCMLNLI) and FLICM (FLICMLNLI) algorithms by integrating both local and non-local information. The aim of these improvements was to preserve image details through the use of local information and enhance the robustness of the algorithms to image noise through the incorporation of non-local information.

To achieve this, they introduced a correlation model process that consists of several steps. Firstly, image patches X_r are constructed for each pixel i in the image. Next, the differences between corresponding patches in different directions are computed using the following equation:

$$d_j(r) = \frac{1}{|N_j|\sum_{r\in N_j}|X_j - X_r|} \tag{3.64}$$

N_j is the set of neighboring pixels with a cardinality of $|N_j|$. Next, the weights and the weighted distances in different directions are retrieved using Eq. (3.65) and Eq. (3.66), respectively.

$$w_{jr} = \frac{\exp(-\alpha d_j(r))}{\sum_{r\in N_j}\exp(-\alpha d_j(r))} \tag{3.65}$$

$$d_j^w(r) = \frac{1}{|N_j|\sum_{r\in N_j}(w_j \otimes |X_j - X_r|)} \tag{3.66}$$

Finally, the relevance between corresponding pixels is obtained using the following equation

$$s(j,r) = \exp(-\gamma d_j^w(r)) \tag{3.67}$$

In FLICMLNLI (FLICM with local and non-local information) algorithm, the cluster center v_i becomes a vector (v_i, v_i^N). The fuzzy factor is then modified using the following equation

$$G_{ij}^{'} = \sum_{r\in N_j} s(j,r)(1-u_{ir})^m (x_r - v_i)^2 + (x_r^N - v_i^N)^2 \tag{3.68}$$

The objective function of FLICMLNLI is formalized according to the following equation:

$$J(U,V) = \sum_{i=1}^{C}\sum_{j=1}^{n} u_{ij}^m (x_j - v_i)^2 + (x_j^N - v_i^N)^2 + G_{ij}^{'} \tag{3.69}$$

The centers and the memberships are updated according to the following equations

$$v_i^N = \frac{\sum_{j=1}^{n} u_{ij}^m x_j^N}{\sum_{j=1}^{n} u_{ij}^m} \tag{3.70}$$

$$u_{ij} = \frac{1}{\sum_{k=1}^{C} \left(\left(\frac{(x_j - v_i)^2 + (x_j^N - v_i^N)^2 + G'_{ij}}{(x_j - v_k)^2 + (x_j^N - v_k^N)^2 + G'_{kj}} \right)^{\frac{1}{m-1}} \right)} \tag{3.71}$$

Where x_j^N is the local information of x_j.

The FCM_S algorithm suffers from three significant drawbacks. Firstly, it only considers the immediate neighborhood and neglects the larger context of the image, which may result in inaccurate segmentation. Secondly, the algorithm may cause a loss of important image details during the segmentation process. Finally, treating all neighboring pixels equally may lead to inaccurate segmentation results, as the impact of each neighboring pixel on the central pixel can vary significantly.

To address the aforementioned drawbacks, the BCFCMLNLI algorithm adopts a larger searching window, allowing for a broader context in the image. Additionally, the cluster center vi is represented as a vector (v_i, v_i^N), where v_i captures the original information of the image, while v_i^N corresponds to the immediate information of neighboring pixels. This combination of local and non-local information allows for a more comprehensive representation of the image characteristics, leading to improved segmentation accuracy and preservation of important image details.

The objective function of BCFCMLNLI algorithm is reformulated as

$$J(U,V) = \sum_{i=1}^{C}\sum_{j=1}^{n} u_{ij}^m (x_j - v_i)^2 + (x_j^N - v_i^N)^2 + \sum_{i=1}^{C}\sum_{j=1}^{n} u_{ij}^m \sum_{r \in N_j} s(j,r)(x_r - v_i)^2 + (x_r^N - v_i^N)^2 \tag{3.72}$$

The optimization process is achieved by updating v_i, and u_{ij} according to the following equations

$$v_i = \frac{\sum_{j=1}^{n} u_{ij}^m (x_j + \sum_{r \in N_j} s(j,r) x_r)}{\sum_{j=1}^{n} u_{ij}^m (1 + \sum_{r \in N_j} s(j,r))} \tag{3.73}$$

$$u_{ij} = \frac{1}{\sum_{k=1}^{C} \left(\left(\frac{(x_j - v_i)^2 + (x_j^N - v_i^N)^2 + \sum_{r \in N_j} s(j,r)(x_r - v_i)^2 + (x_r^N - v_i^N)^2}{(x_j - v_k)^2 + (x_j^N - v_k^N)^2 + \sum_{r \in N_j} s(j,r)(x_r - v_k)^2 + (x_r^N - v_k^N)^2} \right) \right)^{\frac{1}{m-1}}} \tag{3.74}$$

The two proposed algorithms fully utilize the non-local information by incorporating self-similarity and preserving the original image information through back projection, thereby enhancing the robustness of the algorithms. However, a drawback of these algorithms arises when calculating the Euclidean distance between the considered pixel information and the local pixel information. In this calculation, both types of information are given equal weight, which incorrectly amplifies the role of local information in the distance computation. The excessive inclusion of neighborhood information improves denoising capabilities but fails to accurately preserve fine image details.

3.7 Conclusion and discussion

This chapter discusses various approaches aimed at addressing the limitations of the traditional FCM algorithm. Two main challenges of the FCM algorithm are determining the appropriate number of clusters and initializing cluster centers, which can significantly impact the clustering results. To overcome these challenges, methods for automatically involving the number of clusters and improving the initialization process for cluster centers have been explored. Additionally, a range of FCM derivatives have been introduced to enhance the FCM's robustness against noise and other imaging artifacts.

To address the challenges of determining the number of clusters and initializing cluster centers, validity index-based methods have been commonly used. However, these methods have limitations, such as their accuracy being highly dependent on the choice of index and the potential for multiple local optima, which can lead to suboptimal results. In contrast, metaheuristic-based methods offer the advantage of exploring a larger search space and can potentially find better solutions. However, they often require substantial computing time, especially for large datasets, due to their iterative nature. Additionally, the process of parameter setting for metaheuristic-based methods can be challenging, as the performance of these methods is sensitive to the choice of parameters.

Several methods have been proposed in the literature to improve FCM's sensitivity to noise and intensity inhomogeneity in input images, leading to improved contrast between different tissue types and more accurate segmentation results. However, these methods are often sensitive to the choice of a penalty function and require careful parameter specification to balance noise suppression and detail preservation. Determining these parameters can be challenging and may require expertise or trial-and-error approaches. Additionally, incorporating spatial information into the segmentation process may introduce a trade-off between preserving fine details and achieving smooth segmentations.

To address the challenges associated with FCM-based image segmentation, we propose two techniques to enhance its performance. The first technique is an adaptive split and merge approach, which improves the sensitivity of FCM to the initialization scheme. This approach enables more accurate and reliable cluster center initialization and determination of the number of clusters, which can significantly improve the accuracy of segmentation results. The second technique involves fully considering the spatial constraint to make FCM more robust against noise while preserving important image details. By incorporating spatial information into the segmentation process, we can achieve more accurate and robust segmentation results, which is important for a wide range of applications in fields such as medical imaging and computer vision. By employing these techniques, we aim to enhance the accuracy and robustness of FCM, making it a more effective tool for image segmentation. These techniques have the potential to improve the performance of FCM-based segmentation and can be applied to a wide range of image processing tasks,

including object recognition, tracking, and classification.

Chapter 4

An adaptive split and merge method for FCM image segmentation

Contents

4.1 Introduction

Image segmentation is the process of partitioning an image into regions of high similarity, commonly used in pattern recognition, image processing, and data analysis. The widely used Fuzzy C-Means (FCM) algorithm for image segmentation requires specifying the number of clusters, which is not always known in advance, and can lead to sensitivity to initial cluster centers, resulting in local minimum solutions.

To address these issues, this chapter proposes an improved approach that enhances the accuracy of the FCM algorithm. The proposed method employs an adaptive split-merge technique, effectively dividing the image into homogeneous regions using a multi-threshold method based on entropy information. In the merge process, a new distance metric is introduced to combine the homogeneous regions. The FCM algorithm is then applied using the centers of these regions to generate the different fuzzy partitions. Additionally, a

novel fuzzy validity index is introduced, incorporating a new definition for the separation measure. This fuzzy validity index plays a crucial role in selecting the optimal fuzzy partition with high compactness and separation information.

The proposed approach is evaluated quantitatively and qualitatively, and the results demonstrate its superiority over existing methods in terms of evaluation functions and validity indices.

4.2 Automatic initialization process of FCM algorithm

The FCM algorithm is a commonly used clustering algorithm in various domains. However, its effectiveness is highly dependent on the appropriate initialization of its parameters. A poor initialization can lead to suboptimal or even inaccurate clustering results. To enhance the sensitivity of the FCM algorithm to initialization schemes, we propose an adaptive split-merge approach in the following sections. This approach automatically groups the pixels of an image into different homogeneous regions when the number of clusters is not known beforehand, thereby improving the accuracy of the clustering results.

4.2.1 Problem statement

Unlike traditional clustering algorithms, FCM assigns each pixel in the image to multiple clusters based on their membership degrees in cluster centers. This fuzzy membership concept is particularly useful for handling ambiguous points in boundary regions. However, FCM heavily relies on the selection of the number of clusters and the initial cluster centers, but it is not always possible to determine this number in advance, and these initialization difficulties can affect the segmentation quality. While the difficulty of deciding the cluster number can affect the segmented area and region tolerance for feature variance, the difficulty of obtaining the initial cluster centers can affect the cluster compactness and classification accuracy.

The split and merge method is another popular approach for image segmentation. This method initially considers the entire image as a single segment and iteratively splits segments into quarters if a homogeneity criterion is not satisfied. Similarly, the merge step joins adjacent regions if a homogeneity criterion is met. This approach eliminates the need for specifying the number of clusters in advance and avoids the initialization process. However, it lacks adaptability to image semantics due to its rigid quad-tree structure and requires a termination criterion.

To address the limitations of both the FCM algorithm and the split and merge method, we propose a novel method in this chapter. The proposed method aims to enhance the sensitivity of the FCM algorithm to the initialization scheme while incorporating the benefits of the split and merge approach. The proposed method makes the following key

contributions:

1. An adaptive split-stage is included in our algorithm that effectively divides the image into multiple homogeneous regions. This is achieved using a multi-threshold method based on entropy information, which ensures that the image is split into regions with similar characteristics.
2. During the merge process, we introduce a new distance metric that combines homogeneous regions. This distance metric encourages the merging of regions that exhibit high homogeneity within the merged region and well separation from others. By doing so, we achieve more accurate segmentation results.
3. In addition, we introduce a novel fuzzy validity index that incorporates a new definition for the separation measure. This index serves as a criterion for selecting the optimal fuzzy partition, ensuring both high cluster compactness and effective separation between clusters.

4.2.2 Adaptive split and merge method

In this section, we present a methodology to address the issue of the FCM algorithm's sensitivity to initial values, which often leads to suboptimal local minimum solutions. To overcome this limitation, we introduce an adaptive split and merge method.

During the adaptive split stage, we divide the image into multiple homogeneous regions using a multi-threshold method based on entropy information. This ensures that regions with similar characteristics are grouped together. In the merge stage, we combine regions that are both highly similar within the merged region and effectively separated from others using a newly introduced distance metric.

The merge process is iterated again until the number of regions reaches a predefined number of clusters, denoted as C_{min}. In each merging iteration, the cluster centers and the number of clusters obtained from the merge stage serve as initial parameters for the FCM algorithm, which generates its fuzzy partition. We then use the introduced validity index to evaluate each fuzzy partition and determine the optimal number of clusters and the optimal fuzzy partition based on factors such as the compactness and separation of clusters.

4.2.2.1 The Adaptive Split Stage

The optimal entropy automatic threshold value segmentation algorithm is utilized to measure the entropy of the gray histogram of an image, aiming to identify the threshold that maximizes the amount of information between the target and background in the image (Akay, 2013). The gray level values in the image histogram are defined as $0, 1, ..., l-1$. By normalizing the image histogram, the probability distribution is represented as $p_i = n_i/N$,

where $p_i < 1$ and the sum of all probabilities $p_1 + p_2 + ... + p_{l-1}$ equals 1. Here, N denotes the total number of pixels, and n_i represents the number of pixels with gray level i.

To determine the threshold value, the image is partitioned into two classes: $A = 0, 1, ..., t$ and $B = t+1, t+2, ..., l-1$. The total entropy of the image, denoted as $H(t)$, is calculated as the sum of the entropies of class $A(H_A(t))$ and class $B(H_B(t))$. It is defined by the equation:

$$H(t) = H_A(t) + H_B(t) = -\sum_{i=1}^{t} \frac{P_i}{P_t} \ln\left(\frac{P_i}{P_t}\right) - \sum_{i=t+1}^{l-1} \frac{P_i}{1-P_t} \ln\left(\frac{P_i}{1-P_t}\right) \tag{4.1}$$

Here, $H_A(t)$ and $H_B(t)$ represent the entropies of class A and class B, respectively, while P_t corresponds to the probability of class A. The optimal threshold is chosen as the value of t that maximizes $H(t)$ according to the following equation.

$$\theta = \arg \max_{1<t<l-1} H(t) \tag{4.2}$$

The different steps of the adaptive split stage are outlined in the algorithm 2. Our approach involves considering the range of gray-level values $L_{min}, \ldots, L_{max}$ in the image to define it as non-homogeneous. Our objective is to identify a set of optimal thresholds that can split the image into homogeneous regions.

The proposed algorithm involves several steps to identify homogeneous regions in the image. In step 1, we measure the homogeneity of each region (R_i) using the standard deviation (SD). If the SD of a region is below a specified threshold (T) (step 2), the region is considered homogeneous (step 7). However, if the SD is greater than the threshold (T), we move to step 3. In this step, we assign an initial value to the optimal entropy $H(t^{'})$. Then, in step 4, we calculate the corresponding entropy for each gray-level value using Eq. (4.1). This allows us to identify the optimal threshold value that can be used to split the region into smaller, homogeneous regions.

By utilizing this optimal threshold $t^{'}$, we divide the current region into two regions, namely R and $R^{'}$. Region R represents the gray-level values ranging from t_{min} to $t^{'}$, while region $R^{'}$ represents the gray-level values from $t^{''}$ to L_{max}, where $t^{''}$ is the next gray-level value above $t^{'}$ (step 5).

We recursively partition the regions R and $R^{'}$ if they fail to meet the homogeneity criteria (steps 6 and 9) until no non-homogeneous regions remain (steps 8 and 10). This adaptive split-stage approach allows us to effectively divide the image into multiple homogeneous regions.

From the list of obtained thresholds $t_1, t_2, ..., t_n$, we can easily construct the list of clusters LC. The first cluster is defined by $[L_{min}, t_1]$, and each subsequent cluster is defined by $[t_l + 1, t_2]$. Similarly, the remaining clusters are constructed until the last cluster is defined by $[t_n + 1, L_{max}]$.

Algorithm 2 Adaptive Split Stage

Input:

— The input image I,

— $L_{\min}$, $L_{\max}$ are the minimum and maximum gray-level values of the input image I,

— T is a predefined threshold.

Output: List of thresholds

$t_{\min} \leftarrow L_{\min}, \quad t_{\max} \leftarrow L_{\max}, \quad t' \leftarrow L_{\max}$

// R_i initially is the input image, R_i is defined by $t_{\min}$ and $t_{\max}$

Step 1. Calculate the standard deviation (SD) for the current region R_i

Step 2. If SD $\leq T$ then go to **Step 7**

Step 3. $H(t') \leftarrow -\infty$

Step 4.

for t *from* t_{min} *to* t_{max} **do**
  Compute the corresponding $H(t)$ using Eq. (4.1)
  if $H(t) > H(t')$ **then**
    $H(t') \leftarrow H(t)$
  end
end

Step 5. Split the current region R_i by $t^{'}$

Step 6. $t_{\max} \leftarrow t^{'}$ and go to step 1

Step 7. Add t' to the list of thresholds

Step 8. If $t^{'} = L_{max}$ then go to **Step 10**

Step 9. $t_{\min} \leftarrow t_{\max} + 1$, $t_{\max} \leftarrow L_{\max}$ and go to **Step 1**

Step 10. Stop

4.2.2.2 The Merge Stage

The merge stage of the clustering algorithm (see Algorithm 3) involves joining two clusters together in each step. To determine whether two clusters C_i and C_j should be merged, we calculate the distance between them, denoted as Dist(C_i, C_j), using Eq. (4.3). This distance metric measures the compatibility of merging two clusters by considering the sum of squared distances between the data points x_l within their union ($C_i \cup C_j$) and the mean of the merged cluster $m(C_i \cup C_j)$, divided by the sum of squared Euclidean distances between the merged cluster mean $m(C_i \cup C_j)$ and the means of all other clusters $m(C_k)$ excluding C_i and C_j.

$$Dist(C_i, C_j) = \frac{\sum_{x_l \in C_i \cup C_j} \|x_l - m(C_i \cup C_j)\|^2}{\sum_{\substack{k=1 \\ k \neq i, k \neq j}}^{C-1} \|m(C_i \cup C_j) - m(C_k)\|^2} \tag{4.3}$$

Here, C is the total number of clusters, and U denotes the union of two clusters. The merging procedure is applied to each cluster C_i in the list of clusters LC until the

maximum number of clusters C_{max} is reached. For each cluster C_i, we compute ($NCluster$-1) distances using Eq. (4.3). We then identify the cluster C_k with the smallest distance, $Dist(C_i, C_k)$, from C_i, as well as the cluster C_j with the smallest distance, $Dist(C_k, C_j)$, from C_k. If both C_i and C_k "desire" a merger ($i = j$), we merge them. After merging, the cluster count decreases by one, and we update both the cluster list LC and the cluster center list CC. We sequentially add the new cluster C_{ik} and its mean $m(C_{ik})$ to LC and CC, respectively.

The proposed algorithm applies the merging process once again to the list of clusters LC acquired from the previous step, reducing the cluster count by one ($NCluster \leftarrow NCluster - 1$). The cluster center list CC obtained from the merging process serves as the initial centers for the FCM algorithm. The resultant fuzzy partition is then evaluated using the introduced validity index outlined in Eq. (4.7). This iterative process persists until the minimum number of clusters C_{min} is reached. Finally, the optimal number of clusters and the optimal partition are determined based on their effectiveness in terms of compactness and separation using Eq. (4.8).

Algorithm 3 M-FCM (Merge-FCM algorithm)

Input:

- LC: a list of clusters obtained in the adaptive split stage
- $NCluster$: number of clusters obtained in the adaptive split stage
- C_{min}, C_{max}: the minimum and maximum cluster number

Output: Optimal cluster number with associated partition

```
while NCluster > C_max + 1 do
    foreach cluster C_i of LC do
        k ← get the closest cluster of C_i using Eq. (4.3)
        j ← get the closest cluster of C_k using Eq. (4.3)
        if i = j then
            Unified C_i and C_k into one cluster C_ik
            Compute the new center m(C_ik)
            Insert C_ik and m(C_ik) successively in the list LC and CC
            Delete C_i and C_k (and m(C_i), m(C_k)) from the list LC (CC)
            NCluster ← NCluster - 1
        end
    end
end
while NCluster >= C_min do
    foreach cluster C_i of LC do
        k ← get the closest cluster of C_i using Eq. (4.3)
        j ← get the closest cluster of C_k using Eq. (4.3)
        if i = j then
            Unified C_i and C_k into one cluster C_ik
            Compute the new center m(C_ik)
            Insert C_ik and m(C_ik) successively in the list LC and CC
            Delete C_i and C_k (and m(C_i), m(C_k)) from the list LC(CC)
            NCluster ← NCluster- 1
        end
    end
    Apply FCM(CC, NCluster)
    Calculate the corresponding validity index of the obtained partition using Eq. (4.7)
end
Return the optimal number and its corresponding partition using Eq. (4.8)
```

4.2.2.3 The Proposed Validity Index

A reliable validity index for a fuzzy partition should consider both compactness and separation measures. The compactness measure reflects the concentration of data points within the same cluster, while the separation measure evaluates the isolation of cluster centers from one another. Therefore, an optimal fuzzy partition exhibits both high compactness and separation measures (Xie and Beni, 1991).

Our proposed validity index, VI_{CS}, integrates the measures of compactness ($Comp$) and separation (Sep) to effectively evaluate the quality of a fuzzy partition. Compactness

is assessed by measuring the variation of points belonging to the same cluster. To evaluate how well a pixel x_j has been classified, we utilize the term $\max_{1\leq l\leq C} u_{ij}$, where u_{ij} represents the fuzzy membership of the jth pixel to ith cluster. If $\max_{1\leq l\leq C} u_{ij}$ is closer to 1, the pixel x_j is considered to belong to the ith cluster. For a compact fuzzy partition, we aim for a large value of compactness, as indicated by Eq. (4.5).

To compute the compactness of cluster C_i, we calculate the difference D_{ij} between the maximum fuzzy membership of pixel x_j to any cluster and its fuzzy membership to cluster C_i, as depicted in Eq. (4.4). If the pixel x_j certainly belongs to cluster C_i, D_{ij} is set to 0. Otherwise, D_{ij} lies in the interval]0,1]. We use the term $integer\left(\frac{1}{\exp(D_{ij})}\right)$ to retain only the pixels that clearly belong to cluster C_i. This approach ensures that only pixels with a high degree of membership to cluster C_i are considered in the calculation of compactness. The compactness measure is defined in Eq. (4.5), which computes the sum of the membership degrees values of the retained pixels to cluster C_i divided by the sum of the squared membership degrees of the same pixels. Normalizing the compactness measure ensures that its values range from [0, 1[. A higher value of compactness indicates that the pixels in cluster C_i are tightly packed around the cluster center, which is desirable for a good clustering result.

$$D_{ij} = \max_{1\leq l\leq C} u_{lj} - u_{ij} \tag{4.4}$$

$$Comp(C_i) = \frac{\sum_{j=1}^{n} u_{ij}^2 integer\left(\frac{1}{\exp(D_{ij})}\right)}{\sum_{j=1}^{n} u_{ij} integer\left(\frac{1}{\exp(D_{ij})}\right)} \tag{4.5}$$

Typical validity indices used for measuring separation information in cluster analysis often rely solely on centroid information, which overlooks the geometric structures and overall shape of clusters. To address this limitation, we propose a novel measure of separation information called $Sep(C_i, C_k)$, as depicted in Eq. (4.6). Rather than considering only the distance between the centers of two clusters (C_i, C_k)Our approach provides a more comprehensive measure of separation information that considers the overall shape and structure of clusters, rather than just their centroids. Specifically, in order for two clusters to be considered well-separated, all points x_j in cluster C_i must be far from the center C_k, and likewise, all points x_j in cluster C_k should be far from the center C_i. $Sep(C_i, C_k)$ is computed using the formula shown in Eq. (4.6), which takes into account the distances between all pairs of points in the two clusters.

$$Sep(C_i, C_k) = \frac{\sum_{j=1}^{n} u_{kj}^2 integer\left(\frac{1}{\exp(D_{ij})}\right) + \sum_{j=1}^{n} u_{ij}^2 integer\left(\frac{1}{\exp(D_{kj})}\right)}{\sum_{j=1}^{n} u_{kj} integer\left(\frac{1}{\exp(D_{ij})}\right) + \sum_{j=1}^{n} u_{ij} integer\left(\frac{1}{\exp(D_{kj})}\right)} \tag{4.6}$$

This equation evaluates the separation information between clusters C_i and C_k. It consists of two terms, where the first term measures the separation of points in cluster C_i

from the center of cluster C_k, and the second term measures the separation of points in cluster C_k from the center of cluster C_i. When the two clusters (C_i, C_k) are well-separated, the value of $Sep(C_i, C_k)$ tends to reach a minimum value.

By integrating both compactness and separation information, the total proposed validity index is defined as follows:

$$VI_{CS}(c) = \frac{\sum_{i=1}^{c} Comp(C_i)}{\sum_{i=1}^{c-1} \sum_{j=i+1}^{c} Sep(C_i, C_k)} \tag{4.7}$$

The optimal fuzzy partition corresponds to a large value for compactness ($Comp$) and a small value for separation (Sep). To determine the optimal number of clusters ($C_{Optimal}$) that produces the best clustering, the validity index for cluster selection ($VI_{CS}(c)$) is computed for a range of candidate cluster numbers between C_{min} and C_{max}, using the following equation:

$$C_{Optimal} = \max_{C_{\min} \leq c \leq C_{\max}} \mathrm{VI}_{CS}(c) \tag{4.8}$$

4.3 Experiments and Results

In this section, we present the results of our experiments and discuss their implications. Our goal was to demonstrate the effectiveness of our proposed approach for image segmentation and to compare its performance with state-of-the-art methods.

To evaluate the performance of our approach, we conducted tests on a dataset of over 50 images. We randomly selected a subset of 10 images from the dataset and compared the segmentation results of our approach with those of the state-of-the-art methods.

4.3.1 Evaluation on segmentation results

In this section, we present a qualitative evaluation of the segmentation results obtained by our proposed algorithm and the compared approaches. We visually compare the resultant images obtained by our approach and the other methods for the tested images, which are presented in Figure 4.1 to Figure 4.10.

Figure 4.1 shows the segmentation results of the compared algorithms for Capsicum. We can observe that the other methods exhibit a large number of misclassified pixels, which can result in inaccurate segmentation results. However, our proposed algorithm outperforms these approaches in terms of region uniformity and detail preservation, producing more accurate segmentation results.

From Figure 4.2 we can observe that our approach produces more efficient segmentation results, with better homogeneous segmented regions and an adequate number of clusters obtained.

Figure 4.3 demonstrates the efficacy of the proposed approach in achieving superior

segmentation performance compared to other approaches. The resulting regions exhibit greater homogeneity, and the boundaries are efficiently smoothed.

The segmentation results of the onion image (Figure 4.4) demonstrate that all vegetables are well-clustered, and the background is correctly separated from the other partitions.

In the segmentation results of the Gantry Crane image produced by the comparative approaches (Figure 4.5 (b)-(e)), a significant number of pixels are wrongly assigned as a part of the sky region, and the sky is classified into two clusters. On the other hand, the proposed approach generates more uniform regions and considers the sky as a single cluster (Figure 4.5 (f)).

The segmentation results shown in Figure 4.6 highlight the superiority of the proposed approach over other comparative approaches by producing more homogeneous regions for both the walls and the roof.

Figure 4.7 illustrates that the proposed approach effectively segments the trees, sea, hill, sky, and bridge from the background while preserving the detail information of each region, outperforming the comparative approaches. In contrast, the segmentation results of the other approaches exhibit misclassified pixels from the trees being wrongly assigned to the bridge region.

The image segmentation results of the moon image are displayed in Figure 4.8. Figure 4.8 clearly indicates that the compared algorithms generate a significant number of misclassifications by incorrectly assigning pixels from the moon region to the sky region, whereas the proposed algorithm successfully separates the moon region from the sky region, resulting in more homogeneous regions.

The proposed approach outperforms the comparative approaches in determining the optimal partition of the Hill image, as shown in Figure 4.9. It correctly determines the number of clusters and produces a more accurate segmentation result compared to the other approaches, which still contain wrongly detected regions.

In Figure 4.10, it can be observed that the segmentation results of the smarties image using the proposed approach are superior to those obtained using other approaches. The proposed approach achieves better results with fewer background pixels misclassified as smarties. It accurately segments the smarties while maintaining clear boundaries between the smarties and the background, resulting in more homogeneous regions. This leads to a more accurate segmentation overall compared to the other approaches.

4.3.2 Evaluation of cluster number

Based on the qualitative results presented earlier, the proposed technique demonstrates the ability to automatically and adaptively initialize the distribution of cluster centers and centroid values. The adaptive split stage, which is proposed in this technique, provides a better initialization mechanism for cluster centers, ensuring effective classification ca-

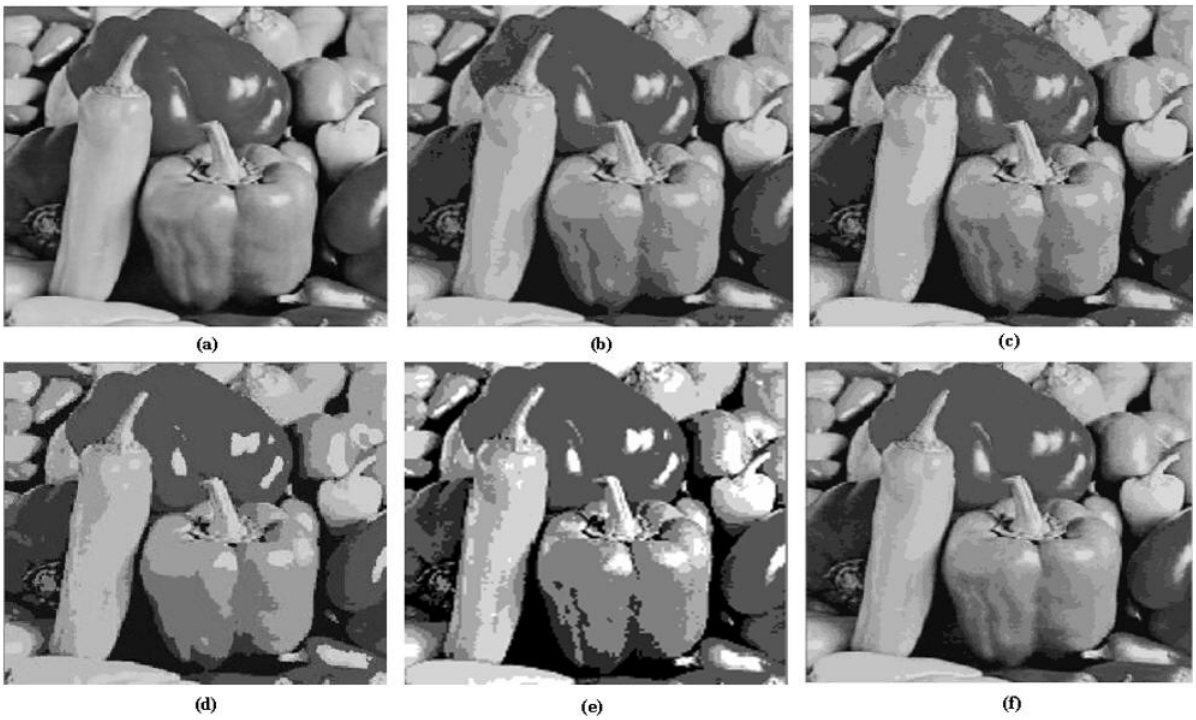

Figure 4.1 – Image segmentation results of the image Capsicums (a) original image (b) FBSA algorithm(c) Fuzzy-VGAPS algorithm(d) MOECA algorithm (e) MSFCA algorithm(f) the proposed approach

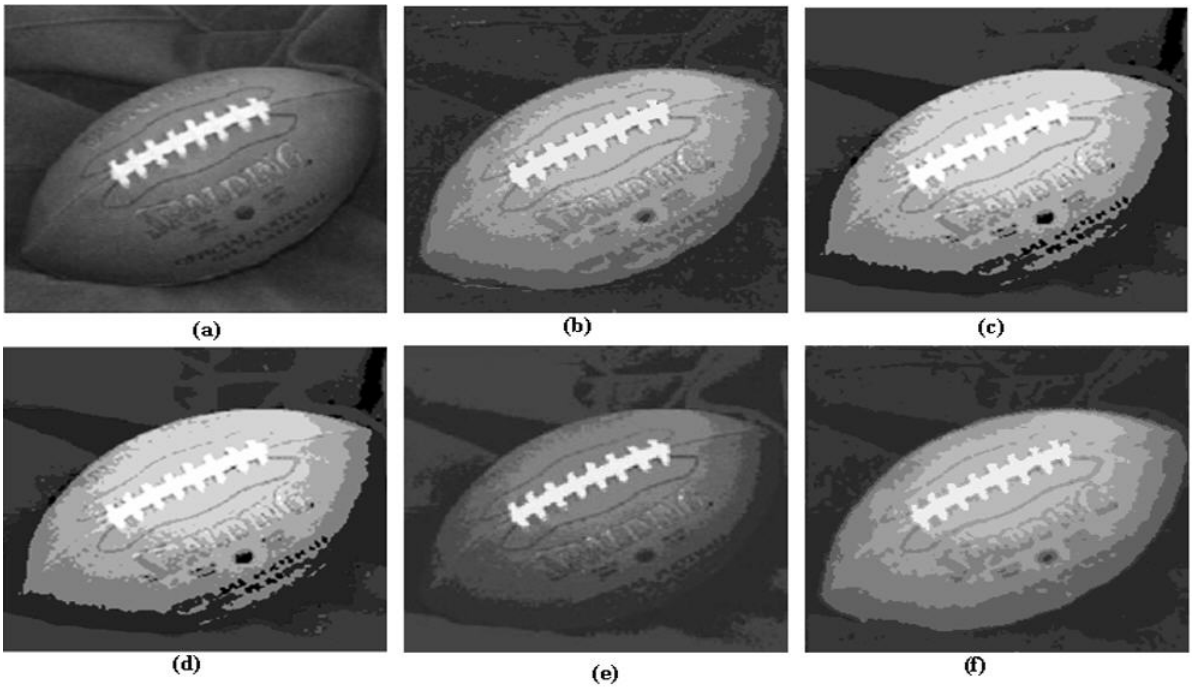

Figure 4.2 – Image segmentation results of the image Football (a) original image (b) FBSA algorithm(c) Fuzzy-VGAPS algorithm(d) MOECA algorithm (e) MSFCA algorithm(f) the proposed approach

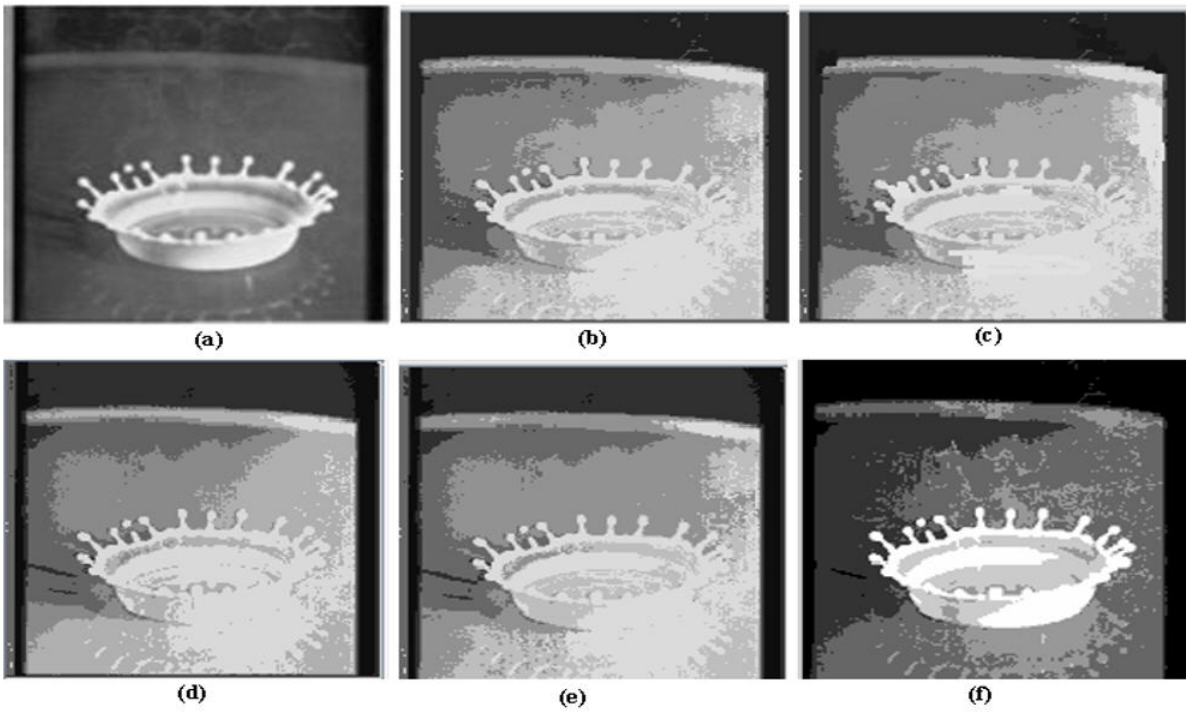

Figure 4.3 – Image segmentation results of the image Crown (a) original image (b) FBSA algorithm(c) Fuzzy-VGAPS algorithm(d) MOECA algorithm (e) MSFCA algorithm(f) the proposed approach

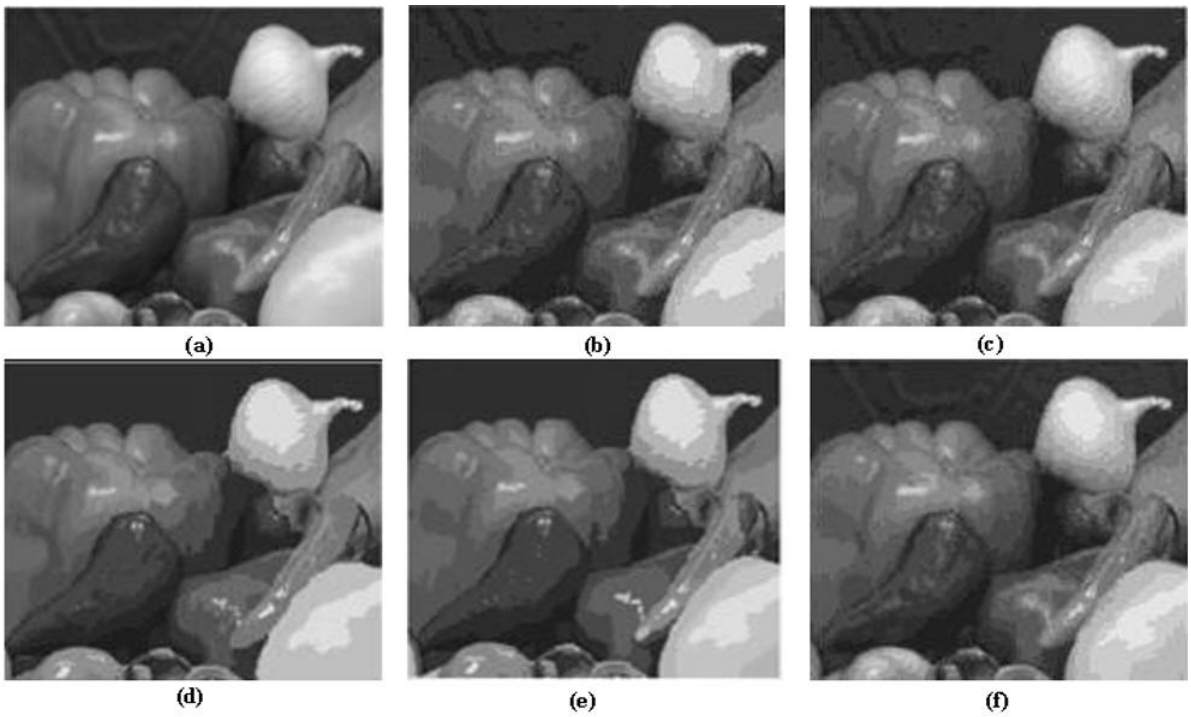

Figure 4.4 – Image segmentation results of the image Onion (a) original image (b) FBSA algorithm(c) Fuzzy-VGAPS algorithm(d) MOECA algorithm (e) MSFCA algorithm(f) the proposed approach

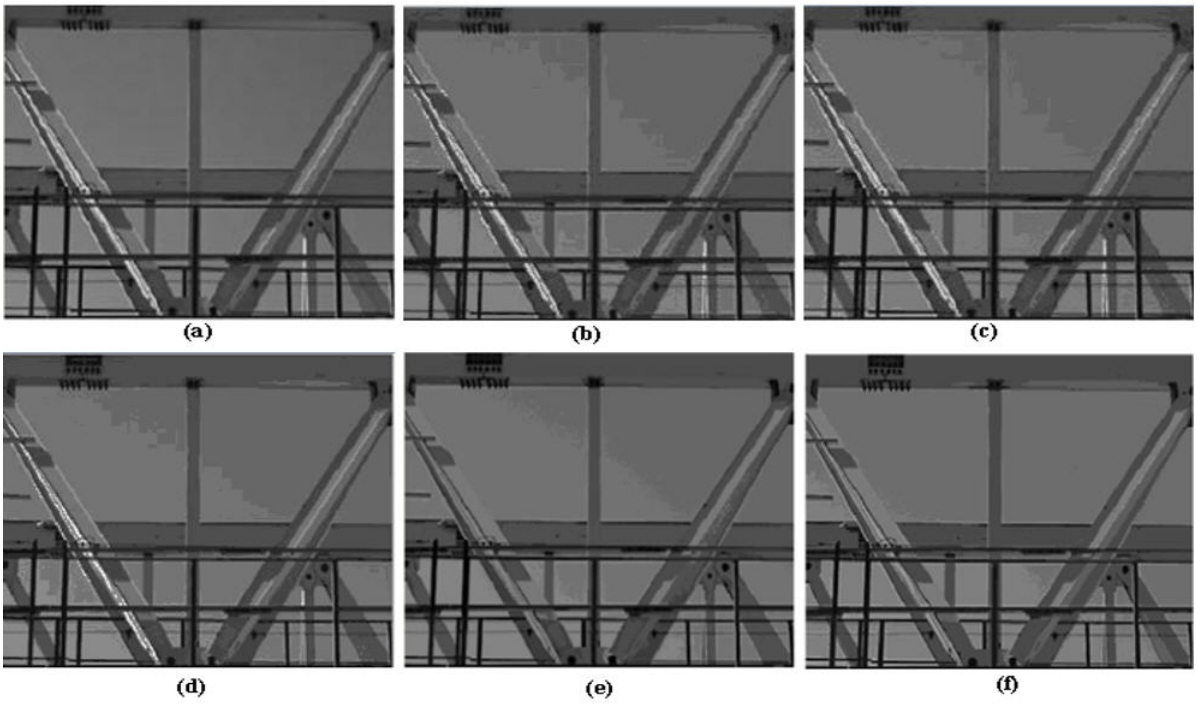

Figure 4.5 – Image segmentation results of the image Gantry Crane (a) original image (b) FBSA algorithm(c) Fuzzy-VGAPS algorithm(d) MOECA algorithm (e) MSFCA algorithm(f) the proposed approach

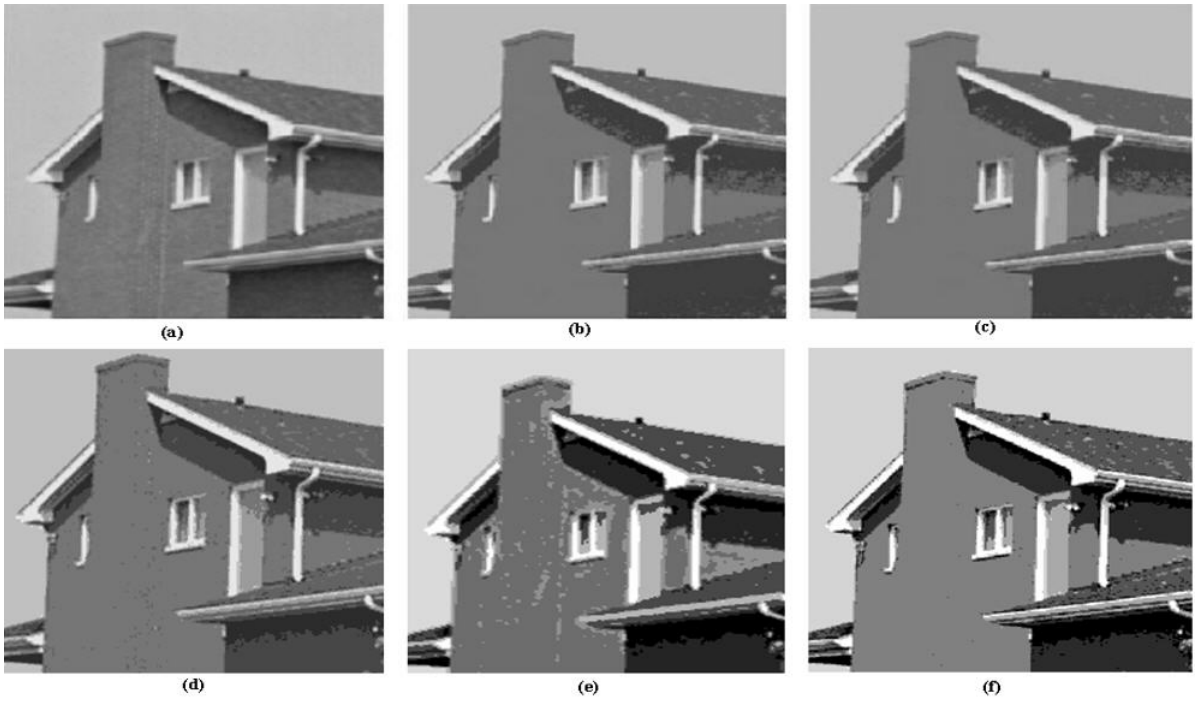

Figure 4.6 – Image segmentation results of the image House (a) original image (b) FBSA algorithm(c) Fuzzy-VGAPS algorithm(d) MOECA algorithm (e) MSFCA algorithm(f) the proposed approach

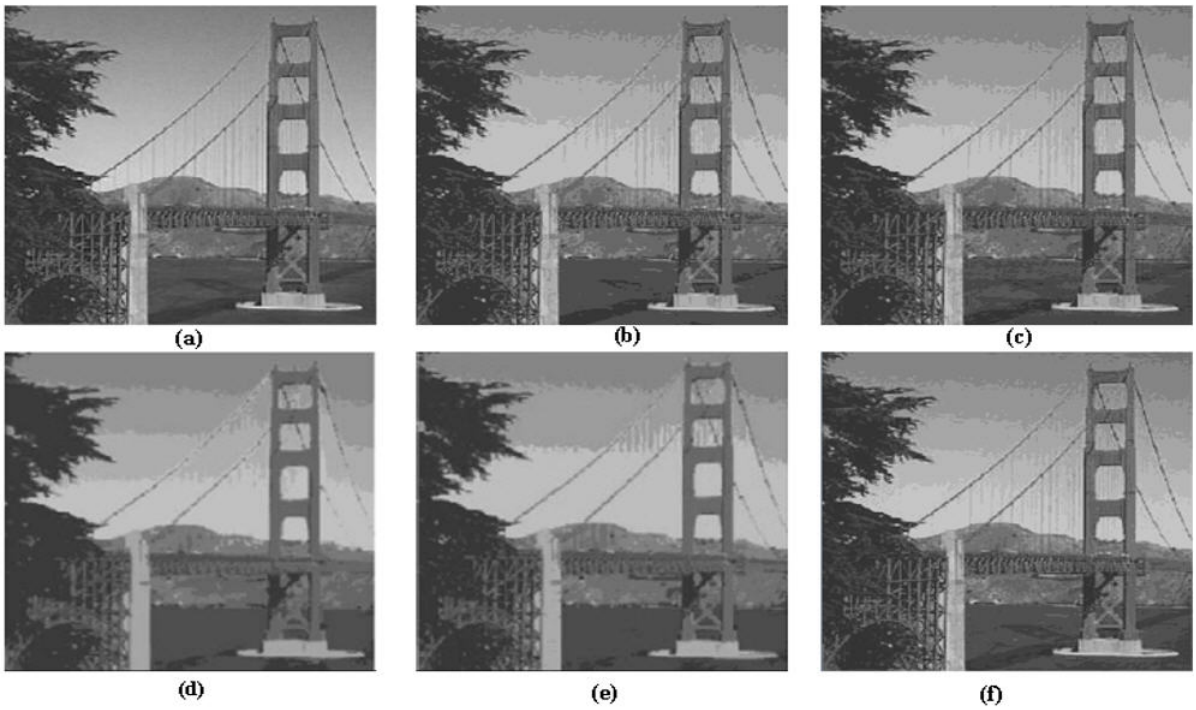

Figure 4.7 – Image segmentation results of the image Golden Gate (a) original image (b) FBSA algorithm(c) Fuzzy-VGAPS algorithm(d) MOECA algorithm (e) MSFCA algorithm(f) the proposed approach

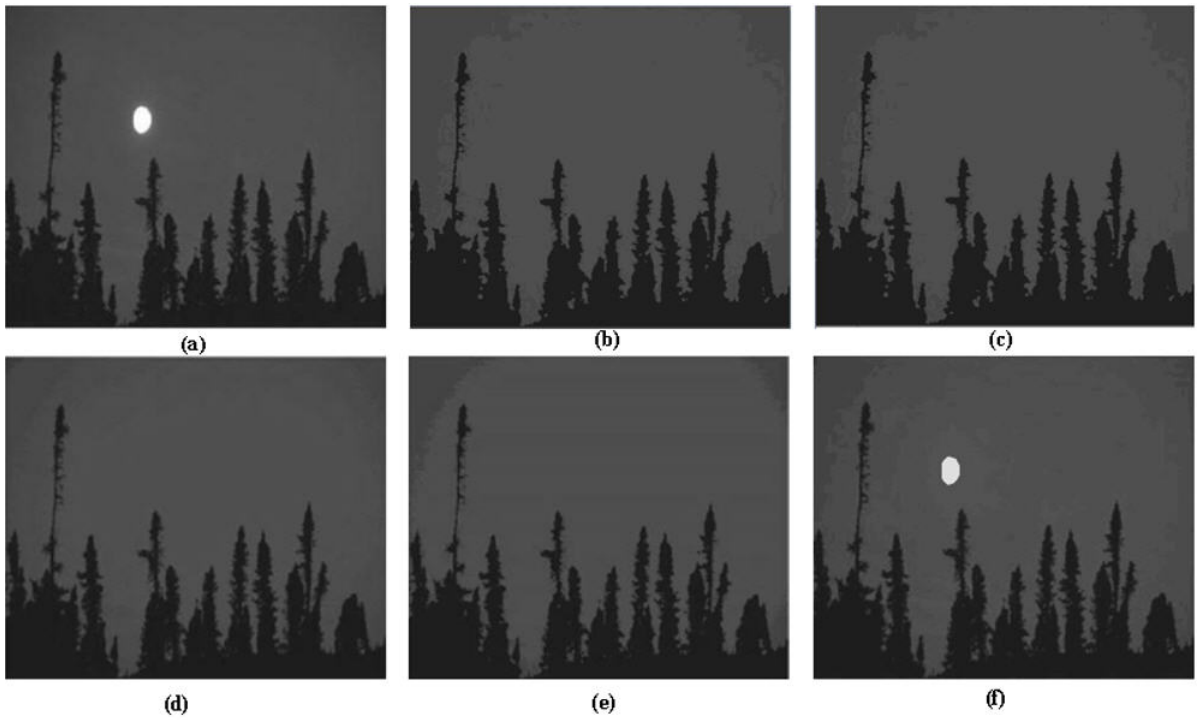

Figure 4.8 – Image segmentation results of the image Moon (a) original image (b) FBSA algorithm(c) Fuzzy-VGAPS algorithm(d) MOECA algorithm (e) MSFCA algorithm(f) the proposed approach

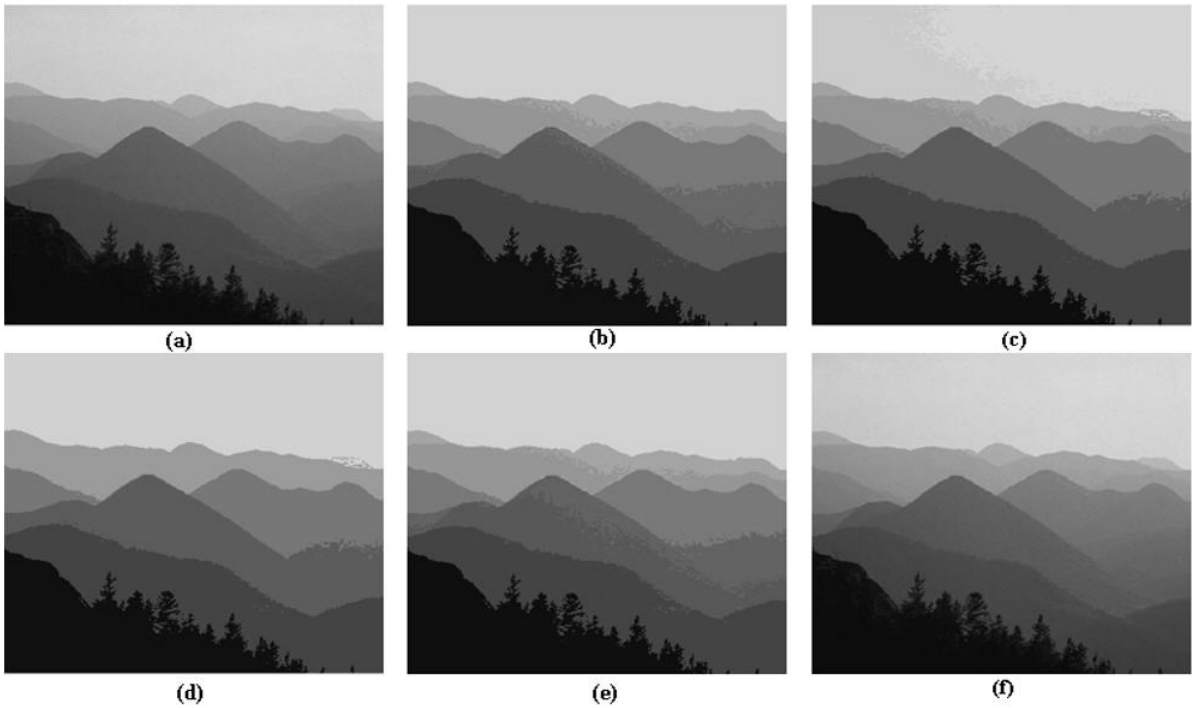

Figure 4.9 – Image segmentation results of the image Hill (a) original image (b) FBSA algorithm(c) Fuzzy-VGAPS algorithm(d) MOECA algorithm (e) MSFCA algorithm(f) the proposed approach

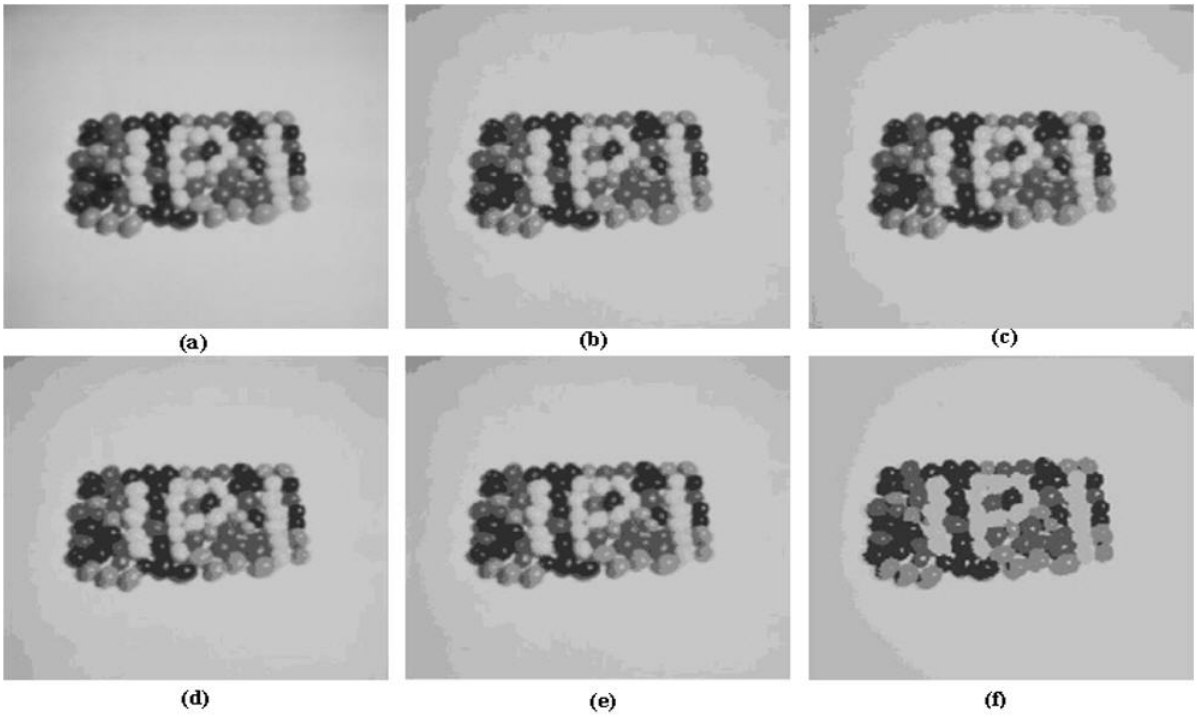

Figure 4.10 – Image segmentation results of the image smarties (a) original image (b) FBSA algorithm(c) Fuzzy-VGAPS algorithm(d) MOECA algorithm (e) MSFCA algorithm(f) the proposed approach

pability and minimal distortion during the segmentation process. It is worth noting that the compared algorithms have their own unique mechanisms for initializing cluster centers. Therefore, it is important to consider the impact of the number of clusters generated by each technique on the segmentation results.

The quality of the clustering result was found to be highly dependent on the cluster center initialization mechanism. A good initialization scheme could ensure high classification accuracy and less distortion during the segmentation process. Therefore, this section aims to investigate the relationship between the quality of segmentation results and the number of clusters produced by each initialization scheme. The number of clusters produced by each technique is tabulated In Table 4.1.

The observation that should be highlighted is that even when different algorithms produce the same number of clusters, there may be significant qualitative and quantitative differences in the segmentation results. While the number of clusters produced is an important performance metric, it is not sufficient to reveal the overall clustering performances of the algorithms. This is an important consideration when evaluating the clustering quality of segmented images. In this section, we emphasize the importance of using multiple performance metrics to assess the clustering quality of segmented images. Specifically, we suggest using metrics such as fuzzy validity indices and quantitative evaluation functions (i.e., the $F(I)$, $F'(I)$, $Q(I)$, and E values) to provide a more comprehensive evaluation of the segmentation results and allow for a fair comparison of the clustering performances of different techniques.

This section aims to explore how the number of clusters affects the quality of segmentation results. According to Table 4.1, MOECA, MSFCA, and the proposed approach generate fewer clusters compared to the FBSA and Fuzzy-VGAPS techniques for the images Capsicums, Crown, and Gantry Crane. As a result, MOECA, MSFCA, and the proposed approach tend to produce larger and more homogeneous regions in these images. On the other hand, for the image Smarties, FBSA, Fuzzy-VGAPS, and the proposed approach generate larger and more homogeneous regions in the segmented image than MOECA and MSFCA techniques by producing fewer clusters.

Regarding the images Football and House, the FBSA and Fuzzy-VGAPS techniques generate larger and more homogeneous regions by producing fewer clusters compared to MOECA, MSFCA, and the proposed approach. However, these techniques tend to misclassify a significant number of pixels in the segmented images, leading to classification errors.

For the Moon image FBSA, Fuzzy-VGAPS share the same number of clusters with the MOECA, and MSFCA, the techniques generate a smaller number of clusters, but the quality of the segmentation result is inferior to that produced by the proposed approach.

For the Hill image, FBSA, Fuzzy-VGAPS, and MOECA, these techniques may generate larger and more homogeneous regions compared to MSFCA and the proposed approach.

However, the segmented image produced by FBSA, Fuzzy-VGAPS, and MOECA techniques tend to have a significant number of falsely assigned pixels. For the Onion and Golden Gate images, the FBSA, Fuzzy-VGAPS, MSFCA, and MOECA techniques generate larger segmented regions than the proposed approach. However, it is evident that the segmented regions produced by these compared techniques contain a significant number of misclassified pixels.

Table 4.1: Number of clusters provided by the different approaches.

Images	FBSA	Fuzzy-VGAPS	MOECA	MSFCA	Proposed approach
Capsicums	12	12	9	9	10
Football	7	7	8	8	9
Crown	8	8	7	7	6
Onion	8	8	8	8	10
Gantry Crane	9	9	8	8	8
House	6	6	7	7	7
Golden Gate	9	9	8	8	11
Moon	3	3	3	3	8
Hill	7	7	6	8	9
Smarties	7	7	9	8	6

4.3.3 Quantitative evaluation of the segmentation results

In this section, we present the experimental results obtained by evaluating the performance of our proposed algorithm on the tested images. To assess the effectiveness of our approach, we employed a range of quantitative evaluation functions and fuzzy validity indices.

4.3.3.1 Quantitative evaluation functions

In this section, we will conduct a quantitative evaluation of the effectiveness of our proposed segmentation approach. To this end, we will employ four evaluation functions: $F(I)$, $F'(I)$, $Q(I)$, and E. Additionally, we will compare our results with those obtained by other methods.

The first evaluation function, $F(I)$ (Liu and Yang, 1994), is defined as follows:

$$F(I) = \sqrt{N} \sum_{j=1}^{M} \frac{e_j^2}{\sqrt{S_j}} \tag{4.9}$$

N represents the total number of pixels in the input image I, while M represents the total number of regions in the segmented image. C_j denotes the set of pixels in the j-th region, and S_j represents the number of pixels in C_j. Finally, e_j denotes the Euclidean distance between the grey levels of the pixels in C_j and the grey level attributed to region j in the segmented image

In addition to $F(I)$, we will also use two modified versions of this function, namely $F'(I)$ and $Q(I)$, proposed by Borsotti et al. (Borsotti et al., 1998),

$$F'(I) = \frac{1}{1000 \cdot S_I} \sqrt{\sum_{a=1}^{\text{Max Area}} [N(a)]^{1+\frac{1}{a}} \sum_{j=1}^{M} \frac{e_j^2}{\sqrt{S_j}}} \tag{4.10}$$

$$Q(I) = \frac{1}{1000 \times N} \sqrt{N} \sum_{j=1}^{M} \left[\frac{e_j^2}{1 + \log S_j} + \left(\frac{N(S_j)}{S_j} \right)^2 \right] \tag{4.11}$$

$N(a)$ denotes the number of regions in image I that have an area of exactly a, and Max Area represents the largest region's size in the segmented image.

To further evaluate the quality of our segmentation approach, we will use an entropy-based information measure E. This measure is frequently used for assessing the performance of segmentation algorithms and provides a comprehensive measure of the overall segmentation quality. E is defined as the sum of the entropy of the regions in the segmented image and incorporates both the layout entropy and the expected region entropy. Mathematically, E is defined as follows:

$$E = H_l(I) + H_r(I) \tag{4.12}$$

The expected entropy of the segmented image region is typically calculated by

$$H_r(I) = \sum_{j=1}^{M} \frac{S_j}{S_I} H_v(R_j) \tag{4.13}$$

Where $H(R_j)$ is the entropy of region j and it is defined as

$$H_v(R_j) = -\sum_{m \in V_j^{(v)}} \frac{L_j(m)}{S_j} \log \left(\frac{L_j(m)}{S_j} \right) \tag{4.14}$$

The layout entropy is defined as

$$H_l(I) = -\sum_{j=1}^{M} \frac{S_j}{S_I} \log \left(\frac{S_j}{S_I} \right) \tag{4.15}$$

Where $L_j(m)$ is the number of pixels in region j that have a value of m for feature v and $V_j^{(v)}$ is the set of all possible values associated with feature v in region j.

The optimal segmentation is obtained when the four evaluation functions reach their minimum values.

To evaluate the performance of our proposed segmentation algorithm, we conducted a quantitative evaluation using four different evaluation functions. The results of this evaluation are presented in Table 4.2, which correspond to the segmented images depicted in Figures 4.1 to 4.10. As shown in Table 4.2, our proposed algorithm exhibited favorable performance across all four evaluation functions, with relatively small values obtained. This indicates that the algorithm has achieved optimal segmentation, surpassing other algorithms in terms of the used evaluation measures. The consistently superior performance of our proposed algorithm in comparison to its counterparts suggests its effectiveness in accurately segmenting the images, as indicated by the evaluation results.

4.3.3.2 Fuzzy validity indices

The fuzzy index, also known as the cluster validity function, plays a crucial role in choosing the best fuzzy partition from a set of alternatives. This is accomplished by utilizing a quality measure that takes into account both compactness and separation metrics. Compactness refers to the variability of data within a cluster, while separation measures the degree of isolation between data from different clusters. By maximizing separation and minimizing compactness, the optimal partition can be achieved.

To evaluate the obtained fuzzy partitions, we utilized five well-known validity functions and the proposed validity index. These validity functions include partition entropy (V_{PE}) (Bezdek, 1973), partition coefficient (V_{PC}) (Bezdek and Dunn, 1975), Fukuyama-Sugno (V_{FS}) (Pal and Bezdek, 1995), Xie-Beni (V_{XB}) (Xie and Beni, 1991), and Bensaid (V_{SC}) function (Bensaid et al., 1996). One of the commonly employed indices for assessing fuzzy partitions is the partition entropy V_{PE}. It is defined as follows:

$$V_{PE} = -\frac{1}{N}\sum_{i=1}^{C}\sum_{j=1}^{N} u_{ij}\log(u_{ij}) \tag{4.16}$$

The optimal clustering is obtained when V_{PE} is minimal. Another validity function introduced by (Bezdek and Dunn, 1975) is the partition coefficient (V_{PC}). It takes on values between $[1/C, 1]$, where C is the number of clusters, and the optimal clustering is achieved when V_{PC} is at its maximum. V_{PC} is defined as follows:

$$V_{PC} = \frac{1}{N}\sum_{i=1}^{C}\sum_{j=1}^{N} u_{ij}^2 \tag{4.17}$$

The V_{FS} is defined by the sum of fuzzy distance between all points to different cluster centers, and the separation that defined as the distance between the cluster centers and the mean of all cluster centers as given in Eq. (4.18), the best fuzzy partition is intended

when V_{FS} is minimal.

$$V_{FS} = \sum_{j=1}^{n} u_{ij}^{m} ||x_j - v_i||^2 - \sum_{j=1}^{n} u_{ij}^{m} ||x_j - \bar{V}||^2 \tag{4.18}$$

The validity function V_{XB} is defined as the ratio of the total compactness of all clusters to the minimum distance with respect to all cluster centers. The minimal value of V_{XB} implies the better fuzzy partition; the V_{XB} is defined as follows:

$$V_{XB} = \frac{\sum_{i=1}^{C} \sum_{j=1}^{N} u_{ij}^{m} ||x_j - v_i||^2}{N \times \min_{i \neq k} ||v_i - v_k||^2} \tag{4.19}$$

The V_{SC} is another one of important validity function, which is defined as the sum of the mean fuzzy distances between points to all cluster centers divided by the sum of separation between all clusters; the minimal value of V_{SC} indicates the best clustering is obtained, and is defined according to the following equation

$$V_{SC} = \sum_{i=1}^{C} \left(\frac{\sum_{j=1}^{n} u_{ij}^{m} ||x_j - v_i||^2}{n_i \sum_{i=1}^{C} ||v_i - v_k||^2} \right) \tag{4.20}$$

where $n_i = \sum_{j=1}^{n} u_{ij}$

The segmentation results of five different algorithms were quantitatively evaluated using various validity functions, as presented in Table 4.3. Notably, the FBSA, Fuzzy-VGAPS, MOECA, and MSFCA algorithms demonstrated satisfactory performance in terms of fuzzy validity measures. However, it was observed that the proposed algorithm outperformed the other comparative algorithms, yielding optimal segmentation results.

The proposed algorithm achieved consistently smaller values of validity measures such as V_{PE}, V_{XB}, V_{SC}, V_{FS}, and the proposed index, as well as a larger value of V_{PC} and VI_{CS} compared to the other algorithms. These results demonstrate the effectiveness of the proposed algorithm in accurately segmenting images.

Table 4.2: A comparative analysis of the evaluation functions over the tested images

Algorithm	Images	$F(I)\times10^8$	$F'(I)$	$Q(I)\times10^3$	E
FBSA	Capsicums	0.4219	4.7122	0.4516	7.9231
	Football	0.4566	3.9830	0.3828	6.6563
	Crown	0.4514	3.8941	0.3705	5.9231
	Onion	0.3755	4.4144	0.3809	6.3765
	Gantry Crane	0.4658	4.1245	0.3654	6.4520
	House	0.3657	3.7138	0.3932	6.5987
	Golden Gate	0.3203	4.0760	0.3705	6.6507

	Moon	0.3968	3.6152	0.4452	6.3097
	Hill	0.3897	4.0994	0.5518	7.4220
	Smarties	0.3976	4.0111	0.3920	6.2545
Fuzzy-VGAPS	Capsicums	0.3124	3.7906	0.4448	6.7758
	Football	0.3262	3.2962	0.3880	5.7923
	Crown	0.3326	4.6331	0.3692	6.6070
	Onion	0.3549	4.8791	0.3338	7.5769
	Gantry Crane	0.4307	3.6299	0.3728	6.6524
	House	0.4398	4.0104	0.3672	6.5401
	Golden Gate	0.4309	3.7794	0.3901	6.9309
	Moon	0.3870	4.8679	0.5870	6.6935
	Hill	0.3936	3.8417	0.4162	7.6070
	Smarties	0.4264	3.9576	0.3822	6.6563
MOECA	Capsicums	0.2935	2.8274	0.2292	5.8821
	Football	0.3538	3.1469	0.3847	5.7449
	Crown	0.3220	3.7013	0.3539	5.2687
	Onion	0.3786	3.0949	0.3344	5.4264
	Gantry Crane	0.3885	3.0047	0.3631	6.7855
	House	0.3957	3.2300	0.3837	6.8960
	Golden Gate	0.3254	2.4832	0.3264	5.5427
	Moon	0.3878	3.9808	0.3208	6.2375
	Hill	0.3540	2.6227	0.2655	6.7855
	Smarties	0.3179	2.4245	0.3689	5.4699
MSFCA	Capsicums	0.2977	3.1012	0.2358	5.4019
	Football	0.3459	2.4976	0.3605	5.4264
	Crown	0.3044	3.3926	0.3743	5.7855
	Onion	0.3615	3.3838	0.3431	5.5949
	Gantry Crane	0.3472	2.9116	0.3814	5.5954
	House	0.3375	2.5443	0.3170	5.4784
	Golden Gate	0.3403	2.9296	0.3581	5.8430
	Moon	0.3449	3.4770	0.3409	5.0421
	Hill	0.3267	2.8094	0.3689	6.1269
	Smarties	0.3237	3.2800	0.3765	5.9854
the proposed approach	Capsicums	0.1395	1.1464	0.1089	3.8822
	Football	0.1444	0.9415	0.1627	2.9349
	Crown	0.1599	1.6019	0.1283	2.5055
	Onion	0.1555	1.0319	0.1701	3.4961
	Gantry Crane	0.2089	1.1643	0.1783	2.5958
	House	0.1293	1.3221	0.1386	3.3860

Golden Gate	0.1588	0.8812	0.1099	3.6772
Moon	0.1083	1.3498	0.1346	3.2513
Hill	0.1478	1.1731	0.1138	1.9984
Smarties	0.1567	1.1715	0.1782	2.4783

Table 4.3: Quantitative evaluation using various validity functions for the five algorithms

Algorithm	**Images**	V_{PE}	V_{PC}	V_{SC}	V_{XB}	V_{FS}	VI_{CS}
FBSA	Capsicums	0.7770	0.0595	0.4062	0.01235	-3.07692E+9	0.8765
	Football	0.8679	0.0781	0.4791	0.04587	-3.95124E+9	0.7523
	Crown	0.8564	0.0439	0.3614	0.04541	-3.79371E+9	0.8234
	Onion	0.7814	0.0475	0.4812	0.04578	-2.75296E+9	0.7901
	Gantry Crane	0.8003	0.0675	0.3969	0.06322	-2.69445E+9	0.7654
	House	0.7430	0.0246	0.4208	0.07854	-3.83120E+9	0.8372
	Golden Gate	0.8454	0.0416	0.4392	0.07541	-4.48511E+9	0.7910
	Moon	0.8094	0.0358	0.4121	0.05356	-5.73007E+9	0.8198
	Hill	0.8230	0.0639	0.4239	0.06546	-3.25140E+9	0.8145
	Smarties	0.7958	0.0529	0.4653	0.05879	-3.95849E+9	0.8087
Fuzzy-	Capsicums	0.8012	0.0388	0.3304	0.07418	-3.34186E+9	0.7712
VGAPS	Football	0.8454	0.0499	0.3828	0.05683	-3.61721E+9	0.7965
	Crown	0.7311	0.0379	0.3958	0.07341	-3.49346E+9	0.8276
	Onion	0.7977	0.0319	0.3898	0.047235	-3.44934E+9	0.8812
	Gantry Crane	0.8236	0.0438	0.4593	0.037129	-4.53833E+9	0.8111
	House	0.7658	0.0346	0.3812	0.045284	-3.60349E+9	0.8457
	Golden Gate	0.8097	0.0458	0.4329	0.041759	-5.31260E+9	0.7612
	Moon	0.8346	0.0587	0.4012	0.039865	-4.16580E+9	0.7326
	Hill	0.8491	0.0496	0.4158	0.049523	-3.27643E+9	0.7881
	Smarties	0.8274	0.0429	0.4035	0.0632	-3.90156E+9	0.8024
MOECA	Capsicums	0.8589	0.0234	0.3100	0.0775	-3.90439E+9	0.8887
	Football	0.8770	0.0497	0.3767	0.02506	-3.9539E+9	0.8275
	Crown	0.8530	0.0552	0.3261	0.02201	-3.94239E+9	0.8045
	Onion	0.8254	0.0291	0.4374	0.04571	-3.89864E+9	0.8167
	Gantry Crane	0.8104	0.0476	0.4403	0.03113	-4.0565E+9	0.8932
	House	0.8854	0.0614	0.3281	0.06522	-4.18616E+9	0.8581
	Golden Gate	0.8501	0.0376	0.4154	0.02748	-4.21707E+9	0.8326
	Moon	0.8712	0.0271	0.3786	0.02471	-4.38651E+9	0.8149

	Hill	0.8469	0.0231	0.3752	0.02712	-4.50832E+9	0.8793
	Smarties	0.8801	0.0563	0.4248	0.02153	-4.51958E+9	0.8976
MSFCA	Capsicums	0.8227	0.3464	0.2947	0.01944	-2.86425E+9	0.8164
	Football	0.8425	0.0319	0.2437	0.02368	-2.72921E+9	0.8402
	Crown	0.8812	0.0247	0.2772	0.03232	-2.89583E+9	0.8294
	Onion	0.8730	0.0273	0.2581	0.02854	-2.85155E+9	0.8012
	Gantry Crane	0.8493	0.0325	0.3549	0.08774	-2.85321E+9	0.8698
	House	0.8632	0.0265	0.3522	0.0356	-3.13161E+9	0.8954
	Golden Gate	0.8196	0.0378	0.3370	0.03232	-3.27178E+9	0.8231
	Moon	0.8990	0.0273	0.3207	0.03523	-3.14067E+9	0.8745
	Hill	0.8119	0.0261	0.3554	0.02569	-3.25068E+9	0.8512
	Smarties	0.8000	0.0292	0.3491	0.04732	-3.20122E+9	0.8398
Proposed	Capsicums	0.9106	0.0176	0.1088	0.00846	-4.02585E+9	0.9525
approach	Football	0.9550	0.0191	0.1258	0.01963	-4.19711E+9	0.9423
	Crown	0.9465	0.0131	0.1490	0.01596	-4.30172E+9	0.9276
	Onion	0.9261	0.0093	0.1906	0.01948	-4.31874E+9	0.9354
	Gantry Crane	0.8992	0.0145	0.1356	0.01860	-4.44668E+9	0.9487
	House	0.9261	0.0105	0.1882	0.01670	-4.58353E+9	0.9741
	Golden Gate	0.9194	0.0152	0.1889	0.01667	-4.61294E+9	0.9378
	Moon	0.9415	0.0117	0.1487	0.01780	-4.68663E+9	0.9467
	Hill	0.9490	0.0235	0.1293	0.02019	-4.81633E+9	0.9632
	Smarties	0.9355	0.0204	0.1484	0.01894	-4.86425E+9	0.9426

4.4 Conclusion

In this chapter, we presented a novel method for automating the determination of the optimal number of clusters and initialization of cluster centers in the FCM algorithm. Our approach involved incorporating an adaptive split stage that used a multithreshold method based on entropy information, which significantly improved the accuracy of cluster determination. Additionally, we introduced a new fuzzy validation index that provided an additional assessment of the quality of the obtained clusters. To evaluate the effectiveness of our proposed approach, we conducted comprehensive quantitative and qualitative assessments using fuzzy validity indices and evaluation functions. The experimental results clearly demonstrate that our method outperformed existing approaches and achieved superior image segmentation results.

Chapter 5

Fully integrated spatial information to improve FCM algorithm

Contents

5.1 Introduction

The FCM algorithm is a popular fuzzy clustering method used for image segmentation. One important characteristic of images is the high correlation among neighboring pixels, which suggests that they often have similar feature values and are likely to belong to the same cluster. However, the traditional FCM algorithm has limitations. It is relatively sensitive to noise and fails to consider the spatial distribution of pixels within an image. Additionally, it is excessively responsive to the initial cluster centers, which can lead to a susceptibility to local minimum solutions. These limitations can result in inaccurate and unreliable segmentation results.

To overcome the limitations of the traditional FCM algorithm, our thesis proposes two techniques aimed at enhancing its performance. In the previous chapter, we introduced an adaptive split and merge approach to improve the sensitivity of the FCM algorithm to the initialization scheme. This approach helps to reduce the sensitivity of the algorithm to the initial cluster centers and improve the accuracy of the segmentation results. In this chapter, we consider a comprehensive integration of the spatial constraint to further improve the performance of the FCM algorithm. This integration involves defining the influence of

neighboring pixels using two proposed terms: a fuzzy similarity measure and the noise level. By incorporating these terms, we aim to capture the complex spatial dependencies among pixels and improve the accuracy and robustness of the segmentation results.

To evaluate the performance of the proposed method, we conducted experiments using synthetic and medical images. The experimental results illustrate that the proposed algorithm achieves a balance between preserving significant image details and removing noise during the image segmentation process. Moreover, the performance of the proposed algorithm surpasses that of several related FCM-based algorithms in terms of segmentation accuracy

5.2 Fully integrated spatial information to improve FCM algorithm

The incorporation of spatial information in the FCM algorithm is essential for achieving accurate image segmentation results, as neighboring pixels often exhibit similar feature values and are likely to belong to the same cluster. To tackle this challenge, we propose a novel spatial FCM algorithm that incorporates comprehensive spatial information to enhance its performance. Our algorithm fully integrates spatial information by assigning varying degrees of importance to each pixel, considering its spatial information. Specifically, we propose two terms to define the influence of neighboring pixels: a fuzzy similarity measure and the noise level. By combining these terms, we aim to capture the complex spatial dependencies among pixels and improve the accuracy and robustness of the segmentation results.

5.2.1 Problem statement

This section introduces a comprehensive spatial FCM algorithm for image segmentation that focuses on incorporating spatial information effectively. In our algorithm, the central pixel's role in fuzzy clustering is determined based on whether it is affected by noise or not. Specifically, if the central pixel is free from noise, it is assigned a critical role in the clustering process. On the other hand, if the central pixel is corrupted by noise, its influence is reduced to avoid distorting the segmentation results. The spatial information is determined according to the fuzzy similarity measure computed between pixels and their respective noise levels. Our contributions can be summarized as follows:

1. The definition of spatial information is not uniform across all pixels. Instead, we highlight the central pixel's importance in fuzzy clustering when it is noise-free, whereas its impact is reduced when it is affected by noise.
2. We aim to improve the accuracy of the segmentation results by determining the

similarity measure between pixels based on their representation within the fuzzy set, rather than relying solely on intensity information.

3. The degree of influence of neighborhood intensity information is determined based on both the fuzzy similarity measure and the noise level present in the neighboring pixels.
4. We aim to enhance the accuracy and robustness of the segmentation results by replacing the central pixel in fuzzy clustering with one of its neighbors that can better contribute to the segmentation result in terms of compactness and separation between clusters.

5.2.2 A fully spatial FCM algorithm for image segmentation (FS-FCM)

Let's consider x_j as a central pixel within a given neighborhood N_j, and C_r as the class to which x_j belongs. If all neighboring pixels of x_j have the same class C_r as x_j (indicating that x_j is not corrupted by noise), the degree of influence of each neighboring pixel x_k is determined based on two factors: the fuzzy similarity measure $S(x_j, x_k)$ between x_j and x_k (section 5.2.2.1), and the level of noise $LN(x_k)$ of x_k (section 5.2.2.2).

On the other hand, if x_j does not have any neighboring pixels belonging to the same class as x_j (indicating that x_j is a noisy pixel), the degree of neighborhood intensity is only defined by the level of noise of its neighboring pixels x_k, thus, reducing the influence of noisy pixels in the fuzzy clustering process.

In the last case, when x_j has some neighboring pixels belonging to the same class as x_j (indicating that x_j is a boundary pixel or partially corrupted by noise), the weight of neighboring pixels is determined using a fuzzy similarity measure and the level of noise of the neighboring pixels. In this case, the new central intensity value x_j^* of x_j is calculated as the average of the mean intensities of the neighboring pixels x_k from the same class, considering all classes to which the neighboring pixels of x_j belong.

To achieve optimal clustering performance in terms of compactness and separation, we explore the local neighborhood N_j of x_j (section 5.2.2.3). If there is a neighboring pixel x_k that has a greater influence than x_j on the accuracy of segmentation, then this pixel is considered instead of x_j. Otherwise, x_j is maintained as the central pixel. Consequently, the new intensity value x_j^* of x_j is given by:

$$x_j^* = \begin{cases} \dfrac{\sum_{x_k \in N_j} (1-LN(x_k)) * x_k}{\sum_{x_k \in N_j} (1-LN(x_k))}, & \text{if } \forall x_k \notin C_r \\ \dfrac{(1-LN(x_j)) * x_j + \sum_{x_k \in N_j} (1-LN(x_k)) * S(x_j, x_k) * x_k}{(1-LN(x_j)) + \sum_{x_k \in N_j} (1-LN(x_k)) * S(x_j, x_k)}, & \text{if } \forall x_k \in C_r \\ \dfrac{\sum_{i=1}^{nc_j} \dfrac{\left(\sum_{x_k \in C_i} (1-LN(x_k)) * S(x_j, x_k) * x_k\right)}{\sum_{x_k \in C_i} (1-LN(x_k)) * S(x_j, x_k)}}{nc_j}, & \text{otherwise} \end{cases} \tag{5.1}$$

Where nc_j is the number of classes to which the neighboring pixels x_k of x_j belong to.

5.2.2.1 The fuzzy similarity measure

To determine the similarity measure between pixel x_j and its neighboring pixels x_k, we propose a fuzzy measure $S(x_j, x_k)$ that indicates the degree of common properties between x_j and x_k. It is defined as the sum of the minimum values between the membership degrees u_{ij} and u_{ik} of x_j and x_k for all cluster centers. The equation for $S(x_j, x_k)$ is as follows:

$$S(x_j, x_k) = \sum_{i=1}^{C} \min(u_{ij}, u_{ik}) \tag{5.2}$$

Where C is the total number of clusters. For the fuzzy similarity measure $S(x_j, x_k)$ we define the following properties

1. $0 \leq S(x_j, x_k) \leq 1$
2. $S(x_j, x_k) = 1$, if $u_{ij} = u_{ik}$ $(i = 1, \ldots, C)$
3. $S(x_j, x_j) = 1$
4. $S(x_j, x_k) = 0$, if $\exists m, l$ $(m \neq l)$ $u_{mj} = 1$ and $u_{lk} = 1$
5. $S(x_j, x_k) = S(x_k, x_j)$

5.2.2.2 The level of noise (LN)

For computing the level of noise $LN(x_j)$ of the pixel x_j within a given neighborhood N_j of x_j, the following conditions are considered:

1. If the set of neighboring pixels x_k of x_j have the same class as that of x_j, then the level of noise of x_j is 0 (Figure 5.1(a)).
2. The level of noise of x_j is 1 if x_j belongs to a class to which none of its neighboring pixels x_k belong (Figure 5.1(b)).
3. If some of the neighboring pixels of x_j belong to the same class as the pixel x_j (Figure 5.1(c)), the level of noise of x_j is defined according to the following equation:

$$\eta_j = \frac{m(j, r)}{\max\left[m(j, l) \mid l \neq r, l = 1 \ldots C\right]} \tag{5.3}$$

where $m(j, r)$ represents the average distance between x_j and its neighboring pixels belonging to the same class C_r to which the pixel x_j belongs, and $m(j, l)$ is the average distance between x_j and its neighboring pixels that belong to the other classes C_l. The level of noise of $LN(x_j)$ is defined as follows:

$$LN(x_j) = \begin{cases} 1, & \text{if } \forall x_k \notin C_r \\ 0, & \text{if } \forall x_k \in C_r \\ \eta_j, & \text{if } \exists x_k \in C_r \end{cases} \tag{5.4}$$

Figure 5.1 – Illustration of three cases of level of noise $LN(x_j)$

5.2.2.3 The quantitative term

In order to improve the accuracy of the proposed segmentation method, we explore an alternative approach to replace the central pixel x_j, with one of its neighboring pixels, x_k, from the same class as x_j. This replacement is considered when x_j is not corrupted by noise or when it is a boundary pixel, and it has been found to yield better segmentation results compared to using x_j alone.

To determine the appropriate neighboring pixel for replacement, we introduce a new quantitative term called a_j. This term aims to assign a higher value to the pixel that minimizes the variation within its cluster while maximizing the separation between clusters. The formulation of a_j is defined as follows:

$$a_j = \frac{1}{C} \sum_{i=1}^{C} \|u_{ij} - (1 - u_{ij})\|^2 \tag{5.5}$$

For this proposed term a_j, we have defined the following properties:

1. $\left(\frac{C-2}{C}\right)^2 \leq a_j \leq 1$
2. $a_j = 1$, if $\exists m$, $u_{mj} = 1$ and $u_{lj} = 0$, $l = 1, \ldots, C$, $l \neq m$
3. $a_j = \left(\frac{C-2}{C}\right)^2$, if $u_{ij} = \frac{1}{C}$, $i = 1, \ldots, C$

Based on these properties, the value of a_j lies between $\left(\frac{C-2}{C}\right)^2$ and 1. When x_j clearly belongs to a specific cluster i, with the maximum degree of membership u_{ij} equal to 1 and all other membership degrees u_{lj} ($l = 1...C$, $l \neq i$) equal to 0, a_j reaches its maximum value of 1. On the other hand, a_j reaches its minimum value of $\left(\frac{C-2}{C}\right)^2$ when x_j belongs to all clusters to the same extent, with all membership degrees u_{ij} ($i = 1...C$) equal to $\frac{1}{C}$.

According to the defined properties of the proposed quantitative term a_j, if the central pixel x_j is not affected by noise or is a boundary pixel, we redefine it using the following equation:

$$x_j = \begin{cases} x_k & \text{if } \exists\, x_k \in C_r \text{ where } k = \arg\max_{l=1,\ldots,|C_r|}(a_l) \\ x_j & \text{otherwise} \end{cases} \tag{5.6}$$

Here, $|C_r|$ denotes the number of neighboring pixels of x_j that belong to the same class as x_j. By applying this alternative approach, we aim to enhance the accuracy of the segmentation method by leveraging neighboring pixels that have a more significant impact on the segmentation result than the central pixel itself.

The key steps of the proposed method can be listed in the following algorithm:

Algorithm 4 : The FSFCM algorithm

Input:

- The input image $X = (x_j, j = 1, \ldots, N)$,
- C is the number of clusters,
- Initial cluster centers $V = (v_1, v_2, \ldots, v_C)$,
- The degree of fuzziness m,
- The threshold termination criterion ϵ.

Output: Fuzzy partition matrix U, Cluster centers $V = (v_1, v_2, \ldots, v_C)$ of the fuzzy partitions.

Step 1: Calculate the membership values u_{ij} using Eq. (2.8);
Step 2: Calculate the cluster centers v_i $(i = 1, 2, \ldots, C)$ according to Eq. (2.9);
Step 3: If $\|V_{\text{new}} - V_{\text{old}}\| < \epsilon$, then stop, otherwise go to Step 1;
Step 4: For each pixel x_j, calculate η_j, $LN(x_j)$, and a_j using Eq. (5.3), Eq. (5.4), and Eq. (5.5);
Step 5: For each pixel x_j
If $LN(x_j) \neq 1$, then
Replace x_j by its novel intensity using Eq. (5.6);
Step 6: For each pixel x_j and for each of its neighboring pixel x_k, calculate the degree of similarity $S(x_j, x_k)$ using Eq. (5.2);
Step 7: Use η_j, $LN(x_j)$, a_j, and $S(x_j, x_k)$ for generating the new image $x^*_{j,j=1,\ldots,N}$ using Eq. (5.1);
Step 8: Update the membership values u_{ij} for each pixel $x^*_{j,j=1,\ldots,N}$ using Eq. (2.8);
Step 9: Update cluster centers v_i $(i = 1, 2, \ldots, C)$ according to Eq. (2.9);
Step 10: If $\|V_{\text{new}} - V_{\text{old}}\| < \epsilon$, then stop, otherwise go to Step 7;

5.2.3 Experiments and Results

This section presents the results of our experiments and a discussion of our algorithm's performance. To evaluate our spatial fuzzy clustering algorithm, we conducted extensive tests on both synthetic and medical images with varying levels of noise. Additionally, we

compared the performance of our algorithm with five other clustering methods in terms of cluster validity functions, segmentation accuracy, and tissue segmentation accuracy to provide a comprehensive evaluation of our algorithm's performance.

Different levels of Gaussian and Salt Pepper noise are added in six synthetic images, SIN1, SIN2, SIN3, SIN4, SIN5, and SIN6; for the medical images, we tested our algorithm on a simulated T1-weighted normal brain MRI obtained from Brainweb (http://www.bic.mni.mcgill.ca/brainweb); Brainweb is a tool designed to address the problem of validation in morphological neuroimaging. Brainweb makes it possible to generate a Simulated Brain Database (SBD), a set of realistic MRI data volumes produced by an MRI simulator. These data can be used by the neuroimaging community to evaluate the performance of various image analysis methods in a situation where the truth is known. The SBD contains simulated brain MRI data based on two anatomical models: healthy normal and multiple sclerosis (MS). For both of these, full 3-dimensional data volumes were simulated using three MRI sequences (T1-, T2-, and proton-density- (PD-) weighted) and a variety of slice thicknesses, noise levels, and levels of intensity non-uniformity (Figure 5.2). These data are available for viewing in three orthogonal views (transversal, sagittal, and coronal), and for downloading. The noise in the simulated images has Rayleigh statistics in the background and Rician statistics in the signal regions. The "percent noise" number represents the percent ratio of the standard deviation of the white Gaussian noise versus the signal for a reference tissue. However, The INU fields were estimated from real MRI scans, so they are realistic. These fields are not linear but are slowly varying fields of a complex shape.

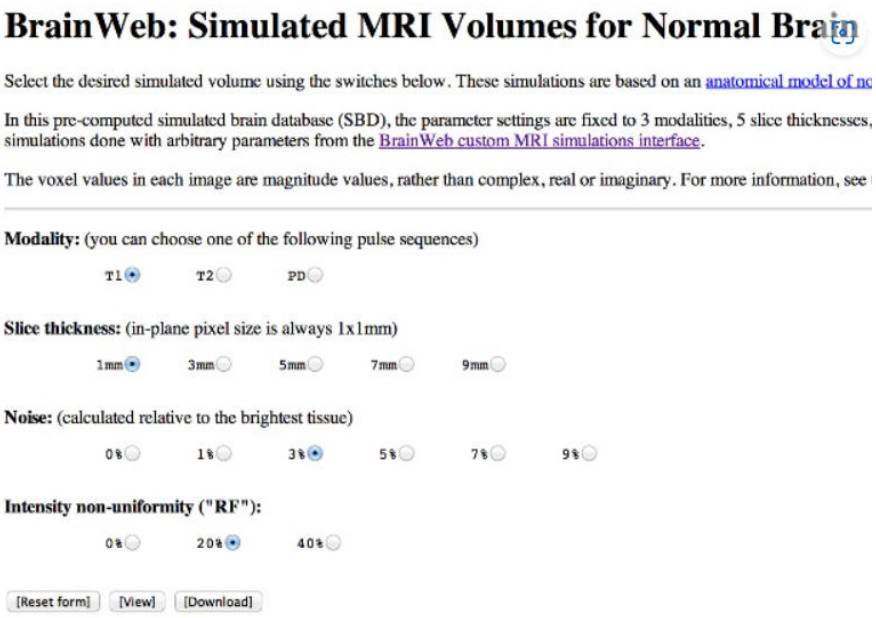

Figure 5.2 – Brain web simulator.

The proposed algorithm is evaluated on six different volumes, each one contains 51 images, corrupted by different levels of noise and inhomogeneity (IH). Volume 1 (5% noise,

20% IH), volume 2 (7% noise, 20% IH), volume 3 (9% noise, 20% IH), volume 4 (5% noise, 40% IH), volume 5 (7% noise, 40% IH), and volume 6 (9% noise, 40% IH).

To evaluate the effectiveness and accuracy of our proposed method, we employed a two-step evaluation process. Firstly, we conducted a qualitative assessment of the experimental results. Subsequently, we performed a quantitative analysis by comparing our approach with several other algorithms, including conventional FCM, sFCM, FCM_S, FGFCM, and csFCM algorithms. This comparison was based on various criteria, such as cluster validity functions, segmentation accuracy (SA), and tissue segmentation accuracy (TSA).

5.2.3.1 Qualitative evaluation

The qualitative evaluations provide valuable insights into the target application, image characteristics, and quality, shortcomings of the segmentation algorithm, and the results of each method step. In this section, qualitative evaluations are employed to compare the segmentation performance of the proposed algorithm with five existing algorithms (FCM, sFCM, FCM_S, FGFCM, and csFCM) on synthetic and MRI brain images. The segmentation results of all six algorithms on synthetic images are illustrated in Figure 5.3-Figure 5.8.

The segmentation results of the six algorithms on the first synthetic image with 30% Salt & Pepper noise are presented in Figure 5.3. From Figure 5.3 (b)-(d), it can be observed that FCM, FCM_S, and sFCM fail to effectively remove the noise from the input image. However, FGFCM and csFCM produce segmentation results with a small number of misclassified pixels. Among all the algorithms, FSFCM achieves the best segmentation result, with well-located boundaries and suppression of the most noisy pixels.

Figure 5.4 illustrates the image segmentation results on the second synthetic image corrupted by 30% Salt & Pepper noise, obtained using the six algorithms. It is evident that the images segmented by FCM, FCM_S, and sFCM exhibit a large number of misclassified pixels, and the boundaries appear blurred. Both FGFCM and csFCM provide segmentation results with a significant number of misclassified pixels and slightly blurred boundaries. On the other hand, the segmentation results obtained by FSFCM demonstrate clearer boundaries and the removal of almost all the noisy pixels.

The segmentation results of the third synthetic image with 30% Salt & Pepper noise are shown in Figure 5.5. From Figure 5.5 (b)-(d), it can be observed that a large number of misclassified pixels are present. Among the FGFCM, csFCM, and FSFCM algorithms (Figure 5.5 (e)-(g)), the proposed algorithm achieves more appropriate results in terms of region homogeneity and detail preservation.

Figure 5.6 depicts the segmentation results of FSFCM and other computing algorithms on the fourth synthetic image with 30% Gaussian noise. The results in Figure 5.6 (b)-(f) exhibit a significant number of incorrectly classified pixels. FSFCM produces the best segmentation results compared to the other five algorithms.

The clustering results of the fifth synthetic image corrupted by 30% Gaussian noise are illustrated in Figure 5.7. The segmentation results of FCM (Figure V6 (b)), sFCM (Figure 5.7 (c)), and FCM_S (Figure 5.7 (d)) are affected by the noise to different extents, indicating a lack of robustness to Gaussian noise. Visually, FGFCM (Figure 5.7 (e)) and csFCM (Figure 5.7 (f)) remove most of the noise but still do not achieve satisfactory results. On the other hand, the proposed algorithm (Figure 5.7 (g)) effectively removes almost all the added noise, yielding satisfactory results.

Figure 5.8 illustrates the segmentation results on the sixth synthetic image corrupted by 30% Gaussian noise, obtained using FCM, sFCM, FCM_S, FGFCM, csFCM, and FSFCM, respectively. In Figure 5.8 (g), the segmentation results obtained from FSFCM exhibit smoother regions and clearer image boundaries, effectively removing almost all the added noise.

Figures 5.9 to 5.11 present the qualitative segmentation results of a T1-weighted MRI brain image (slice 90) contaminated by 5% noise and 40% inhomogeneity, 7% noise and 40% inhomogeneity, and 9% noise and 40% inhomogeneity, respectively.

In Figure 5.9 (a), the input image contaminated by 5% noise and 40% inhomogeneity is shown. The segmentation results of the three tissues (CSF, GM, WM) and the final segmentation by different computing algorithms are depicted in Figure 5.9 (b)-(y). It can be observed that FCM, sFCM, and FCM_S struggle to handle the presence of many noise points, resulting in compromised segmentation performance. Although csFCM and FGFCM show some improvement with fewer noise points, the proposed algorithm achieves superior segmentation results by effectively suppressing almost all the noise points in the segmentation images.

Figure 5.10 (a) presents the original image contaminated by 7% noise and 40% inhomogeneity. The segmentation results of the three tissues (CSF, GM, WM) and the final segmentation by FCM, sFCM, FCM_S, FGFCM, csFCM, and the proposed algorithm are depicted in Figure 5.10 (b)-(y). From the results shown in Figure 5.10 (b)-(m), it is evident that FCM, sFCM, and FCM_S are highly sensitive to the high level of inhomogeneity, resulting in a significant loss of image details. FGFCM and csFCM (Figure 5.10 (n)-(u)) still exhibit numerous noise points and suppress certain image details. However, the segmentation results shown in Figure 5.10 (v)-(y) highlight the superior performance of the proposed algorithm compared to the other considered algorithms.

Figure 5.11 (a) displays the input image corrupted by 9% noise and 40% inhomogeneity. The segmented images of the three main tissues and the final segmentation by the compared algorithms are shown in Figure 5.11 (b)-(u). It is evident that the segmentation performance of the compared algorithms is significantly affected by the presence of high levels of noise and inhomogeneity. The segmentation results of the other five algorithms still contain numerous noise points, and the CSF, GM, and WM tissues are often misclassified, particularly in the case of FCM, sFCM, and FCM_S algorithms. In contrast, the

proposed algorithm's segmentation results in Figure 5.11 (v)-(y) demonstrate its effective ability to remove almost all the noisy points while preserving image details.

5.2.3.2 Quantitative evaluation

Quantitative evaluation plays a crucial role in comparing the results of different segmentation methods. In our study, we conducted three types of quantitative evaluations, including cluster validity functions, segmentation accuracy (SA), and tissue segmentation accuracy (TSA).

a- Cluster validity function

To evaluate the quality of clusters, various cluster validity functions have been proposed in prior studies on fuzzy clustering. In this section, we utilize five evaluation functions as quantitative measures to assess the quality of image segmentation results.

Table 5.1 presents the cluster validity functions obtained by six algorithms on synthetic images corrupted by different levels of noise. It is evident that FSFCM outperforms the other five approaches, exhibiting the highest V_{PC} values and the smallest values for V_{PE}, V_{FS}, V_{XB}, and V_{SC}.

Table 5.2 provides the mean values of the validity functions across 51 MRI images with varying levels of noise (5%, 7%, and 9%) and inhomogeneity (20%, 40%). Clearly, the segmentation performance of all algorithms deteriorates as the noise level and inhomogeneity in the image increase. However, even in the presence of high levels of noise and inhomogeneity, the proposed algorithm surpasses the other five algorithms, demonstrating the lowest values for V_{PE}, V_{FS}, V_{XB}, V_{SC}, and the highest values for V_{PC}.

Figure 5.12 illustrates the average values of cluster validity functions (V_{PE}, V_{PC}, V_{FS}, V_{XB}, and V_{SC}) for the segmented regions of CSF, GM, and WM obtained by FCM, sFCM, FCM_S, FGFCM, csFCM, and the proposed algorithm over 51 MRI images corrupted by 9% noise and 40% inhomogeneity. These results clearly demonstrate that the proposed algorithm achieves the highest segmentation accuracy among the compared algorithms over all the MRI images.

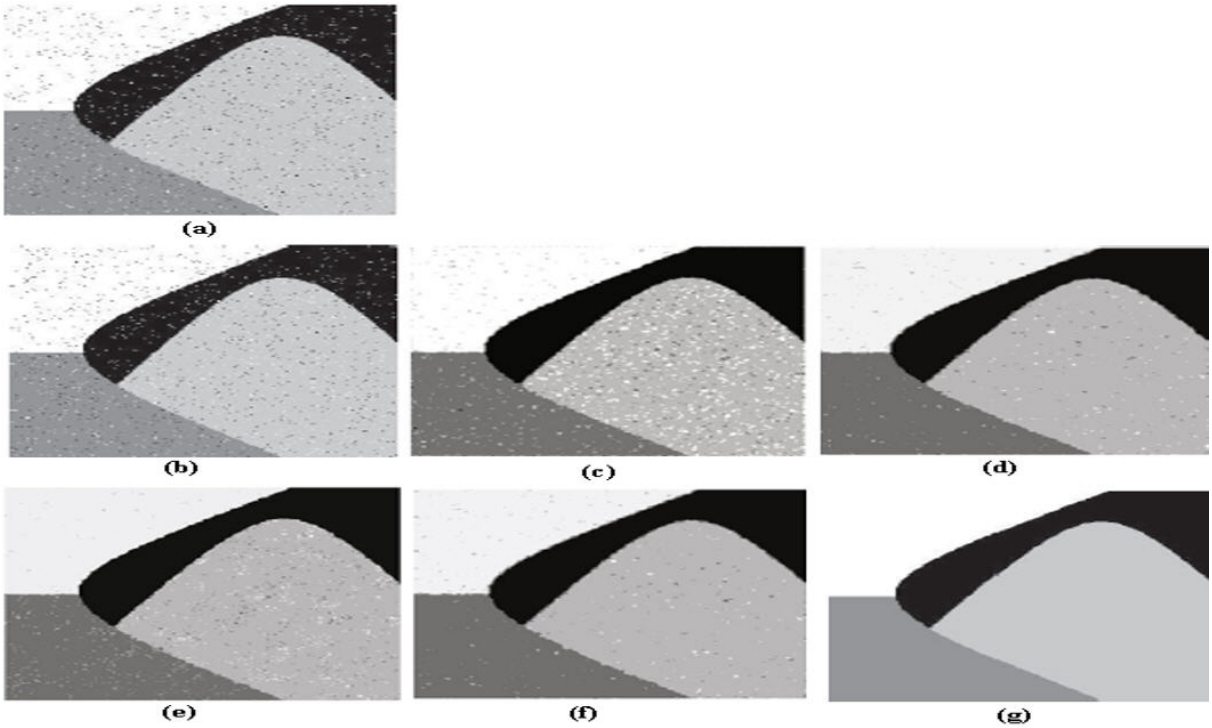

Figure 5.3 – Qualitative segmentation results on the first synthetic image (SIN1) corrupted by salt & Pepper noise (30%) by different computing algorithms.

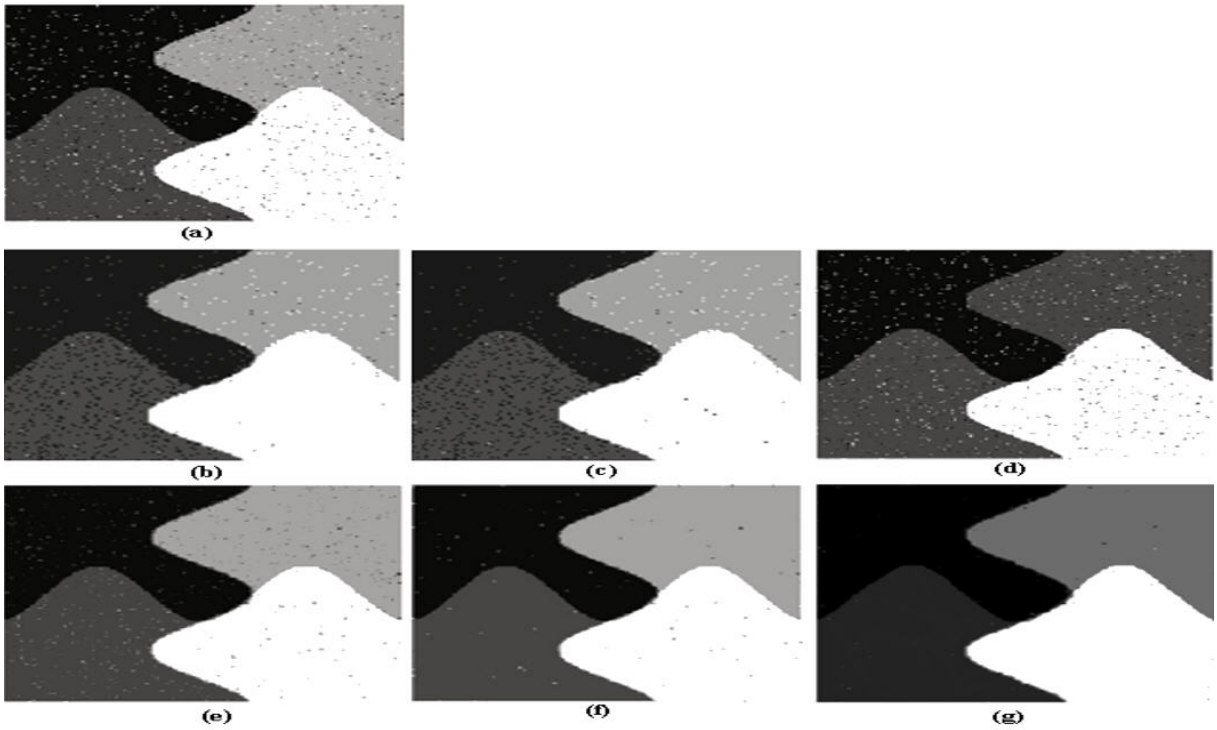

Figure 5.4 – Qualitative segmentation results on the second synthetic image (SIN2) corrupted by salt & Pepper noise (30%) by different computing algorithms.

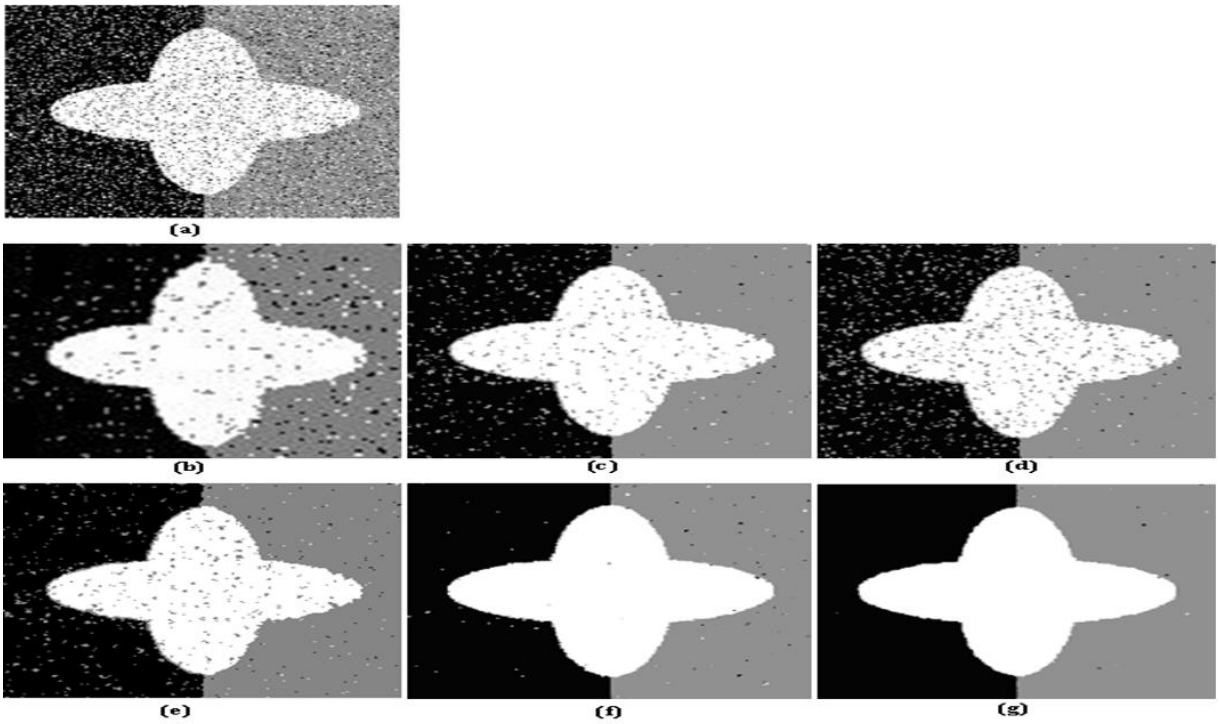

Figure 5.5 – Qualitative segmentation results on the third synthetic image (SIN3) corrupted by salt & Pepper noise (30%) by different computing algorithms.

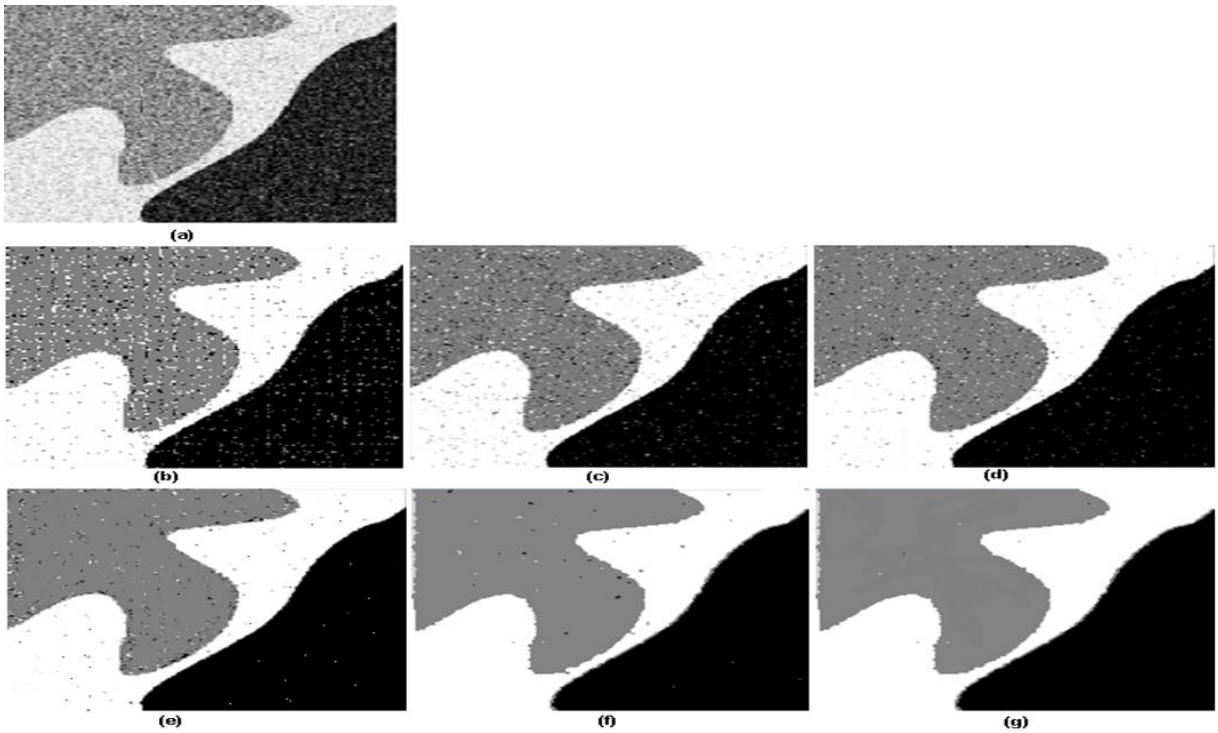

Figure 5.6 – Qualitative segmentation results on the fourth synthetic image (SIN4) corrupted by Gaussian noise (30%) by different computing algorithms.

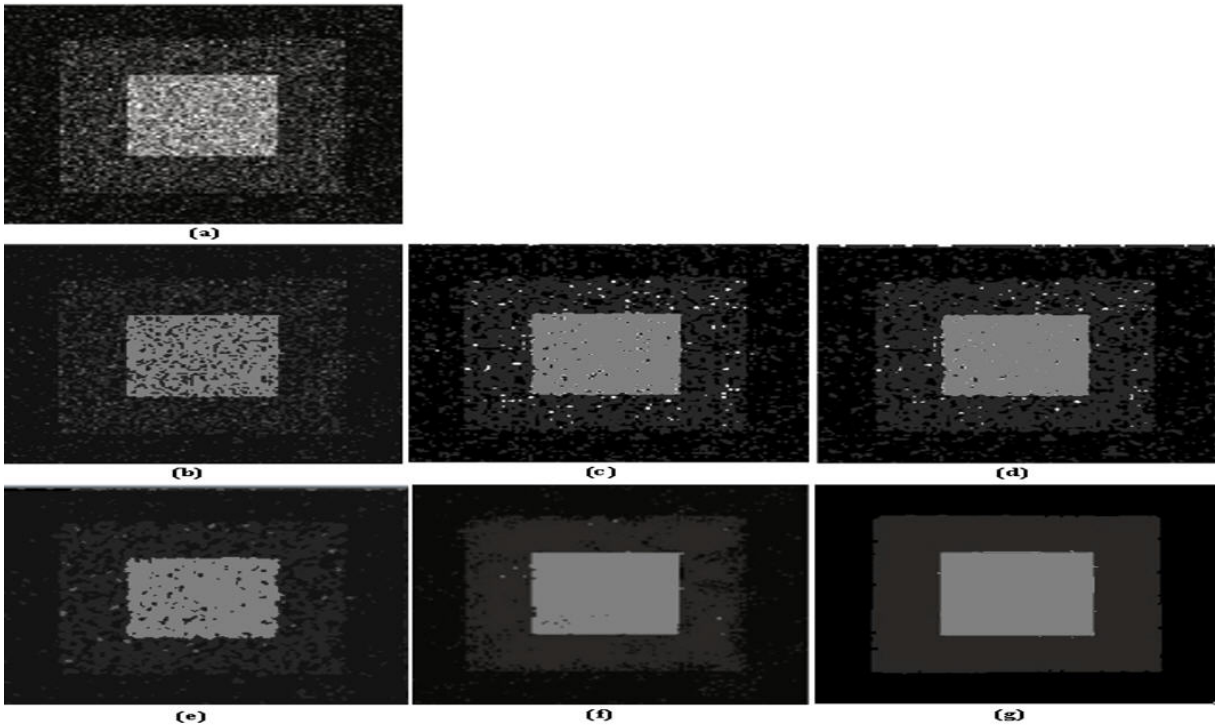

Figure 5.7 – Qualitative segmentation results on the fifth synthetic image (SIN5) corrupted by Gaussian noise (30%) by different computing algorithms.

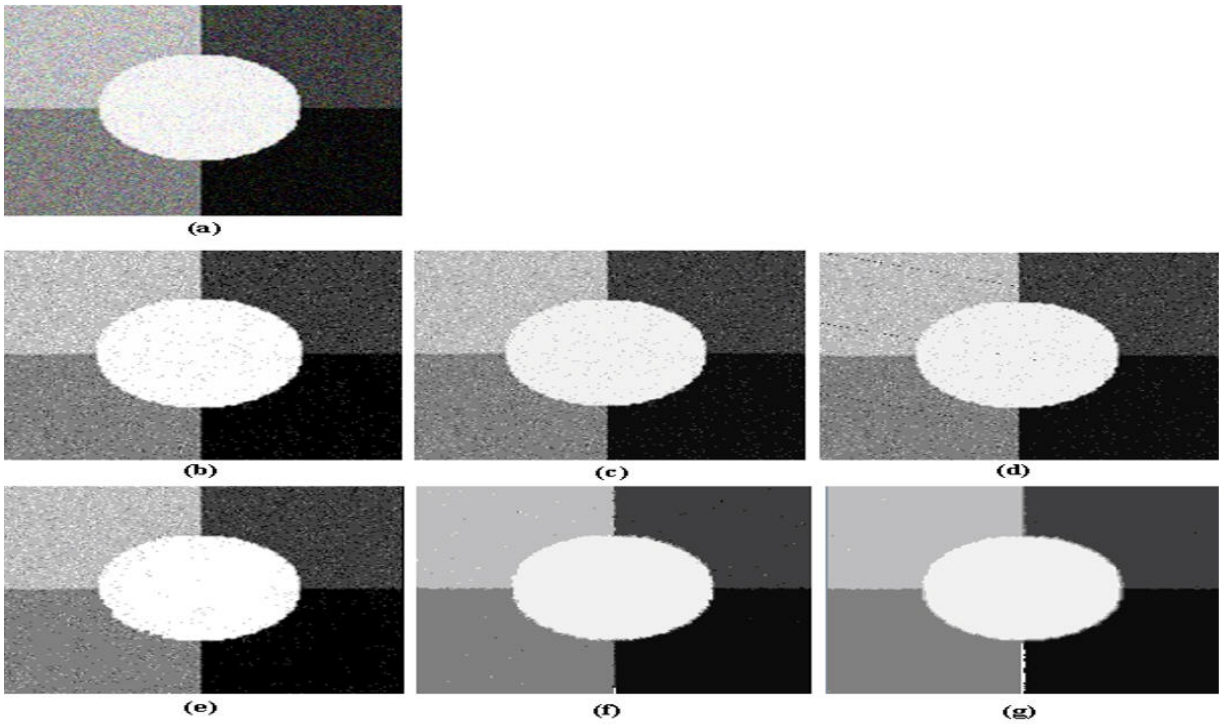

Figure 5.8 – Qualitative segmentation results on the sixth synthetic image (SIN6) corrupted by Gaussian noise (30%) by different computing algorithms.

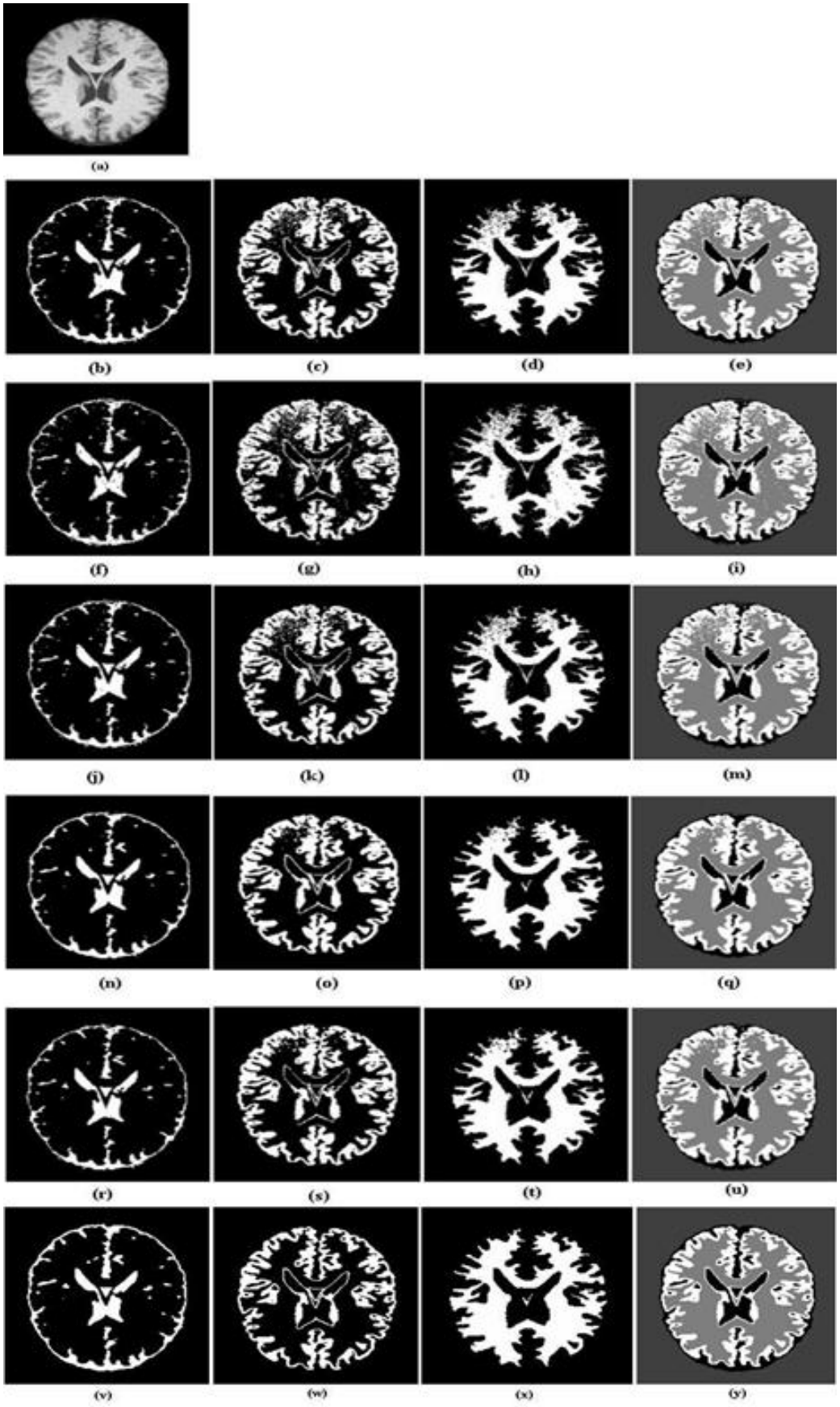

Figure 5.9 – Qualitative segmentation results on a MRI brain image with 5% noise and 40% inhomogeneity by different computing algorithms.

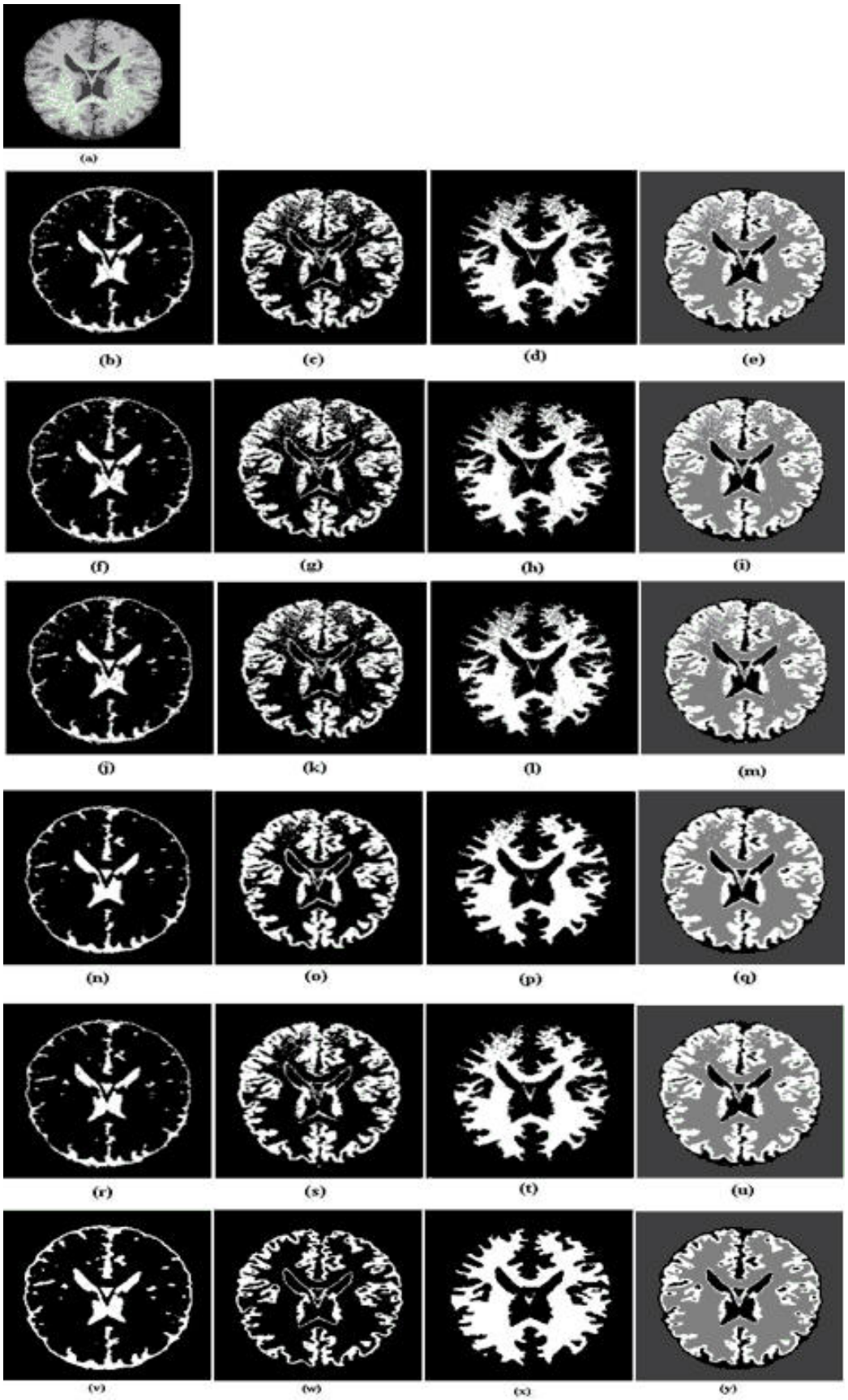

Figure 5.10 – Qualitative segmentation results on a MRI brain image with 7% noise and 40% inhomogeneity by different computing algorithms.

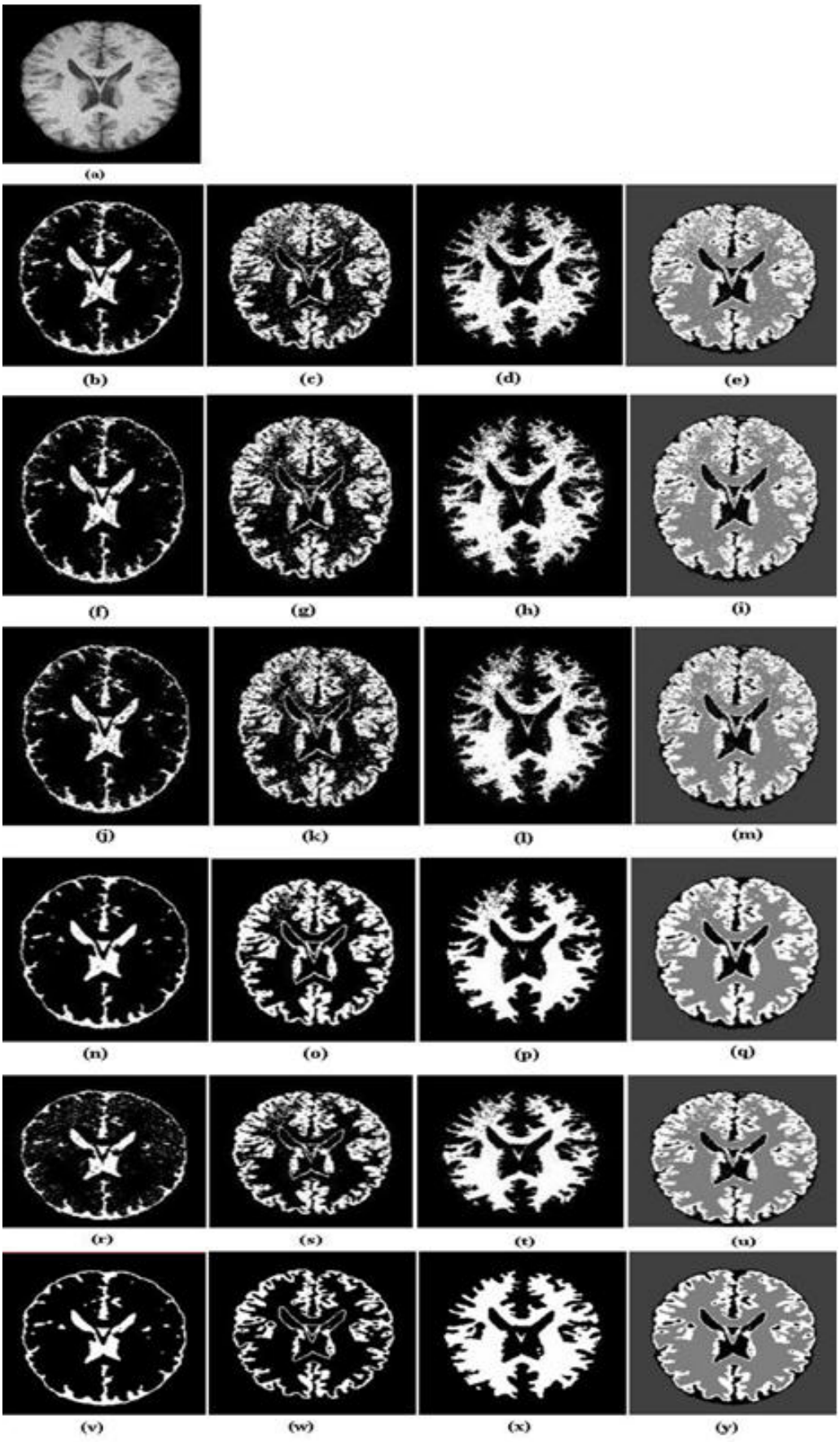

Figure 5.11 – Qualitative segmentation results on a MRI brain image with 9% noise and 40% inhomogeneity by different computing algorithms.

Table 5.1: The results of using validity functions produced by six algorithms on the synthetic images with various levels of noise

Image	Segmented Methods	Cluster Validity Function				
		V_{PE}	V_{PC}	V_{FS}	V_{XB}	V_{SC}
SIN1 with 30% Gaussian noise	FCM	0.32002	0.84752	-2.98861	0.10526	0.04514
	sFCM	0.30689	0.85941	-3.05147	0.09562	0.03401
	FCM_S	0.29856	0.86780	-3.18552	0.09125	0.03048
	FGFCM	0.25468	0.87012	-3.45012	0.06372	0.02894
	csFCM	0.26356	0.88045	-3.50012	0.05272	0.02507
	FSFCM	***0.20101***	***0.90562***	***-3.64370***	***0.01501***	***0.02098***
SIN1 with 30% Salt and Pepper noise	FCM	0.28472	0.85098	-3.16381	0.01766	0.03217
	sFCM	0.26984	0.86817	-3.21578	0.01702	0.02895
	FCM_S	0.25841	0.86541	-3.35602	0.01685	0.02901
	FGFCM	0.22745	0.87342	-3.65351	0.01512	0.02663
	csFCM	0.20941	0.89624	-3.45399	0.01485	0.02578
	FSFCM	***0.16458***	***0.92236***	***-4.29881***	***0.0085***	***0.02084***
SIN2 with 30% Gaussian noise	FCM	0.43100	0.80459	-3.58368	0.08569	0.07024
	sFCM	0.39895	0.82549	-3.65231	0.06478	0.05982
	FCM_S	0.38012	0.84780	-3.75489	0.06945	0.06047
	FGFCM	0.34989	0.86979	-4.05298	0.03985	0.04702
	csFCM	0.33844	0.87026	-4.18481	0.03178	0.04796
	FSFCM	***0.21589***	***0.90841***	***-4.58216***	***0.01547***	***0.02350***
SIN2 with 30% Salt and Pepper noise	FCM	0.44297	0.79531	-2.58961	0.09755	0.06942
	sFCM	0.42103	0.83125	-2.84215	0.07854	0.06589
	FCM_S	0.40953	0.84025	-2.72358	0.07402	0.05998
	FGFCM	0.35136	0.86478	-2.83881	0.04199	0.04942
	csFCM	0.34408	0.86558	-3.02984	0.03460	0.04527
	FSFCM	***0.21478***	***0.89945***	***-3.64370***	***0.02471***	***0.02159***
SIN3 with 30% Gaussian noise	FCM	0.49647	0.79541	-2.95012	0.18542	0.16272
	sFCM	0.45216	0.79428	-3.00005	0.16985	0.15892
	FCM_S	0.49125	0.78652	-3.01785	0.16524	0.14856
	FGFCM	0.41025	0.82014	-3.14269	0.13025	0.09518
	csFCM	0.44028	0.81590	-3.16029	0.11685	0.08932
	FSFCM	***0.34021***	***0.87453***	***-3.58096***	***0.06992***	***0.04835***
SIN3 with 30% Salt and Pepper noise	FCM	0.54953	0.78302	-2.89477	0.17951	0.20707
	sFCM	0.49852	0.79025	-2.94586	0.16589	0.20025
	FCM_S	0.48965	0.79149	-2.98543	0.15978	0.18936
	FGFCM	0.40953	0.82302	-3.29708	0.12951	0.16153
	csFCM	0.43785	0.82406	-3.25081	0.11798	0.15848
	FSFCM	***0.36526***	***0.88007***	***-3.75088***	***0.05102***	***0.05233***
SIN4 with 30% Gaussian noise	FCM	0.26163	0.86272	-3.15685	0.04615	0.03094
	sFCM	0.25998	0.86901	-3.17446	0.03998	0.02908
	FCM_S	0.25602	0.87006	-3.18098	0.03759	0.02781

	FGFCM	0.23370	0.88031	-3.26731	0.01828	0.02296
	csFCM	0.23066	0.88552	-3.26366	0.01943	0.02083
	FSFCM	***0.193859***	***0.90202***	***-3.78053***	***0.00905***	***0.01509***
SIN4 with 30% Salt and Pepper noise	FCM	0.25220	0.85272	-3.46289	0.04182	0.02938
	sFCM	0.24086	0.86378	-3.48122	0.03854	0.02800
	FCM_S	0.23845	0.86945	-3.50014	0.03695	0.02768
	FGFCM	0.21323	0.88031	-3.58162	0.02257	0.02323
	csFCM	0.20816	0.88352	-3.66698	0.01445	0.02132
	FSFCM	***0.18956***	***0.91202***	***-4.35897***	***0.00566***	***0.01382***
SIN5 with 30% Gaussian noise	FCM	0.3859	0.8034	-2.3458E+9	0.04801	0.03123
	sFCM	0.3664	0.8192	-3.0134E+9	0.03812	0.02901
	FCM_S	0.3599	0.8256	-3.3474E+9	0.03417	0.02727
	FGFCM	0.2559	0.8576	-4.0134E+9	0.03022	0.02981
	csFCM	0.2819	0.8489	-4.6796E+9	0.02626	0.02323
	FSFCM	***0.2189***	***0.8901***	***-5.2876E+9***	***0.01242***	***0.01234***
SIN5 with 30% Salt and Pepper noise	FCM	0.3729	0.8011	-2.6810E+9	0.04603	0.03345
	sFCM	0.2884	0.8209	-3.0120E+9	0.03615	0.02828
	FCM_S	0.2754	0.8465	-3.16216E+9	0.03273	0.02901
	FGFCM	0.2104	0.8532	-3.6810E+9	0.02789	0.02456
	csFCM	0.2494	0.8378	-4.3204E+9	0.02533	0.02121
	FSFCM	***0.1064***	***0.9023***	***-4.9204E+9***	***0.01440***	***0.01123***
SIN6 with 30% Gaussian noise	FCM	0.3079	0.8023	-2.7529E+9	0.04405	0.03094
	sFCM	0.2299	0.8254	-3.5590E+9	0.03219	0.02567
	FCM_S	0.2429	0.8123	-3.6703E+9	0.03475	0.02789
	FGFCM	0.2234	0.8379	-3.8312E+9	0.02331	0.02012
	csFCM	0.2169	0.8587	-4.9774E+9	0.02486	0.02285
	FSFCM	***0.1324***	***0.9145***	***-5.3579E+9***	***0.01338***	***0.01012***
SIN6 with 30% Salt and Pepper noise	FCM	0.3144	0.8054	-2.6944E+9	0.04010	0.03234
	sFCM	0.2624	0.8165	-3.0769E+9	0.02869	0.02584
	FCM_S	0.2364	0.8492	-3.7937E+9	0.02824	0.02678
	FGFCM	0.1909	0.8523	-3.9512E+9	0.02391	0.02123
	csFCM	0.1974	0.8654	-4.4851E+9	0.02596	0.02234
	FSFCM	***0.1259***	***0.9223***	***-5.4620E+9***	***0.01045***	***0.01345***

Table 5.2: The mean values of validity functions over the MRI images with various levels of noise and inhomogeneity

Image	Segmented Methods	Cluster Validity Function				
		V_{PE}	V_{PC}	V_{FS}	V_{XB}	V_{SC}
Noise 5%, IH=20%	FCM	0.18960	0.90066	-3.32001	0.01625	0.02101
	sFCM	0.18393	0.90510	-3.36894	0.01600	0.02081
	FCM_S	0.17847	0.90622	-3.37679	0.01613	0.02056
	FGFCM	0.15942	0.91329	-3.45942	0.01592	0.01958
	csFCM	0.15843	0.91511	-3.48027	0.01329	0.01853
	FSFCM	***0.15724***	***0.92419***	***-4.41607***	***0.01222***	***0.01689***
Noise 7%, IH=20%	FCM	0.20692	0.89155	-3.29695	0.01931	0.02338
	sFCM	0.18960	0.90066	-3.32001	0.01911	0.02268
	FCM_S	0.18547	0.90389	-3.33674	0.01865	0.02252
	FGFCM	0.18846	0.90257	-3.48545	0.01641	0.02058
	csFCM	0.18742	0.90866	-3.51848	0.01501	0.01955
	FSFCM	***0.16029***	***0.92365***	***-4.28821***	***0.01374***	***0.01778***
Noise 9%, IH=20%	FCM	0.21977	0.88907	-3.48120	0.02072	0.02626
	sFCM	0.21263	0.88994	-3.54394	0.01990	0.02512
	FCM_S	0.21018	0.88944	-3.56894	0.02042	0.02490
	FGFCM	0.19098	0.89456	-3.61634	0.01490	0.02202
	csFCM	0.19016	0.89578	-3.63718	0.01572	0.02223
	FSFCM	***0.16901***	***0.91329***	***-3.94283***	***0.01422***	***0.01936***
Noise 5%, IH=40%	FCM	0.19932	0.89562	-3.56865	0.01551	0.02229
	sFCM	0.19773	0.89743	-3.57325	0.01586	0.02168
	FCM_S	0.18979	0.89965	-3.57821	0.01507	0.02139
	FGFCM	0.17402	0.91170	-3.58557	0.01480	0.02133
	csFCM	0.17431	0.91059	-3.59596	0.01431	0.02029
	FSFCM	***0.15397***	***0.93183***	***-4.56466***	***0.01248***	***0.01867***
Noise 7%, IH=40%	FCM	0.21964	0.87242	-3.48839	0.02894	0.02889
	sFCM	0.21172	0.88286	-3.56016	0.02681	0.02789
	FCM_S	0.21100	0.88960	-3.56304	0.02605	0.02750
	FGFCM	0.19317	0.89953	-3.59851	0.01764	0.02288
	csFCM	0.20041	0.89241	-3.59602	0.01701	0.02464
	FSFCM	***0.16616***	***0.90960***	***-4.09950***	***0.01468***	***0.01915***
Noise 9%, IH=40%	FCM	0.22838	0.88358	-3.47568	0.02922	0.02753
	sFCM	0.21961	0.88807	-3.49818	0.02609	0.02656
	FCM_S	0.21918	0.88906	-3.51894	0.02567	0.02609
	FGFCM	0.19840	0.89148	-3.58410	0.02123	0.02342
	csFCM	0.19652	0.89308	-3.61334	0.02096	0.02387
	FSFCM	***0.17193***	***0.90982***	***-3.98324***	***0.01621***	***0.02023***

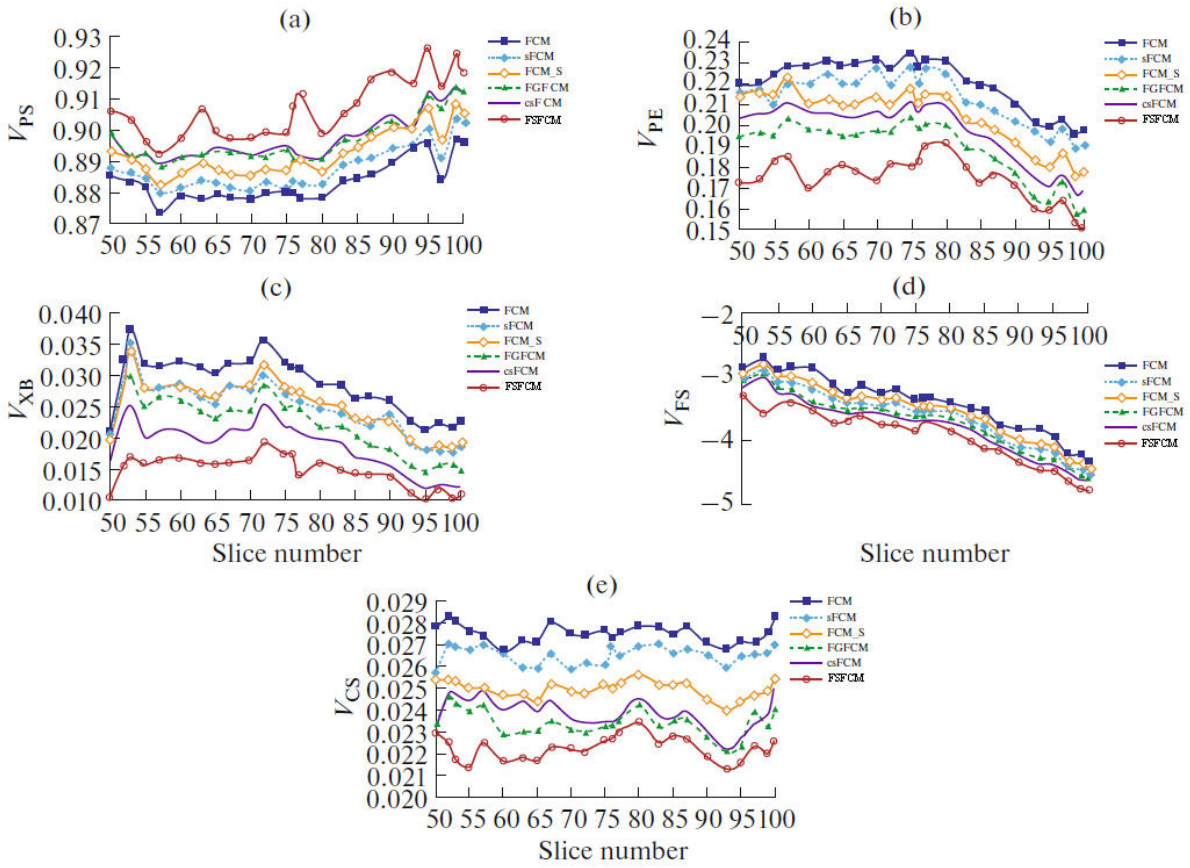

Figure 5.12 – Validity function values of V_{PE}, V_{PC}, V_{XB}, V_{FS}, and V_{SC} over the 51 simulated MRI brain images corrupted by 9% noise and 40% inhomogeneity.

b- Segmentation Accuracy (SA)

In this section, we evaluate the proposed algorithm and the compared algorithms in terms of segmentation accuracy measure (SA), which can be expressed as:

$$SA = \frac{\text{number of correctly classified pixels}}{\text{total number of pixels}} \tag{5.7}$$

From the results shown in Table 5.3, it can be seen that the SA values of FGFCM and csFCM are larger than those of FCM, sFCM, and FCM_S algorithms. Furthermore, FSFCM has much larger SA values in Table 5.3. It indicates that the proposed method achieves superior segmentation performance in terms of the segmentation accuracy measure.

Table 5.4 presents the average values of SA for the three segmented regions of the MRI brain images: CSF, GM, and WM, obtained by the six different algorithms with different levels of noise and inhomogeneity. It can be seen from Table 5.4 that the SA values of the proposed algorithm for CSF, GM, and WM tissues are larger than those of the compared computing algorithms. It reflects that the FSFCM algorithm achieves superior segmentation performance even with increased noise in the MRI images.

Figure 5.13 displays the average values of the SA measure over the 51 MRI images with 9% noise and 40% inhomogeneity of the three brain tissues obtained by the proposed algorithm (FSFCM) and the compared algorithms (FCM, sFCM, FCM_S, FGFCM, and csFCM). From Figure 5.13, we can observe that the proposed algorithm performs well in the segmentation of WM, GM, and CSF tissues across all MRI images. The proposed algorithm demonstrates a powerful capacity to accurately segment the three brain tissues compared to the other five algorithms.

Table 5.3: Comparison of SA measure on the synthetic images with various levels of noise.

Image	Method	SA	Image	Method	SA
SIN1 with 30% Salt and Pepper noise	FCM	0.78023	SIN4 with 30% Salt and Pepper noise	FCM	0.67529
	sFCM	0.80002		sFCM	0.68047
	FCM_S	0.80475		FCM_S	0.68259
	FGFCM	0.83470		FGFCM	0.77025
	csFCM	0.84021		csFCM	0.78691
	FSFCM	***0.91952***		***FSFCM***	***0.90902***
SIN1 with 30% Gaussian noise	FCM	0.75828	SIN4 with 30% Gaussian noise	FCM	0.68045
	sFCM	0.76852		sFCM	0.69417
	FCM_S	0.76524		FCM_S	0.69924
	FGFCM	0.81256		FGFCM	0.76982
	csFCM	0.82014		csFCM	0.77328
	FSFCM	***0.91651***		***FSFCM***	***0.90032***
SIN2 with 30% Salt and Pepper noise	FCM	0.72045	SIN5 with 30% Salt and Pepper noise	FCM	0.76521
	sFCM	0.75210		sFCM	0.77059
	FCM_S	0.75861		FCM_S	0.77928
	FGFCM	0.80426		FGFCM	0.80025
	csFCM	0.80578		csFCM	0.81965
	FSFCM	***0.91452***		***FSFCM***	***0.91023***
SIN2 with 30% Gaussian noise	FCM	0.68452	SIN5 with 30% Gaussian noise	FCM	0.75820
	sFCM	0.69425		sFCM	0.77458
	FCM_S	0.69014		FCM_S	0.79025
	FGFCM	0.78025		FGFCM	0.82036
	csFCM	0.79258		csFCM	0.84473
	FSFCM	***0.91254***		***FSFCM***	***0.91486***
SIN3 with 30% Salt and Pepper noise	FCM	0.7023	SIN6 with 30% Salt and Pepper noise	FCM	0.7127
	sFCM	0.7293		sFCM	0.7413
	FCM_S	0.8049		FCM_S	0.8026
	FGFCM	0.8172		FGFCM	0.8369

	csFCM	0.8684		csFCM	0.8426
	FSFCM	***0.9465***		***FSFCM***	***0.9514***
	FCM	0.7165		FCM	0.7044
SIN3 with	sFCM	0.7837	SIN6 with	sFCM	0.7638
30%	FCM_S	0.8017	30%	FCM_S	0.8105
Gaussian	FGFCM	0.8716	Gaussian	FGFCM	0.8496
noise	csFCM	0.8379	noise	csFCM	0.8502
	FSFCM	***0.9382***		***FSFCM***	***0.9649***

Table 5.4: Comparison of SA measure over the different using MRI brain images with various levels of noise and inhomogeneity

Image	Method	SA		
		CSF	GM	WM
Noise 5%, IH=20%	FCM	0.94240	0.92805	0.95168
	sFCM	0.94278	0.92823	0.95160
	FCM_S	0.94521	0.92841	0.95245
	FGFCM	0.94765	0.92881	0.96086
	csFCM	0.94688	0.92837	0.95200
	FSFCM	***0.95885***	***0.93960***	***0.97128***
Noise 7%, IH=20%	FCM	0.90154	0.88198	0.89472
	sFCM	0.90234	0.88567	0.90012
	FCM_S	0.90743	0.88997	0.90459
	FGFCM	0.91582	0.90456	0.92158
	csFCM	0.91680	0.89110	0.92350
	FSFCM	***0.94743***	***0.92997***	***0.94459***
Noise 9%, IH=20%	FCM	0.86844	0.83909	0.84124
	sFCM	0.87098	0.85422	0.85342
	FCM_S	0.87162	0.86031	0.84520
	FGFCM	0.88386	0.89000	0.91964
	csFCM	0.89105	0.88212	0.91666
	FSFCM	***0.93893***	***0.92188***	***0.93797***
Noise 5%, IH=40%	FCM	0.94101	0.93662	0.91867
	sFCM	0.94121	0.93666	0.91877
	FCM_S	0.94123	0.93694	0.92187
	FGFCM	0.94049	0.93822	0.92869
	csFCM	0.94139	0.93812	0.92919
	FSFCM	***0.95587***	***0.95879***	***0.96848***

Noise 7%, IH=40%	FCM	0.86089	0.84233	0.91391
	sFCM	0.86348	0.85752	0.91987
	FCM_S	0.87190	0.86359	0.91926
	FGFCM	0.87526	0.87211	0.92424
	csFCM	0.86921	0.86330	0.93310
	FSFCM	***0.93972***	***0.91417***	***0.94822***
Noise 9%, IH=40%	FCM	0.81652	0.78311	0.81728
	sFCM	0.84604	0.81637	0.82691
	FCM_S	0.81035	0.84714	0.81028
	FGFCM	0.88018	0.86915	0.89111
	csFCM	0.88514	0.85074	0.89197
	FSFCM	***0.91484***	***0.90081***	***0.92867***

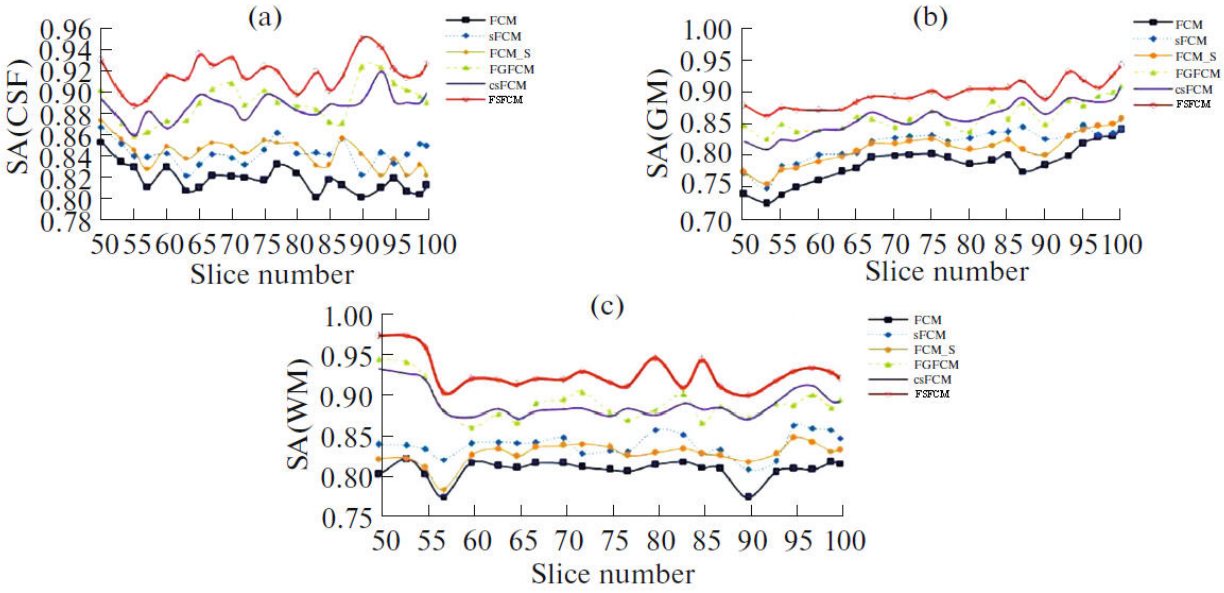

Figure 5.13 – The various values of segmentation accuracy measure of the brain tissues obtained by FSFCM and the compared algorithms on the simulated MRI brain images corrupted by 9% noise and 40% inhomogeneity.

c- Tissue Segmentation Accuracy (TSA)

In this section, we present the third evaluation measure in our quantitative analysis, namely tissue segmentation accuracy (TSA) (Adhikari et al., 2015). The TSA measure is calculated as follows:

$$TSA = \frac{2N_{CTK}}{N_{CITK} + N_{GTK}} \tag{5.8}$$

where N_{CTK} represents the number of pixels correctly assigned to tissue k by a given method within the ground truth mask, N_{GTK} is the number of pixels assigned to tissue k in the ground

truth mask, and N_{CITK} is the total number of pixels assigned to tissue k (inside and outside the ground truth mask).

Table 5.5 presents a comparison of the tissue segmentation accuracy measure for CSF, GM, and WM tissues using images with (5%, 7%, 9%) noise and (20%, 40%) inhomogeneity. The table includes the results for the proposed algorithm (FSFCM) and the compared algorithms. It can be observed that the proposed algorithm achieves the highest TSA values for the three brain tissues. On the other hand, the segmentation performance of the compared algorithms deteriorates under high levels of noise and inhomogeneity. This demonstrates the superior effectiveness of the proposed algorithm in segmenting the main brain tissues.

Figure 5.14 illustrates the average values of the TSA measure for CSF, GM, and WM tissues over the 51 MRI images with 9% noise and 40% inhomogeneity. The results are obtained using the proposed algorithm and the compared algorithms. It is evident that our proposed algorithm consistently outperforms the compared algorithms in segmenting CSF, GM, and WM tissues across the entire set of MRI images.

Table 5.5: Comparison of TSA measure over the different using images with various levels of noise and inhomogeneity

Image	Method	Tissue Segmentation Accuracy (TSA)		
		CSF	GM	WM
Noise 5%, IH=20%	FCM	0.90077	0.90589	0.93303
	sFCM	0.90112	0.90764	0.93765
	FCM_S	0.90328	0.90715	0.93860
	FGFCM	0.90521	0.91850	0.94756
	csFCM	0.90422	0.91936	0.94607
	FSFCM	***0.92854***	***0.93974***	***0.95821***
Noise 7%, IH=20%	FCM	0.85403	0.83752	0.87632
	sFCM	0.85712	0.84541	0.88420
	FCM_S	0.85879	0.84831	0.88783
	FGFCM	0.86140	0.87191	0.90973
	csFCM	0.86319	0.87079	0.90369
	FSFCM	***0.89444***	***0.91286***	***0.93303***
Noise 9%, IH=20%	FCM	0.78030	0.81782	0.85424
	sFCM	0.80007	0.82986	0.86543
	FCM_S	0.80439	0.82994	0.88493
	FGFCM	0.83750	0.87517	0.90384
	csFCM	0.83284	0.86656	0.90106
	FSFCM	***0.89157***	***0.90760***	***0.92746***
Noise 5%, IH=40%	FCM	0.89545	0.87942	0.90869
	sFCM	0.89698	0.88410	0.91006
	FCM_S	0.89876	0.88943	0.91311
	FGFCM	0.90076	0.89903	0.92104
	csFCM	0.90429	0.89465	0.92408
	FSFCM	***0.92930***	***0.92104***	***0.92429***
Noise 7%, IH=40%	FCM	0.84861	0.85732	0.89070
	sFCM	0.85000	0.86210	0.89119
	FCM_S	0.85157	0.86760	0.89746
	FGFCM	0.86803	0.88214	0.91402
	csFCM	0.89226	0.87171	0.91236
	FSFCM	***0.91996***	***0.91301***	***0.93810***
Noise 9%, IH=40%	FCM	0.77821	0.80477	0.80103
	sFCM	0.8069	0.82084	0.83866
	FCM_S	0.79030	0.82782	0.82424
	FGFCM	0.82679	0.86222	0.87251
	csFCM	0.83114	0.86383	0.88697
	FSFCM	***0.88024***	***0.89029***	***0.92918***

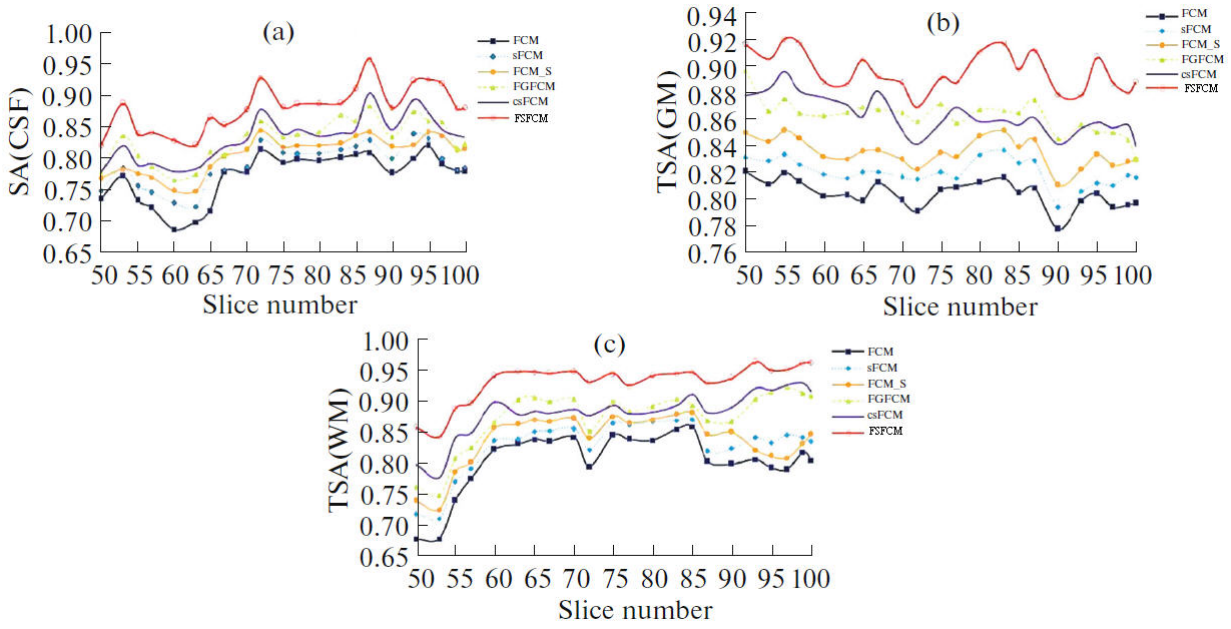

Figure 5.14 – The various values of tissue segmentation accuracy measure of the brain tissues obtained by FSFCM and the compared algorithms on the simulated MRI brain images corrupted by 9% noise and 40% inhomogeneity.

5.2.4 Conclusion

In this chapter, we proposed a novel fuzzy clustering algorithm termed as the Fully Spatial FCM Algorithm for Brain MRI Image Segmentation. The key feature of our algorithm is its comprehensive consideration of neighboring pixels' contribution during the fuzzy clustering process. By adjusting the influence of the central pixel in defining its new intensity, we incorporated a spatial constraint that effectively balances the reduction of sensitivity to imaging artifacts and the preservation of image detail information.

To evaluate the performance of the FSFCM algorithm, we conducted experiments on synthetic and brain MR images corrupted by various levels of noise. Additionally, we compared the performance of our algorithm with existing fuzzy clustering algorithms. The results demonstrate the effectiveness of the FSFCM algorithm in achieving accurate segmentation while effectively handling image artifacts.

Chapter 6

General Conclusions and Perspectives

Contents

6.1 Summary of contributions

The FCM algorithm is known to be sensitive to noise because it does not incorporate any spatial information. Additionally, FCM is a local optimum searching algorithm that depends mainly on the choice of the number of clusters and the initial cluster centers. These limitations can result in suboptimal segmentation results, particularly in medical imaging applications where accurate and reliable segmentation is crucial for diagnosis and treatment planning. To address these shortcomings, in this thesis, we proposed an automatic method for brain MRI image segmentation.

To address the main shortcomings of the FCM algorithm, our contributions are twofold. First, we propose a new adaptive initialization method that automatically evolves the number of clusters and improves the conventional process of initializing centers in the FCM algorithm. Second, we introduce a full spatial FCM algorithm that fully considers the contribution of neighboring pixels in the fuzzy clustering process, thereby improving the FCM algorithm's sensitivity to noise.

In Chapter 2, we first introduced the concept of image segmentation and its importance in a wide range of applications, such as medical imaging. Second, we discussed the principles of MRI imaging, including the underlying physics and the different types of MRI sequences commonly used in medical imaging. After that, we provided a detailed explanation of brain MRI segmentation, including its challenges and key applications. Following this, we presented a comprehensive survey of classical and modern state-of-the-art approaches for image segmentation. Our goal is to provide useful references to fundamental concepts accessible to the broad community of image segmentation techniques, in particular, we presented a taxonomy of clustering techniques, which are widely used in image segmentation, and discussed their strengths and weaknesses.

In Chapter 3, we first provided an overview of several fuzzy c-means (FCM) based image clustering concepts. Next, we presented the main limitations of the FCM algorithm, including its

sensitivity to initialization, poor performance in noisy environments, and difficulty in determining the optimal number of clusters. To address these limitations, we summarized various approaches aimed at automatically evolving the number of clusters and improving the conventional process of initializing centers in the FCM algorithm. Additionally, we proposed a large number of FCM derivatives that aim to either speed up the clustering process or provide improved or more robust clustering performance against noise. The derivatives that aim to improve the sensitivity of FCM algorithm can be essentially divided into two categories: input image generation-based methods and objective function modification-based methods. In the input image generation-based methods, the input data is preprocessed to extract features that are then used to generate a new image for clustering. This new image is expected to have better clustering properties than the original image. On the other hand, the objective function modification-based methods involve modifying the objective function used in FCM to incorporate additional constraints or penalties to improve the clustering performance.

In Chapter 4, we proposed a novel strategy to address the issue of the FCM algorithm's sensitivity to initialization schemes. Our proposed method is based on an adaptive split-stage technique that effectively divides the image into several homogeneous regions using a multi-threshold approach based on entropy information. To merge these regions, we introduced a new distance metric that combines the homogeneous regions, and then applied the FCM algorithm using the centers of the obtained regions. Additionally, we introduced a novel fuzzy validity index that incorporated a new definition for the separation measure. This allowed us to select the optimal fuzzy partition with high compactness and separation between clusters.

In Chapter 5, we introduce a robust fuzzy clustering algorithm that considers spatial information to improve the accuracy and reliability of FCM-based image segmentation. Our proposed algorithm assigns an important role to the central pixel if it is not a noisy pixel, and suppresses its influence from the fuzzy clustering if it is corrupted with noise. The degree of similarity between pixels is calculated using a fuzzy measure, and a new term is introduced to indicate the noise level of pixels. These measures are combined to construct neighborhood intensity information and enhance the algorithm's performance. The proposed algorithm aims to balance the reduction of sensitivity of the FCM algorithm to imaging artifacts and the preservation of image detail information.

6.2 Perspectives

When an image is corrupted by noise, accurately identifying the pixels that belong to a specific object or region in the image can be a challenging task. Relying solely on local spatial information, which considers only the pixels adjacent to a given pixel, may not provide sufficient information to accurately segment the image. However, incorporating non-local information, such as information about the entire image structure, can significantly improve the segmentation performance. By considering the global image structure, the proposed segmentation method can better distinguish between different regions and objects in the image, leading to more precise and reliable segmentation results.

In some cases, the proposed segmentation method may take longer to compute than other state-of-the-art methods. However, adopting a parallel strategy, such as utilizing parallel processing techniques or distributed computing, can significantly improve the computational time of the algorithm.

The validity index is a crucial metric that evaluates the quality of the segmentation results obtained by the algorithm. By incorporating overlap information, which measures the degree of

similarity between clusters, the validity index can be further improved. This approach provides a more comprehensive assessment of the segmentation performance, enabling the algorithm to better distinguish between different regions and objects in the image.

Moreover, a fuzzy representation of cluster centers as vectors can significantly enhance the algorithm's accuracy by effectively capturing the complex interrelationships between pixels in an image.

Publications

The publications directly related to this thesis are:

Fouzia Chighoub, Rachida Saouli, Fully Integrated Spatial Information to Improve FCM Algorithm for Brain MRI Image Segmentation. Aut. Control Comp. Sci. 56, 67–82 (2022). https://doi.org/10.3103/S0146411622010047

Bibliography

Adhikari, S. K., Sing, J. K., Basu, D. K., and Nasipuri, M. (2015). Conditional spatial fuzzy c-means clustering algorithm for segmentation of mri images. *Applied soft computing*, 34:758–769.

Agarwal, P., Kumar, S., Singh, R., Agarwal, P., and Bhattacharya, M. (2015). A combination of bias-field corrected fuzzy c-means and level set approach for brain mri image segmentation. In *2015 Second International Conference on Soft Computing and Machine Intelligence (ISCMI)*, pages 84–87. IEEE.

Ahmadvand, A. and Daliri, M. R. (2015). Improving the runtime of mrf based method for mri brain segmentation. *Applied Mathematics and Computation*, 256:808–818.

Ahmed, M. N., Yamany, S. M., Mohamed, N., Farag, A. A., and Moriarty, T. (2002). A modified fuzzy c-means algorithm for bias field estimation and segmentation of mri data. *IEEE transactions on medical imaging*, 21(3):193–199.

Akay, B. (2013). A study on particle swarm optimization and artificial bee colony algorithms for multilevel thresholding. *Applied Soft Computing*, 13(6):3066–3091.

Aljabar, P., Heckemann, R. A., Hammers, A., Hajnal, J. V., and Rueckert, D. (2009). Multi-atlas based segmentation of brain images: atlas selection and its effect on accuracy. *Neuroimage*, 46(3):726–738.

Alomoush, W., Alrosan, A., Alomari, Y. M., Alomoush, A. A., Almomani, A., and Alamri, H. S. (2022). Fully automatic grayscale image segmentation based fuzzy c-means with firefly mate algorithm. *Journal of Ambient Intelligence and Humanized Computing*, 13(9):4519–4541.

Alsmadi, M. K. (2014). A hybrid firefly algorithm with fuzzy-c mean algorithm for mri brain segmentation. *American Journal of Applied Sciences*, 11(9):1676–1691.

Assam, M., Kanwal, H., Farooq, U., Shah, S. K., Mehmood, A., and Choi, G. S. (2021). An efficient classification of mri brain images. *IEEE Access*, 9:33313–33322.

Atek, S., Mehidi, I., Jabri, D., and Belkhiat, D. E. (2022). Swint-unet: hybrid architecture for medical image segmentation based on swin transformer block and dual-scale information. In *2022 7th International Conference on Image and Signal Processing and their Applications (ISPA)*, pages 1–6. IEEE.

Ayman, A., Mabrouk, E., and Elnomery, Z. (2013). Adaptation of region growing thresholds using memetic programming algorithm. In *2013 IEEE/ACIS 12th International Conference on Computer and Information Science (ICIS)*, pages 29–34. IEEE.

Baillard, C. and Barillot, C. (2000). Robust 3d segmentation of anatomical structures with level sets. In *International Conference on Medical Image Computing and Computer-Assisted Intervention*, pages 236–245. Springer.

Balafar, M. A., Ramli, A. R., Saripan, M. I., and Mashohor, S. (2010). Review of brain mri image segmentation methods. *Artificial Intelligence Review*, 33:261–274.

Banerjee, A. and Maji, P. (2016). Rough-probabilistic clustering and hidden markov random field model for segmentation of hep-2 cell and brain mr images. *Applied Soft Computing*, 46:558–576.

Benaichouche, A. N., Oulhadj, H., and Siarry, P. (2013). Improved spatial fuzzy c-means clustering for image segmentation using pso initialization, mahalanobis distance and post-segmentation correction. *Digital Signal Processing*, 23(5):1390–1400.

Benos, L., Tagarakis, A. C., Dolias, G., Berruto, R., Kateris, D., and Bochtis, D. (2021). Machine learning in agriculture: A comprehensive updated review. *Sensors*, 21(11):3758.

Bensaid, A. M., Hall, L. O., Bezdek, J. C., Clarke, L. P., Silbiger, M. L., Arrington, J. A., and Murtagh, R. F. (1996). Validity-guided (re) clustering with applications to image segmentation. *IEEE Transactions on fuzzy systems*, 4(2):112–123.

Beringer, J. and Hullermeier, E. (2007). Adaptive optimization of the number of clusters in fuzzy clustering. In *2007 IEEE International Fuzzy Systems Conference*, pages 1–6. IEEE.

Bezdek, J. C. (1973). Cluster validity with fuzzy sets.

Bezdek, J. C. and Dunn, J. C. (1975). Optimal fuzzy partitions: A heuristic for estimating the parameters in a mixture of normal distributions. *IEEE Transactions on Computers*, 100(8):835–838.

Bian, Z. (2022). Mr brain tissue classification based on the spatial information enhanced gaussian mixture model. *Technology and Health Care*, 30(S1):81–89.

Borsotti, M., Campadelli, P., and Schettini, R. (1998). Quantitative evaluation of color image segmentation results. *Pattern recognition letters*, 19(8):741–747.

Cai, W., Chen, S., and Zhang, D. (2007). Fast and robust fuzzy c-means clustering algorithms incorporating local information for image segmentation. *Pattern recognition*, 40(3):825–838.

Chan, T. F. and Vese, L. A. (2001). Active contours without edges. *IEEE Transactions on image processing*, 10(2):266–277.

Chang, C.-I., Chen, K., Wang, J., and Althouse, M. L. (1994). A relative entropy-based approach to image thresholding. *Pattern recognition*, 27(9):1275–1289.

Chen, M. and Ludwig, S. A. (2014). Particle swarm optimization based fuzzy clustering approach to identify optimal number of clusters. *Journal of Artificial Intelligence and Soft Computing Research*, 4(1):43–56.

Chen, S. and Zhang, D. (2004). Robust image segmentation using fcm with spatial constraints based on new kernel-induced distance measure. *IEEE Transactions on Systems, Man, and Cybernetics, Part B (Cybernetics)*, 34(4):1907–1916.

Chen, Y. and Wu, M. (2019). A level set method for brain mr image segmentation under asymmetric distributions. *Signal, Image and Video Processing*, 13(7):1421–1429.

Chouhan, S. S., Kaul, A., and Singh, U. P. (2019). Image segmentation using computational intelligence techniques. *Archives of Computational Methods in Engineering*, 26:533–596.

Chuang, K.-S., Tzeng, H.-L., Chen, S., Wu, J., and Chen, T.-J. (2006). Fuzzy c-means clustering with spatial information for image segmentation. *computerized medical imaging and graphics*, 30(1):9–15.

Cocosco, C. A., Zijdenbos, A. P., and Evans, A. C. (2003). A fully automatic and robust brain mri tissue classification method. *Medical image analysis*, 7(4):513–527.

Davé, R. N. and Krishnapuram, R. (1997). Robust clustering methods: a unified view. *IEEE Transactions on fuzzy systems*, 5(2):270–293.

De, A. and Guo, C. (2015). An adaptive vector quantization approach for image segmentation based on som network. *Neurocomputing*, 149:48–58.

Dehdasht-Heydari, R. and Gholami, S. (2019). Automatic seeded region growing (asrg) using genetic algorithm for brain mri segmentation. *Wireless Personal Communications*, 109(2):897–908.

Deserno, T. M. (2010). Fundamentals of biomedical image processing. In *Biomedical Image Processing*, pages 1–51. Springer.

Despotović, I., Goossens, B., and Philips, W. (2015). Mri segmentation of the human brain: challenges, methods, and applications. *Computational and mathematical methods in medicine*, 2015.

Ding, Y. and Fu, X. (2016). Kernel-based fuzzy c-means clustering algorithm based on genetic algorithm. *Neurocomputing*, 188:233–238.

Dokur, Z. and Ölmez, T. (2003). Segmentation of mr and ct images by using a quantiser neural network. *Neural Computing & Applications*, 11:168–177.

Dong, F. and Peng, J. (2014). Brain mr image segmentation based on local gaussian mixture model and nonlocal spatial regularization. *Journal of Visual Communication and Image Representation*, 25(5):827–839.

Dora, L., Agrawal, S., Panda, R., and Abraham, A. (2017). State-of-the-art methods for brain tissue segmentation: A review. *IEEE reviews in biomedical engineering*, 10:235–249.

Dubey, Y. K. and Mushrif, M. M. (2016). Fcm clustering algorithms for segmentation of brain mr images. *Advances in Fuzzy Systems*, 2016.

Duda, R. O., Hart, P. E., et al. (1973). *Pattern classification and scene analysis*, volume 3. Wiley New York.

El-Dahshan, E.-S. A., Mohsen, H. M., Revett, K., and Salem, A.-B. M. (2014). Computer-aided diagnosis of human brain tumor through mri: A survey and a new algorithm. *Expert systems with Applications*, 41(11):5526–5545.

Ezugwu, A. E., Shukla, A. K., Agbaje, M. B., Oyelade, O. N., José-García, A., and Agushaka, J. O. (2021). Automatic clustering algorithms: a systematic review and bibliometric analysis of relevant literature. *Neural Computing and Applications*, 33:6247–6306.

Fraz, M. M., Remagnino, P., Hoppe, A., Uyyanonvara, B., Rudnicka, A. R., Owen, C. G., and Barman, S. A. (2012). An ensemble classification-based approach applied to retinal blood vessel segmentation. *IEEE Transactions on Biomedical Engineering*, 59(9):2538–2548.

Gong, M., Su, L., Jia, M., and Chen, W. (2013). Fuzzy clustering with a modified mrf energy function for change detection in synthetic aperture radar images. *IEEE Transactions on Fuzzy Systems*, 22(1):98–109.

Greenspan, H., Ruf, A., and Goldberger, J. (2006). Constrained gaussian mixture model framework for automatic segmentation of mr brain images. *IEEE transactions on medical imaging*, 25(9):1233–1245.

Guha, S., Rastogi, R., and Shim, K. (1998). Cure: An efficient clustering algorithm for large databases. *ACM Sigmod record*, 27(2):73–84.

Hammouche, K., Diaf, M., and Siarry, P. (2010). A comparative study of various meta-heuristic techniques applied to the multilevel thresholding problem. *Engineering Applications of Artificial Intelligence*, 23(5):676–688.

Held, K., Kops, E. R., Krause, B. J., Wells, W. M., Kikinis, R., and Muller-Gartner, H.-W. (1997). Markov random field segmentation of brain mr images. *IEEE transactions on medical imaging*, 16(6):878–886.

Höppner, F., Klawonn, F., Kruse, R., and Runkler, T. (1999). *Fuzzy cluster analysis: methods for classification, data analysis and image recognition*. John Wiley & Sons.

Isa, N. A. M., Salamah, S. A., and Ngah, U. K. (2009). Adaptive fuzzy moving k-means clustering algorithm for image segmentation. *IEEE Transactions on Consumer Electronics*, 55(4):2145–2153.

Jain, A. K., Murty, M. N., and Flynn, P. J. (1999). Data clustering: a review. *ACM computing surveys (CSUR)*, 31(3):264–323.

Jansi, S. and Subashini, P. (2014). Modified fcm using genetic algorithm for segmentation of mri brain images. In *2014 IEEE International Conference on Computational Intelligence and Computing Research*, pages 1–5. IEEE.

Jena, M., Mishra, S. P., and Mishra, D. (2018). A survey on applications of machine learning techniques for medical image segmentation. *Internationa Journal of Engineering & Technology*, 7(4):4489–4495.

Ji, Z.-X., Chen, Q., Sun, Q.-S., Xia, D.-S., and Heng, P.-A. (2010). Mr image segmentation and bias field estimation using coherent local and global intensity clustering. In *2010 Seventh International Conference on Fuzzy Systems and Knowledge Discovery*, volume 2, pages 578–582. IEEE.

Jialun, P., Chen, W., and Dong, X. (2017). Magnetic resonance imaging brain image segmentation method based on adaptive clustering algorithm. *Journal of Medical Imaging and Health Informatics*, 7:1629–1635.

Kapur, J. N., Sahoo, P. K., and Wong, A. K. (1985). A new method for gray-level picture thresholding using the entropy of the histogram. *Computer vision, graphics, and image processing*, 29(3):273–285.

Khairuzzaman, A. K. M. and Chaudhury, S. (2019). Brain mr image multilevel thresholding by using particle swarm optimization, otsu method and anisotropic diffusion. *International Journal of Applied Metaheuristic Computing (IJAMC)*, 10(3):91–106.

Khaled, A., Han, J.-J., Ghaleb, T. A., and Mohamed, R. (2023). Fully convolutional neural network for improved brain segmentation. *Arabian Journal for Science and Engineering*, 48(2):2133–2146.

Khalili, N., Lessmann, N., Turk, E., Claessens, N., de Heus, R., Kolk, T., Viergever, M. A., Benders, M. J., and Išgum, I. (2019). Automatic brain tissue segmentation in fetal mri using convolutional neural networks. *Magnetic resonance imaging*, 64:77–89.

Khorram, B. and Yazdi, M. (2019). A new optimized thresholding method using ant colony algorithm for mr brain image segmentation. *Journal of digital imaging*, 32:162–174.

Kittler, J. and Illingworth, J. (1986). Minimum error thresholding. *Pattern recognition*, 19(1):41–47.

Kleesiek, J., Urban, G., Hubert, A., Schwarz, D., Maier-Hein, K., Bendszus, M., and Biller, A. (2016). Deep mri brain extraction: A 3d convolutional neural network for skull stripping. *NeuroImage*, 129:460–469.

Kotte, S., Pullakura, R. K., and Injeti, S. K. (2018). Optimal multilevel thresholding selection for brain mri image segmentation based on adaptive wind driven optimization. *Measurement*, 130:340–361.

Krinidis, S. and Chatzis, V. (2010). A robust fuzzy local information c-means clustering algorithm. *IEEE transactions on image processing*, 19(5):1328–1337.

Krishna, K. and Murty, M. N. (1999). Genetic k-means algorithm. *IEEE Transactions on Systems, Man, and Cybernetics, Part B (Cybernetics)*, 29(3):433–439.

Lai, J. Z., Huang, T.-J., and Liaw, Y.-C. (2009). A fast k-means clustering algorithm using cluster center displacement. *Pattern Recognition*, 42(11):2551–2556.

Li, C., Huang, R., Ding, Z., Gatenby, J. C., Metaxas, D. N., and Gore, J. C. (2011). A level set method for image segmentation in the presence of intensity inhomogeneities with application to mri. *IEEE transactions on image processing*, 20(7):2007–2016.

Li, H., He, H., and Wen, Y. (2015). Dynamic particle swarm optimization and k-means clustering algorithm for image segmentation. *Optik*, 126(24):4817–4822.

Li, Y.-l. and Shen, Y. (2010). An automatic fuzzy c-means algorithm for image segmentation. *Soft Computing*, 14:123–128.

Liang, Z., Zhang, P., and Zhao, J. (2010). Optimization of the number of clusters in fuzzy clustering. In *2010 International Conference On Computer Design and Applications*, volume 3, pages V3–580. IEEE.

Liu, J. and Yang, Y.-H. (1994). Multiresolution color image segmentation. *IEEE Transactions on Pattern Analysis and Machine Intelligence*, 16(7):689–700.

Lötjönen, J. M., Wolz, R., Koikkalainen, J. R., Thurfjell, L., Waldemar, G., Soininen, H., Rueckert, D., Initiative, A. D. N., et al. (2010). Fast and robust multi-atlas segmentation of brain magnetic resonance images. *Neuroimage*, 49(3):2352–2365.

Lu, X., Wu, J., Ren, X., Zhang, B., and Li, Y. (2014). The study and application of the improved region growing algorithm for liver segmentation. *Optik*, 125(9):2142–2147.

Malladi, R., Sethian, J. A., and Vemuri, B. C. (1993). Topology-independent shape modeling scheme. In *Geometric Methods in Computer Vision II*, volume 2031, pages 246–258. SPIE.

Manikandan, S., Ramar, K., Iruthayarajan, M. W., and Srinivasagan, K. (2014). Multilevel thresholding for segmentation of medical brain images using real coded genetic algorithm. *Measurement*, 47:558–568.

Martin, D., Fowlkes, C., Tal, D., and Malik, J. (2001). A database of human segmented natural images and its application to evaluating segmentation algorithms and measuring ecological statistics. In *Proceedings Eighth IEEE International Conference on Computer Vision. ICCV 2001*, volume 2, pages 416–423. IEEE.

Maulik, U. and Bandyopadhyay, S. (2003). Fuzzy partitioning using a real-coded variable-length genetic algorithm for pixel classification. *IEEE Transactions on geoscience and remote sensing*, 41(5):1075–1081.

Maulik, U. and Saha, I. (2009). Modified differential evolution based fuzzy clustering for pixel classification in remote sensing imagery. *Pattern Recognition*, 42(9):2135–2149.

Mehidi, I., Belkhiat, D. E. C., and Jabri, D. (2020). A fast k-means clustering algorithm for separation of brain tissues in mri. In *2020 2nd International Conference on Mathematics and Information Technology (ICMIT)*, pages 132–137. IEEE.

Mehnert, A. and Jackway, P. (1997). An improved seeded region growing algorithm. *Pattern Recognition Letters*, 18(10):1065–1071.

Mekhmoukh, A. and Mokrani, K. (2015). Improved fuzzy c-means based particle swarm optimization (pso) initialization and outlier rejection with level set methods for mr brain image segmentation. *Computer methods and programs in biomedicine*, 122(2):266–281.

Mirjalili, S., Gandomi, A. H., Mirjalili, S. Z., Saremi, S., Faris, H., and Mirjalili, S. M. (2017). Salp swarm algorithm: A bio-inspired optimizer for engineering design problems. *Advances in engineering software*, 114:163–191.

Mittal, H., Pandey, A. C., Saraswat, M., Kumar, S., Pal, R., and Modwel, G. (2021). A comprehensive survey of image segmentation: clustering methods, performance parameters, and benchmark datasets. *Multimedia Tools and Applications*, pages 1–26.

Moeskops, P., Viergever, M. A., Mendrik, A. M., De Vries, L. S., Benders, M. J., and Išgum, I. (2016). Automatic segmentation of mr brain images with a convolutional neural network. *IEEE transactions on medical imaging*, 35(5):1252–1261.

Mumford, D. B. and Shah, J. (1989). Optimal approximations by piecewise smooth functions and associated variational problems. *Communications on pure and applied mathematics*.

Nie, S., Zhang, Y., Li, W., and Chen, Z. (2007). A fast and automatic segmentation method of mr brain images based on genetic fuzzy clustering algorithm. In *2007 29th Annual International Conference of the IEEE Engineering in Medicine and Biology Society*, pages 5628–5633. IEEE.

Nilakant, R., Menon, H. P., and Vikram, K. (2017). A survey on advanced segmentation techniques for brain mri image segmentation. *International Journal on Advanced Science, Engineering and Information Technology*, 7(4):1448–1456.

Oliva, D., Hinojosa, S., Cuevas, E., Pajares, G., Avalos, O., and Gálvez, J. (2017). Cross entropy based thresholding for magnetic resonance brain images using crow search algorithm. *Expert Systems with Applications*, 79:164–180.

Ortiz, A., Gorriz, J., Ramirez, J., and Salas-Gonzalez, D. (2014). Improving mr brain image segmentation using self-organising maps and entropy-gradient clustering. *Information Sciences*, 262:117–136.

Osher, S. and Sethian, J. A. (1988). Fronts propagating with curvature-dependent speed: Algorithms based on hamilton-jacobi formulations. *Journal of computational physics*, 79(1):12–49.

Otsu, N. (1979). A threshold selection method from gray-level histograms. *IEEE transactions on systems, man, and cybernetics*, 9(1):62–66.

Pal, N. R. and Bezdek, J. C. (1995). On cluster validity for the fuzzy c-means model. *IEEE Transactions on Fuzzy systems*, 3(3):370–379.

Pan, Z. and Lu, J. (2007). A bayes-based region-growing algorithm for medical image segmentation. *Computing in science & Engineering*, 9(4):32–38.

Panda, R., Samantaray, L., Das, A., Agrawal, S., and Abraham, A. (2021). A novel evolutionary row class entropy based optimal multi-level thresholding technique for brain mr images. *Expert Systems with Applications*, 168:114426.

Papachary, B., Amru, M., and Reddy, S. R. K. (2021). An effective segmentation of tissues from mr brain images. In *Journal of Physics: Conference Series*, volume 1964, page 062029. IOP Publishing.

Pateria, N., Kumar, D., and Kumar, S. (2021). Magnetic resonance imaging classification methods: A review. *Nanoelectronics, Circuits and Communication Systems: Proceeding of NCCS 2019*, pages 417–427.

Pham, D. L. and Prince, J. L. (1999). An adaptive fuzzy c-means algorithm for image segmentation in the presence of intensity inhomogeneities. *Pattern recognition letters*, 20(1):57–68.

Pham, D. L., Xu, C., and Prince, J. L. (2000). Current methods in medical image segmentation. *Annual review of biomedical engineering*, 2(1):315–337.

Pohle, R. and Toennies, K. D. (2001). Segmentation of medical images using adaptive region growing. In *Medical Imaging 2001: Image Processing*, volume 4322, pages 1337–1346. SPIE.

Puttagunta, M. and Ravi, S. (2021). Medical image analysis based on deep learning approach. *Multimedia tools and applications*, 80:24365–24398.

Rajapakse, J. C., Giedd, J. N., and Rapoport, J. L. (1997). Statistical approach to segmentation of single-channel cerebral mr images. *IEEE transactions on medical imaging*, 16(2):176–186.

Ramzan, F., Khan, M. U. G., Iqbal, S., Saba, T., and Rehman, A. (2020). Volumetric segmentation of brain regions from mri scans using 3d convolutional neural networks. *IEEE Access*, 8:103697–103709.

Ren, M., Liu, P., Wang, Z., and Yi, J. (2016). A self-adaptive fuzzy c-means algorithm for determining the optimal number of clusters. *Computational intelligence and neuroscience*, 2016.

Rogowska, J. (2000). Overview and fundamentals of medical image segmentation. *Handbook of medical imaging, processing and analysis*, pages 69–85.

Rostami, M. T., Ezoji, M., Ghaderi, R., and Ghasemi, J. (2013). Brain mri segmentation using the mixture of fcm and rbf neural network. In *2013 8th Iranian Conference on Machine Vision and Image Processing (MVIP)*, pages 425–429. IEEE.

Sezgin, M. and Sankur, B. l. (2004). Survey over image thresholding techniques and quantitative performance evaluation. *Journal of Electronic imaging*, 13(1):146–168.

Shen, S., Sandham, W., Granat, M., and Sterr, A. (2005). Mri fuzzy segmentation of brain tissue using neighborhood attraction with neural-network optimization. *IEEE transactions on information technology in biomedicine*, 9(3):459–467.

Shi, Z., Lihuang, S., Hongyan, W., and Hua, Z. (2013). Brain mr image segmentation and bias field estimation using coherent local and non-local spatial constraints. In *2013 25th Chinese Control and Decision Conference (CCDC)*, pages 4454–4459. IEEE.

Siddiqui, F. and Mat Isa, N. (2012). Optimized k-means (okm) clustering algorithm for image segmentation. *Opto-Electronics Review*, 20:216–225.

Sikka, K., Sinha, N., Singh, P. K., and Mishra, A. K. (2009). A fully automated algorithm under modified fcm framework for improved brain mr image segmentation. *Magnetic Resonance Imaging*, 27(7):994–1004.

Singh, M., Venkatesh, V., Verma, A., and Sharma, N. (2020). Segmentation of mri data using multi-objective antlion based improved fuzzy c-means. *Biocybernetics and Biomedical Engineering*, 40(3):1250–1266.

Stadlbauer, A., Moser, E., Gruber, S., Buslei, R., Nimsky, C., Fahlbusch, R., and Ganslandt, O. (2004). Improved delineation of brain tumors: an automated method for segmentation based on pathologic changes of 1h-mrsi metabolites in gliomas. *Neuroimage*, 23(2):454–461.

Sun, H., Wang, S., and Jiang, Q. (2004). Fcm-based model selection algorithms for determining the number of clusters. *Pattern recognition*, 37(10):2027–2037.

Szilagyi, L., Benyo, Z., Szilágyi, S. M., and Adam, H. (2003). Mr brain image segmentation using an enhanced fuzzy c-means algorithm. In *Proceedings of the 25th annual international conference of the IEEE engineering in medicine and biology society (IEEE Cat. No. 03CH37439)*, volume 1, pages 724–726. IEEE.

Tarkhaneh, O. and Shen, H. (2019). An adaptive differential evolution algorithm to optimal multi-level thresholding for mri brain image segmentation. *Expert Systems with Applications*, 138:112820.

Tohka, J., Dinov, I. D., Shattuck, D. W., and Toga, A. W. (2010). Brain mri tissue classification based on local markov random fields. *Magnetic resonance imaging*, 28(4):557–573.

Torbati, N., Ayatollahi, A., and Kermani, A. (2014). An efficient neural network based method for medical image segmentation. *Computers in biology and medicine*, 44:76–87.

Tripathi, P. C. and Bag, S. (2020). Segmentation of brain magnetic resonance images using a novel fuzzy clustering based method. *IET Image Processing*, 14(15):3705–3717.

Valdés-Cristerna, R., Medina-Bañuelos, V., and Yáñez-Suárez, O. (2004). Coupling of radial-basis network and active contour model for multispectral brain mri segmentation. *IEEE Transactions on Biomedical Engineering*, 51(3):459–470.

Van Leemput, K., Maes, F., Vandermeulen, D., and Suetens, P. (1999). Automated model-based tissue classification of mr images of the brain. *IEEE transactions on medical imaging*, 18(10):897–908.

Vovk, U., Pernus, F., and Likar, B. (2007). A review of methods for correction of intensity inhomogeneity in mri. *IEEE transactions on medical imaging*, 26(3):405–421.

Wang, J., Kong, J., Lu, Y., Qi, M., and Zhang, B. (2008). A modified fcm algorithm for mri brain image segmentation using both local and non-local spatial constraints. *Computerized medical imaging and graphics*, 32(8):685–698.

Wang, Q., Wang, X., Fang, C., and Yang, W. (2020). Robust fuzzy c-means clustering algorithm with adaptive spatial & intensity constraint and membership linking for noise image segmentation. *Applied Soft Computing*, 92:106318.

Warfield, S. K., Kaus, M., Jolesz, F. A., and Kikinis, R. (2000). Adaptive, template moderated, spatially varying statistical classification. *Medical image analysis*, 4(1):43–55.

Wen, L., Wang, X., Wu, Z., Zhou, M., and Jin, J. S. (2015). A novel statistical cerebrovascular segmentation algorithm with particle swarm optimization. *Neurocomputing*, 148:569–577.

Xie, X. L. and Beni, G. (1991). A validity measure for fuzzy clustering. *IEEE Transactions on Pattern Analysis & Machine Intelligence*, 13(08):841–847.

Xu, D. and Tian, Y. (2015). A comprehensive survey of clustering algorithms. *Annals of Data Science*, 2:165–193.

Yang, M.-S. and Nataliani, Y. (2017). Robust-learning fuzzy c-means clustering algorithm with unknown number of clusters. *Pattern Recognition*, 71:45–59.

Yang, M.-S. and Tsai, H.-S. (2008). A gaussian kernel-based fuzzy c-means algorithm with a spatial bias correction. *Pattern recognition letters*, 29(12):1713–1725.

Yazdani, S., Yusof, R., Karimian, A., Pashna, M., and Hematian, A. (2015). Image segmentation methods and applications in mri brain images. *IETE Technical Review*, 32(6):413–427.

Yong, Y., Chongxun, Z., and Pan, L. (2004). A novel fuzzy c-means clustering algorithm for image thresholding. *Measurement science review*, 4(1):11–19.

Zanaty, E. (2012). Determining the number of clusters for kernelized fuzzy c-means algorithms for automatic medical image segmentation. *Egyptian Informatics Journal*, 13(1):39–58.

Zanaty, E. and Asaad, A. (2013). Probabilistic region growing method for improving magnetic resonance image segmentation. *Connection Science*, 25(4):179–196.

Zanaty, E. and Ghoniemy, S. (2016). Medical image segmentation techniques: an overview. *International Journal of informatics and medical data processing*, 1(1):16–37.

Zhan, T., Zhang, J., Xiao, L., Chen, Y., and Wei, Z. (2013). An improved variational level set method for mr image segmentation and bias field correction. *Magnetic Resonance Imaging*, 31(3):439–447.

Zhang, T., Ramakrishnan, R., and Livny, M. (1996). Birch: an efficient data clustering method for very large databases. *ACM sigmod record*, 25(2):103–114.

Zhang, X., Sun, Y., Liu, H., Hou, Z., Zhao, F., and Zhang, C. (2021). Improved clustering algorithms for image segmentation based on non-local information and back projection. *Information Sciences*, 550:129–144.

Zhang, X., Sun, Y., Wang, G., Guo, Q., Zhang, C., and Chen, B. (2017). Improved fuzzy clustering algorithm with non-local information for image segmentation. *Multimedia Tools and Applications*, 76:7869–7895.

Zhang, Y., Brady, M., and Smith, S. (2001). Segmentation of brain mr images through a hidden markov random field model and the expectation-maximization algorithm. *IEEE transactions on medical imaging*, 20(1):45–57.

Zhao, F. (2013). Fuzzy clustering algorithms with self-tuning non-local spatial information for image segmentation. *Neurocomputing*, 106:115–125.

Zhao, F., Fan, J., Liu, H., Lan, R., and Chen, C. W. (2018). Noise robust multiobjective evolutionary clustering image segmentation motivated by the intuitionistic fuzzy information. *IEEE Transactions on Fuzzy Systems*, 27(2):387–401.

Zhao, F., Liu, H., and Fan, J. (2015). A multiobjective spatial fuzzy clustering algorithm for image segmentation. *Applied Soft Computing*, 30:48–57.

Zhu, H. (2003). Medical image processing overview. *University of Calgary*, pages 1–27.